Dynamics of The Cytosolic Ca^{2+} Concentration in Acutely Dissociated Subfornical Organ Neurons of Rats: Mechanisms of Angiotensin II-induced Activation and GABA-mediated Inhibition

（ラット急性単離脳弓下器官ニューロンにおける細胞内Ca^{2+}動態:
それに対するAngiotensin IIとGABAの作用機序）

2021

The Joint Graduate School of Veterinary Sciences,
Tottori University

Yu Izumisawa

CONTENTS

PREFACE …… 1

1. **Subfornical organ, SFO**
2. **Cytosolic Ca^{2+} concentration**
3. **Angiotensin II in the SFO**
4. **γ-amino butyric acid (GABA)**
5. **About my study during the graduate course**

References

Chapter 1: The cytosolic Ca^{2+} concentration in acutely dissociated subfornical organ (SFO) neurons of rats: spontaneous Ca^{2+} oscillations and Ca^{2+} oscillations induced by picomolar concentrations of angiotensin II

…… 15

- **Abstract**
- **Introduction**
- **Results**
- **Discussion**
- **Graphical abstract**
- **Experiment procedure**
- **References**

Chapter 2: Persistent cytosolic Ca^{2+} increase induced by angiotensin II at nanomolar concentrations in acutely dissociated subfornical organ (SFO) neurons of rats

…… 59

- **Abstract**
- **Introduction**
- **Results**
- **Discussion**
- **Graphical abstract**
- **Experiment procedure**
- **References**

Chapter 3: Mechanisms of GABA-mediated inhibition of the angiotensin II-induced cytosolic Ca^{2+} increase in rat subfornical organ neurons

…… 103

- **Abstract**
- **Introduction**
- **Results**
- **Discussion**
- **Graphical abstract**
- **Experiment procedure**
- **References**

SUMMARY

…… 155

- **INTRODUCTION & PURPOSE**

- **MATERIALS AND METHODS**
- **RESULTS**
- **DISCUSSION & CONCLUSION**

ACKNOWLEDGEMENTS 159

PREFACE

1. Subfornical organ, SFO

The Subfornical organ (SFO), one of the circumventricular organs, is located in the middle of the anterior wall of the third ventricle and protrudes toward the ventricle (Dellmann, 1998b; Johnson and Gross, 1993). Since the SFO lacks the blood-brain barrier (BBB) due to the fenestrated capillaries, it can directly sense molecules in the circulating blood (Cottrell and Ferguson, 2004; Ferguson and Li, 1996; Gross, 1992; McKinley et al., 1998; Mimee et al., 2013; Smith and Ferguson, 2010). In addition, SFO neurons project to multiple brain regions and play an important role in the sensing circulating substances in the central nervous system (Dellmann, 1998a). Specifically, they project to the median preoptic nucleus (MnPO) and the organum vasculosum laminae terminalis (OVLT) involved in fluid homeostasis, nuclei in the hypothalamus such as the paraventricular nucleus (PVN) and supraoptic nucleus (SON), and the limbic system such as the bed nucleus of the stria terminalis (BST) and amygdala. Moreover, PVN neurons project to the rostral ventrolateral medulla (RVLM), the center of cardiovascular regulation, and contain neurosecretory neurons secreting the arginine vasopressin (AVP), the antidiuretic hormone at the posterior pituitary. When electrical stimulation is applied to the SFO, the RVLM is activated via the PVN and also promotes the secretion of the vasopressin from the posterior pituitary, resulting in an increase in the blood pressure (Ferguson and Kasting, 1986; Ferguson and Renaud, 1984; Gutman et al., 1985). Since the above-mentioned brain regions except for the OVLT possess BBB, it has been considered that the SFO is the entry point for sensing various substances in the circulating blood and sending the information to other brain regions. In fact, since SFO neurons sense the plasma Na^+ concentration (Hiyama and Noda,

2016), angiotensin II (AII) (Ferguson et al., 1990), and AVP (Anthes et al., 1997), it has been regarded as the most important sensor site for maintaining the homeostasis of blood pressure and circulating fluid volume in the central nervous system. In recent years, several results have been reported that SFO neurons sense not only circulating molecules related to the fluid homeostasis but also those related to feeding and immune responses. From these results, it has been suggested that the SFO may be the integrated site of multiple physiologically important information (Cancelliere and Ferguson, 2017; Cottrell and Ferguson, 2004; Fitzsimons, 1998; Simpson and Ferguson, 2017; Simpson and Ferguson, 2018; Yu et al., 2018).

2. Cytosolic Ca^{2+} concentration

Ca^{2+} acts as the key second messenger in cells of various organs (Berridge et al., 1998). For example, it plays an important role in hormone secretion, muscle contraction, immune response, and fertilization. In neurons, Ca^{2+} is the most universal intracellular signaling substance, and is known as a factor that triggers important cell functions such as release of neurotransmitters, neuroplasticity, gene expression, and cell death. Normally, in the resting state, the intracellular Ca^{2+} concentration ($[Ca^{2+}]_i$) is precisely maintained at around 100 nM, which is 1 / 10,000 or less of that outside the cell. However, it increases more than 10 times when a stimulus is applied from outside the cell. This is because various types of Ca^{2+} channels exist in the cell membrane and are opened by extracellular stimuli to cause extracellular Ca^{2+} influx. In addition, there are multiple types of Ca^{2+} stores inside the cell. Second messengers such as inositol triphosphates (IP_3) are generated by extracellular stimuli open Ca^{2+} channels on the Ca^{2+} store membrane and cause Ca^{2+} release. Furthermore, Ca^{2+} ATPases are present both in

the plasma membrane and Ca^{2+} store membrane, and rapidly removes intracellular Ca^{2+} to maintain the basal $[Ca^{2+}]_i$. Most types of cells possess an accurate and elaborate mechanism that keeps $[Ca^{2+}]_i$ extremely low when the cell is inactive and raises $[Ca^{2+}]_i$ for a short period when it is active. When the cell is stimulated, there are many patterns in which $[Ca^{2+}]_i$ rises sharply after stimulation and gradually decreases to the baseline. However, in some cells, the increase and decrease of $[Ca^{2+}]_i$ are repeatedly observed depending on the cell type and the stimulus condition. The phenomenon is called Ca^{2+} oscillations. There are two types of Ca^{2+} oscillations, namely, “store oscillations” caused by Ca^{2+} release from Ca^{2+} stores and “membrane oscillations” caused by Ca^{2+} influx from the extracellular space. The former is often found in non-excitatory cells, and the latter is found in certain excitatory cells. Ca^{2+} oscillations have been reported in leukocytes (Jaconi et al., 1988), exocrine gland cells (Petersen et al., 1991), smooth muscle cells (Savineau and Marthan, 2000), hepatocytes (Rooney et al., 1991), mammalian eggs (Miyazaki et al., 1993), and pituitary endocrine cells (Shibuya et al., 1997). It has been suggested that it is involved in various physiological mechanisms such as release of hormones and digestive enzymes, immunity, and gene expression. In neurons, it has been reported in striatum (Song et al., 2016; Tamura et al., 2014) and SON neurons (Shibuya et al., 1998; Kortus et al., 2016). For SFO neurons, Gebke et al. have already reported that a very high concentration (100 nM) of AII caused Ca^{2+} oscillations in about 3% of SFO neurons (Gebke et al., 1998). However, whether or not Ca^{2+} oscillation occurs in SFO neurons in physiological conditions and the mechanism of the AII-induced Ca^{2+} oscillation is still unclear.

Moreover, Ca^{2+} oscillations have been observed without any stimulus in certain types of cells (Busik et al., 1996; Shibuya et al., 1997) Kortus et al., x2016). Whether or not

such spontaneous Ca^{2+} oscillations can be seen in SFO neurons is not known.

3. Angiotensin II in the SFO

AII is an octapeptide produced in the circulating blood by the renin-angiotensin pathway that regulates body fluid homeostasis as well as circulatory and renal functions. Promotion of aldosterone secretion from the adrenal cortex and vasoconstriction are well known as direct effects of AII. However, it also has a potent effect on the central nervous system (Uijl et al., 2018). AII cannot pass through BBB (Harding et al., 1988). It is reported that AII receptors are expressed at a high density in SFO neurons (Mendelsohn et al., 1984) and SFO neurons are activated by AII (Okuya et al., 1987a). It is widely accepted that the activation of SFO is responsible for the drinking behavior induced by AII and the promotion of AVP secretion (Phillips and Sumners, 1998). Itwas reported that mechanical distraction of SFO abolished drinking behaviors induced by intravenous administration of AII to rats (Simpson et al., 1978). There are also reports that SFO send excitatory projections to PVN and SON, which release AVP into the systemic circulation (Li and Ferguson, 1993b). In addition, many electrophysiological studies with SFO slices and isolated SFO cells have also demonstrated that AII directly activates SFO neurons (Cancelliere and Ferguson, 2017; Felix and Akert, 1974; Gutman et al., 1988; Li and Ferguson, 1993a; Okuya et al., 1987b; Ono et al., 2005; Schmid and Simon, 1992; Tanaka et al., 1987).

It was reported that two types of AII receptors, AT1 and AT2 receptors, are expressed in the SFO (Premer et al., 2013). Mice in which the AT1 receptor gene is genetically disrupted show significantly reduced AII-evoked drinking behavior (Li et al., 2003). It has also been reported that administration of losartan, a selective antagonist

of the AT1 receptor, attenuated the response of SFO to AII (Beresford and Fitzsimons, 1992; Weisinger et al., 1997). From these results, it has been suggested that the AT receptor responsible for the excitatory effects in the SFO is the AT1 receptor subclass.

AII also plays a pivotal role in the development of cardiovascular disease, including hypertension (Kobori et al., 2007). Inhibitors of angiotensin converting enzyme (ACE) and blockers of the AII receptor are the first-choice drugs for the chronic hypertension. When the SFO receives AII, the blood pressure rises by inducing drinking behaviors increasing AVP release and the sympathetic activity via PVN. Therefore, it is highly possible that the SFO is involved in the pathological mechanism of hypertension (Hendel and Collister, 2005). In fact, treatment of the SFO with reactive oxygen species or agents causing endoplasmic reticulum stress enhanced the sympathetic stimulating effect of AII, leading to chronic hypertension (Campese et al., 2005; Young et al., 2012; Zimmerman et al., 2004). In addition, it has been reported that the presence of inflammatory substances enhanced the sensitivity of SFO to AII (Simpson and Ferguson, 2017; Simpson and Ferguson, 2018). In recent years, studies investigating the role of AII in the SFO during the progress of hypertension are currently attracting attention.

4. γ -amino butyric acid (GABA)

GABA is one of the most important inhibitory neurotransmitters in the central nervous system (CNS) and it is widely distributed throughout the CNS. GABA activates two kinds of GABA receptor subtypes, the $GABA_A$ and the $GABA_B$ receptors. The $GABA_A$ receptor is known to be ligand-gated Cl^- channels located in the plasma membrane. On the other hand, the $GABA_B$ receptor is a G protein-coupled receptor,

activation of which causes a decrease in the intracellular cAMP concentration, opening of inwardly rectifying K^+ (IRK) channels, and inhibition of voltage-gated Ca^{2+} channels (Misgeld, Bijak and Jarolimek, 1995; Bettler et al. ,2004). Studies using immunohistochemistry have reported the presence of $GABA_A$ receptors on the cell membrane of SFO neurons (Weindl et al., 1992). *In vivo* studies using rats also reported that administration of GABA to the intracerebroventricular space suppresses the effects of AII such as increasing water intake and increasing blood pressure (Abe et al.,1988). In addition, studies of extracellular recordings reported that GABA suppresses the spontaneous electrical activity of SFO neurons, mainly via $GABA_A$ receptors (Inenaga et al., 1995). In general, GABA is a dominant neurotransmitter generating inhibitory postsynaptic potentials (IPSPs) in CNS neurons. It is reported that IPSPs recorded in slice preparations of SFO is due to the action of GABA mediated by $GABA_A$ receptors (Honda et al. 2001). These results suggest that GABA plays a critical role in the inhibitory regulation of the spontaneous activity of SFO neurons. However, whether or not GABA can suppress the activity of SFO neurons evoked by AII or other stimulatory ligands.

5. About my study during the graduate course

To investigate the function of SFO neurons and to identify molecules that affect the activity of SFO neurons *in vivo* and *in vitro*, several electrophysiological studies using cultured neurons and brain slices have been reported so far (Cancelliere and Ferguson, 2017; Felix and Akert, 1974; Gutman et al., 1988; Li and Ferguson, 1993a; Okuya et al., 1987b; Ono et al., 2005; Schmid and Simon, 1992; Tanaka et al., 1987). On the other hand, there are only a few studies using Ca^{2+} Imaging techniques in cultured SFO

neurons (Gebke et al., 1998; Jurzak et al., 1995), and there is no report using Ca^{2+} Imaging with acutely dissociated SFO neurons as this study. Since acutely dissociated SFO neurons which are superfused at a rapid rate have little or no influence from surrounding cells, direct effects of various agents on SFO neurons can be investigated. In this study, I investigated the basic $[Ca^{2+}]_i$ behavior of SFO neurons using acutely dissociated preparations of SFO neurons. Furthermore, I studied the properties and mechanisms of the $[Ca^{2+}]_i$ increase induced by AII and the $[Ca^{2+}]_i$ decrease by GABA. This thesis consists of chapters 1: **The cytosolic Ca^{2+} concentration in acutely dissociated subfornical organ (SFO) neurons of rats: spontaneous Ca^{2+} oscillations and Ca^{2+} oscillations induced by picomolar concentrations of angiotensin II,** 2: **Persistent cytosolic Ca^{2+} increase induced by angiotensin II at nanomolar concentrations in acutely dissociated subfornical organ (SFO) neurons of rats, and** 3: **Mechanisms of GABA-mediated inhibition of the angiotensin II-induced cytosolic Ca^{2+} increase in rat subfornical organ neurons.** Chapter 1 describes 1) discrimination between neurons and glia present in SFO, 2) basic $[Ca^{2+}]_i$ response to various physiologically relevant ligands, 3) spontaneous Ca^{2+} oscillations, and 4) induction and enhancement of Ca^{2+} oscillations by low concentrations of AII. Chapter 2 describes 1) the persistent $[Ca^{2+}]_i$ increase induced by high concentrations of AII and 2) the mechanism of AII-induced persistent $[Ca^{2+}]_i$ increase. Chapter 3 describes 1) the effects of the inhibitory transmitters on the AII-induced persistent $[Ca^{2+}]_i$ increase and 2) the mechanism of inhibition by GABA.

References

Anthes, N., Schmid, H.A., Hashimoto, M., Riediger, T., Simon, E., 1997. Heterogeneous actions of vasopressin on ANG II-sensitive neurons in the subfornical organ of rats. Am J Physiol. 273**,** R2105-11.

Beresford, M.J., Fitzsimons, J.T., 1992. Intracerebroventricular angiotensin II-induced thirst and sodium appetite in rat are blocked by the AT_1 receptor antagonist, Losartan (DuP 753), but not by the AT_2 antagonist, CGP 42112B. Exp Physiol. 77**,** 761-4.

Berridge, M.J., 1990. Calcium oscillations. J Biol Chem. 265**,** 9583-6.

Berridge, M.J., Bootman, M.D., Lipp, P., 1998. Calcium - a life and death signal. Nature. 395**,** 645-648.

Campese, V.M., Shaohua, Y., Huiquin, Z., 2005. Oxidative stress mediates angiotensin II-dependent stimulation of sympathetic nerve activity. Hypertension. 46**,** 533-9.

Cancelliere, N.M., Ferguson, A.V., 2017. Subfornical organ neurons integrate cardiovascular and metabolic signals. Am J Physiol Regul Integr Comp Physiol. 312**,** R253-r262.

Cottrell, G.T., Ferguson, A.V., 2004. Sensory circumventricular organs: central roles in integrated autonomic regulation. Regul. Pept. 117**,** 11-23.

Dellmann, H.D., 1998b. Structure of the subfornical organ: a review. Microsc Res Tech. 41**,** 85-97.

Felix, D., Akert, K., 1974. The effect of angiotensin II on neurones of the cat subfornical organ. Brain Res. 76**,** 350-3.

Ferguson, A.V., Day, T.A., Renaud, L.P., 1984. Subfornical organ stimulation excites paraventricular neurons projecting to dorsal medulla. Am J Physiol. 247**,** R1088-

92.

Ferguson, A.V., Renaud, L.P., 1984. Hypothalamic paraventricular nucleus lesions decrease pressor responses to subfornical organ stimulation. Brain Res. 305**,** 361-4.

Ferguson, A.V., Kasting, N.W., 1986. Electrical stimulation in subfornical organ increases plasma vasopressin concentrations in the conscious rat. Am J Physiol. 251**,** R425-8.

Ferguson, A.V., Donevan, S.D., Papas, S., Smith, P.M., 1990. Circumventricular structures: CNS sensors of circulating peptides and autonomic control centres. Endocrinol Exp. 24**,** 19-27.

Ferguson, A.V., Li, Z., 1996. Whole cell patch recordings from forebrain slices demonstrate angiotensin II inhibits potassium currents in subfornical organ neurons. Regul Pept. 66**,** 55-8.

Fitzsimons, J.T., 1998. Angiotensin, thirst, and sodium appetite. Physiol. Rev. 78**,** 583-686.

Gebke, E., Muller, A.R., Jurzak, M., Gerstberger, R., 1998. Angiotensin II-induced calcium signalling in neurons and astrocytes of rat circumventricular organs. Neuroscience. 85**,** 509-520.

Gross, P.M., 1992. Circumventricular organ capillaries. *Prog Brain Res*. 91**,** 219-233.

Gutman, M.B., Ciriello, J., Mogenson, G.J., 1985. Effect of paraventricular nucleus lesions on cardiovascular responses elicited by stimulation of the subfornical organ in the rat. Can J Physiol Pharmacol. 63**,** 816-24.

Gutman, M.B., Ciriello, J., Mogenson, G.J., 1988. Effects of plasma angiotensin-ii and hypernatremia on subfornical organ neurons. Am J Physiol. 254**,** R746-R754.

Harding, J.W., Sullivan, M.J., Hanesworth, J.M., Cushing, L.L., Wright, J.W., 1988. Inability of [^{125}I]Sar^{1}, Ile8-angiotensin II to move between the blood and cerebrospinal fluid compartments. J Neurochem. 50**,** 554-7.

Hendel, M.D., Collister, J.P., 2005. Contribution of the subfornical organ to angiotensin II-induced hypertension. Am J Physiol Heart Circ Physiol. 288**,** H680-5.

Hiyama, T.Y., Noda, M., 2016. Sodium sensing in the subfornical organ and body-fluid homeostasis. Neurosci Res. 113**,** 1-11.

Iino, M., 2007. Regulation of cell functions by Ca^{2+} oscillation. Adv Exp Med Biol. 592**,** 305-12.

Jaconi, M.E., Rivest, R.W., Schlegel, W., Wollheim, C.B., Pittet, D., Lew, P.D., 1988. Spontaneous and chemoattractant-induced oscillations of cytosolic free calcium in single adherent human neutrophils. J Biol Chem. 263**,** 10557-60.

Johnson, A.K., Gross, P.M., 1993. Sensory circumventricular organs and brain homeostatic pathways. Faseb J. 7**,** 678-686.

Jurzak, M., Muller, A.R., Gerstberger, R., 1995. Characterization of vasopressin receptors in cultured-cells derived from the region of rat-brain circumventricular organs. Neuroscience. 65**,** 1145-1159.

Kobori, H., Nangaku, M., Navar, L.G., Nishiyama, A., 2007. The intrarenal renin-angiotensin system: from physiology to the pathobiology of hypertension and kidney disease. Pharmacol Rev. 59**,** 251-87.

Kortus, S., Srinivasan, C., Forostyak, O., Ueta, Y., Sykova, E., Chvatal, A., Zapotocky, M., Verkhratsky, A., Dayanithi, G., 2016. Physiology of spontaneous $[Ca^{2+}]_i$ oscillations in the isolated vasopressin and oxytocin neurones of the rat supraoptic nucleus. Cell Calcium. 59**,** 280-8.

Li, Z., Ferguson, A.V., 1993a. Angiotensin-ii responsiveness of rat paraventricular and subfornical organ neurons in-vitro. Neuroscience. 55**,** 197-207.

Li, Z., Ferguson, A.V., 1993b. Subfornical organ efferents to paraventricular nucleus utilize angiotensin as a neurotransmitter. Am J Physiol. 265**,** R302-9.

Li, Z., Iwai, M., Wu, L., Shiuchi, T., Jinno, T., Cui, T.X., Horiuchi, M., 2003. Role of AT2 receptor in the brain in regulation of blood pressure and water intake. Am J Physiol Heart Circ Physiol. 284**,** H116-21.

McKinley, M.J., Allen, A.M., Burns, P., Colvill, L.M., Oldfield, B.J., 1998. Interaction of circulating hormones with the brain: The roles of the subfornical organ and the organum vasculosum of the lamina terminalis. Clin. Exp. Pharmacol. Physiol. 25**,** S61-S67.

Mendelsohn, F.A., Quirion, R., Saavedra, J.M., Aguilera, G., Catt, K.J., 1984. Autoradiographic localization of angiotensin II receptors in rat brain. Proc Natl Acad Sci U S A. 81**,** 1575-9.

Mimee, A., Smith, P.M., Ferguson, A.V., 2013. Circumventricular organs: Targets for integration of circulating fluid and energy balance signals? Physiol. Behav. 121**,** 96-102.

Miyazaki, S., Shirakawa, H., Nakada, K., Honda, Y., 1993. Essential role of the inositol 1,4,5-trisphosphate receptor/Ca^{2+} release channel in Ca^{2+} waves and Ca^{2+} oscillations at fertilization of mammalian eggs. Dev Biol. 158**,** 62-78.

Okuya, S., Inenaga, K., Kaneko, T., Yamashita, H., 1987a. Angiotensin II sensitive neurons in the supraoptic nucleus, subfornical organ and anteroventral third ventricle of rats in vitro. Brain Res. 402**,** 58-67.

Okuya, S., Inenaga, K., Kaneko, T., Yamashita, H., 1987b. Angiotensin II sensitive

neurons in the supraoptic nucleus, subfornical organ and anteroventral third ventricle of rats in vitro. Brain Res. 402**,** 58-67.

Ono, K., Toyono, T., Honda, E., Inenaga, K., 2005. Transient outward K^+ currents in rat dissociated subfornical organ neurones and angiotensin II effects. J Physiol. 568**,** 979-91.

Petersen, C.C., Toescu, E.C., Petersen, O.H., 1991. Different patterns of receptor-activated cytoplasmic Ca^{2+} oscillations in single pancreatic acinar cells: dependence on receptor type, agonist concentration and intracellular Ca^{2+} buffering. Embo j. 10**,** 527-33.

Phillips, M.I., Sumners, C., 1998. Angiotensin II in central nervous system physiology. Regul Pept. 78**,** 1-11.

Premer, C., Lamondin, C., Mitzey, A., Speth, R.C., Brownfield, M.S., 2013. Immunohistochemical Localization of AT_{1a}, AT_{1b}, and AT2 Angiotensin II Receptor Subtypes in the Rat Adrenal, Pituitary, and Brain with a Perspective Commentary. Int J Hypertens. 2013**,** 175428.

Rooney, T.A., Renard, D.C., Sass, E.J., Thomas, A.P., 1991. Oscillatory cytosolic calcium waves independent of stimulated inositol 1,4,5-trisphosphate formation in hepatocytes. J Biol Chem. 266**,** 12272-82.

Savineau, J.P., Marthan, R., 2000. Cytosolic Calcium Oscillations in Smooth Muscle Cells. News Physiol Sci. 15**,** 50-55.

Schmid, H.A., Simon, E., 1992. Effect of angiotensin II and atrial natriuretic factor on neurons in the subfornical organ of ducks and rats in vitro. Brain Res. 588**,** 324-8.

Shibuya, I., Kongsamut, S., Douglas, W.W., 1997. Both $GABA_A$ and $GABA_B$ receptors participate in suppression of $[Ca^{2+}]_i$ pulsing in toad melanotrophs. Eur J Pharmacol.

321, 241-6.

Simpson, J.B., Epstein, A.N., Camardo, J.S., 1978. Localization of receptors for the dipsogenic action of angiotensin II in the subfornical organ of rat. J Comp Physiol Psychol. 92, 581-601.

Simpson, N.J., Ferguson, A.V., 2017. The proinflammatory cytokine tumor necrosis factor-alpha excites subfornical organ neurons. J Neurophysiol. 118, 1532-1541.

Simpson, N.J., Ferguson, A.V., 2018. Tumor necrosis factor α potentiates the effects of angiotensin II on subfornical organ neurons. Am J Physiol Regul Integr Comp Physiol.

Smith, P.M., Ferguson, A.V., 2010. Circulating signals as critical regulators of autonomic state-central roles for the subfornical organ. Am. J. Physiol. Regul. Integr. Comp. Physiol. 299, R405-R415.

Song, S.C., Beatty, J.A., Wilson, C.J., 2016. The ionic mechanism of membrane potential oscillations and membrane resonance in striatal LTS interneurons. J Neurophysiol. 116, 1752-1764.

Tamura, A., Yamada, N., Yaguchi, Y., Machida, Y., Mori, I., Osanai, M., 2014. Both neurons and astrocytes exhibited tetrodotoxin-resistant metabotropic glutamate receptor-dependent spontaneous slow Ca^{2+} oscillations in striatum. PLoS One. 9, e85351.

Tanaka, J., Saito, H., Kaba, H., 1987. Subfornical organ and hypothalamic paraventricular nucleus connections with median preoptic nucleus neurons - an electrophysiological study in the rat. Exp. Brain Res. 68, 579-585.

Uijl, E., Ren, L., Danser, A.H.J., 2018. Angiotensin generation in the brain: a re-evaluation. Clin Sci (Lond). 132, 839-850.

Weisinger, R.S., Blair-West, J.R., Burns, P., Denton, D.A., Tarjan, E., 1997. Role of brain angiotensin in thirst and sodium appetite of rats. Peptides. 18**,** 977-84.

Young, C.N., Cao, X., Guruju, M.R., Pierce, J.P., Morgan, D.A., Wang, G., Iadecola, C., Mark, A.L., Davisson, R.L., 2012. ER stress in the brain subfornical organ mediates angiotensin-dependent hypertension. J Clin Invest. 122**,** 3960-4.

Yu, Y., Wei, S.G., Weiss, R.M., Felder, R.B., 2018. Angiotensin II Type la Receptors in the Subfornical Organ Modulate Neuroinflammation in the Hypothalamic Paraventricular Nucleus in Heart Failure Rats. Neuroscience. 381**,** 46-58.

Zimmerman, M.C., Lazartigues, E., Sharma, R.V., Davisson, R.L., 2004. Hypertension caused by angiotensin II infusion involves increased superoxide production in the central nervous system. Circ Res. 95**,** 210-6.

Chapter 1

The cytosolic Ca^{2+} concentration in acutely dissociated subfornical organ (SFO) neurons of rats: spontaneous Ca^{2+} oscillations and Ca^{2+} oscillations induced by picomolar concentrations of angiotensin II

Highlights

1. $[Ca^{2+}]_i$ of SFO neurons were examined in acutely dissociated neurons of rats
2. SFO neurons but not glial cells exhibited spontaneous Ca^{2+} oscillations
3. Ca^{2+} oscillations were arrested by the Ca^{2+}-free condition and inhibited by nicardipine
4. Angiotensin II at picomolar concentrations evoked Ca^{2+} oscillations in silent cells
5. The primary inhibitory transmitter, GABA, arrested spontaneous Ca^{2+} oscillations

Abstract

Characteristics of subfornical organ (SFO) neurons were examined by measuring the cytosolic Ca^{2+} concentration ($[Ca^{2+}]_i$) in acutely dissociated neurons of the rat. SFO neurons, defined by the responsiveness to 50 mM K^+ (n = 67) responded to glutamate (86%), angiotensin II (AII) (50%), arginine vasopressin (AVP) (66%) and/or carbachol (CCh) (61%), at their maximal concentrations, with marked increases in $[Ca^{2+}]_i$. More than a half (174/307) of SFO neurons examined exhibited spontaneous Ca^{2+} oscillations, while the remainder showed a relatively stable baseline under unstimulated conditions. Spontaneous Ca^{2+} oscillations were suppressed when extracellular Ca^{2+} was removed and were inhibited when extracellular Na^+ was replaced with equimolar N-methyl-D-glucamine. Ca^{2+} oscillations were unaffected by the inhibitor of Ca^{2+}-dependent ATPases cyclopiazonic acid, the N-type Ca^{2+} channel blocker ω-conotoxin GVIA and the P/Q-type Ca^{2+} channel blocker ω-agatoxin IVA, but significantly inhibited by the high-voltage-activated Ca^{2+} channel blocker Cd^{2+} and the L-type Ca^{2+} channel blocker nicardipine. Ca^{2+} oscillations were also completely arrested by the voltage-gated Na^+ channel blocker tetrodotoxin in 50 % of SFO neurons but only partially in the remaining neurons. These results suggest that SFO neurons exhibit spontaneous membrane Ca^{2+} oscillations that are dependent in part on Ca^{2+} entry through L-type Ca^{2+} channels, whose activation may result from burst firing. Moreover, AII at picomolar concentrations induced Ca^{2+} oscillations in neurons showing no spontaneous Ca^{2+} oscillations, while spontaneous Ca^{2+} oscillations were arrested by gamma-aminobutyric acid (10 μM), suggesting that rises in $[Ca^{2+}]_i$ during Ca^{2+} oscillations may play an important role in the modulation of SFO neuron function.

1. Introduction

The subfornical organ (SFO) is a circumventricular organ located at the top of the dorsal third ventricle (Dellmann and Linner, 1979; Johnson and Gross, 1993; Mimee et al., 2013). While the SFO is within the central nervous system (CNS), an interesting functional characteristic of this central structure is its lack of a normal blood-brain barrier due to fenestrated capillaries, allowing it to interact directly with blood-borne molecules (Cottrell and Ferguson, 2004; Gross, 1992; McKinley et al., 1998; Smith and Ferguson, 2010). In addition, the SFO contains neuronal cell bodies with efferent projections to other brain regions, such as the hypothalamic paraventricular and supraoptic nuclei, the medulla oblongata, and the spinal cord (Dellmann, 1998). Considering these anatomical properties, the SFO appears to play a key role in the transmission of information from the periphery circulation to the CNS. Indeed, the SFO serves as a target of circulatory molecules involved in body fluid homeostasis, including water, salt, and food intake, and in immune responses (Cottrell and Ferguson, 2004; Fitzsimons, 1998; Simpson and Ferguson, 2017; Simpson and Ferguson, 2018; Yu et al., 2018). One of the best-characterized functions of the SFO is an increase in water intake in response to blood-borne angiotensin II (AII) (Fitzsimons, 1998). Although many studies have been performed to examine the function of the SFO and to identify molecules that affect the activity of SFO neurons *in vivo* and/or *in vitro* using techniques for electrophysiology to address intracellular signaling mechanisms of these neurons at the single-cell level (Okuya et al., 1987), few have examined SFO neuronal characteristics using Ca^{2+} measurements in individual SFO neurons (Gebke et al., 1998; Jurzak et al., 1995a).

Ca^{2+} is one of the most common intracellular signals in neurons and mediates variety

of important neuronal cell functions, such as neurotransmitter release, synaptic plasticity, gene expression and cell survival (Augustine et al., 2003). Some agonists, including AII, increase the intracellular Ca^{2+} concentration ($[Ca^{2+}]_i$) in dissociated and cultured SFO neurons (Gebke et al., 1998; Johnson et al., 2001; Jurzak et al., 1995b; Pulman et al., 2006; Simpson and Ferguson, 2018), suggesting that these agonists activate Ca^{2+}-dependent neuronal cell mechanisms as well as modulate neural activity (Ferguson and Bains, 1996). Although these previous studies have used primary cultures of SFO neurons and have provided important information about the responsiveness of SFO neurons to various physiological ligands, there are inconsistencies between the results of these studies and those obtained from electrophysiology performed *in vivo* and/or *in vitro* (Felix and Akert, 1974; Gebke et al., 1998; Johnson et al., 2001). For example, the response rates of cultured SFO neurons to physiological ligands such as AII range from a few percent to approximately 20 % (Gebke et al., 1998; Johnson et al., 2001), which is much lower than that reported by electrophysiological studies using *in vivo* preparations or brain slices (more than 50 %) (Felix and Akert, 1974; Gutman et al., 1988; Li and Ferguson, 1993; Okuya et al., 1987; Schmid and Simon, 1992; Tanaka et al., 1987). Moreover, the $[Ca^{2+}]_i$ responses to AII and other ligands are quickly desensitized (Gebke et al., 1998; Johnson et al., 2001; Jurzak et al., 1995a; Jurzak et al., 1995b), which does not match the suggested property of SFO neurons as a sensor of these ligands. These discrepancies raise the possibility that properties in SFO neurons may be altered during primary cultures. Furthermore, the precise cellular mechanisms as to how $[Ca^{2+}]_i$ is regulated in SFO neurons, such as how basal $[Ca^{2+}]_i$ is maintained and whether intracellular Ca^{2+} stores play a role, are poorly understood.

In the present study, an acutely dissociated SFO preparation was used to measure $[Ca^{2+}]_i$ and to characterize the properties of Ca^{2+} signals in SFO neurons. The results of this study indicate that in acutely dissociated SFO neurons, the response rates to physiological ligands were more than 50 %, and desensitization of $[Ca^{2+}]_i$ responses was not observed by repeated applications of the ligands. Additionally, it was observed that a considerable portion of SFO neurons exhibited spontaneous repeated elevations in $[Ca^{2+}]_i$, called Ca^{2+} oscillations, and that these Ca^{2+} oscillations could be induced by several stimuli, including picomolar concentrations of AII, identifying a new properties of the Ca^{2+} signaling mechanism of SFO neurons.

2. Results

After dissociation, two distinct types of cell populations could be seen; cells with and without dendritic-like processes (Fig. 1B-C). The diameter of the dissociated SFO cells ranged from approximately 10 to 20 μm Cells with smaller diameter tended to be round cells (Fig. 1B-b), whereas larger cells often had more than one process, although most had only one dendritic-like process (Fig. 1B-a). The immunohistochemical analysis using an antibody against the astrocyte marker GFAP confirmed that cells having one or a few dendritic-like processes did not stain for GFAP, suggesting that these cells were likely neurons. Only a very small portion of cells with no processes were GFAP positive.

2.1 Basal $[Ca^{2+}]_i$ activity and responses to various $[Ca^{2+}]_i$-increasing treatments of acutely dissociated SFO cells

To know the basic characteristics of cells acutely dissociated from SFO tissues, basal $[Ca^{2+}]_i$ activity and $[Ca^{2+}]_i$ responses to treatments that were likely to raise $[Ca^{2+}]_i$ in SFO cells was monitored. Examples of the time course of such $[Ca^{2+}]_i$ activities are shown in Fig. 2. Most SFO cells, regardless of the existance of dendrites and the cell size, responded to 50 mM K^+ with a sharp and large rise in $[Ca^{2+}]_i$ (Fig. 2A). The mean amplitude of the $[Ca^{2+}]_i$ rise above the baseline ($\Delta[Ca^{2+}]_i$) was 2454 ± 409 nM (n = 67). In this study, cells showing such responses to high K^+ were regarded as SFO neurons. The basal $[Ca^{2+}]_i$ in these cells was 136 ± 8 nM. On the other hand, some SFO cells did not show any response to high K^+ (Fig. 2B). The majority of these cells (n = 27) exhibited a marked rise in $[Ca^{2+}]_i$ in response to the P2X7 receptor agonist BzATP (100 μM; Fig. 2B). As glial cells express high levels of P2X7 receptors and exhibit a large response to BzATP (Shibuya et al., 1999), cells that showed large responses to BzATP but no

response to high K^+ were regarded as SFO glial cells in the present study (Fig. 2B). The basal $[Ca^{2+}]_i$ in these cells was 97 ± 6 nM (n = 36).

Of the 67 SFO neurons used in this series of experiments, the majority (86 %) responded to glutamate (100 μM; Fig. 2A), previously identified as a primary excitatory neurotransmitter in the SFO (Gutman et al., 1985; Osaka et al., 1992a; Schmid, 1998; Weindl et al., 1992), with a sharp and large rise in $[Ca^{2+}]_i$ (328 ± 43 nM). More than a half of SFO neurons showed a clear $[Ca^{2+}]_i$ response to arginine vasopressin (AVP) (66 %), carbachol (CCh) (61 %) and angiotensin II (AII) (50 %) when given individually at their maximally effective concentrations (AVP, 100 nM; CCh, 100 μM; AII, 100 nM) (Fig. 2A). The average $\Delta[Ca^{2+}]_i$ to the three ligands was 209 ± 55 (n = 44), 425 ± 167 (n = 41), and 283 ± 67 nM (n = 33), respectively (Fig. 2B, inset). When $[Ca^{2+}]_i$ responses to high K^+, glutamate and AII were observed twice in the same cells with an interval longer than 5 min, there was no significant difference between the amplitudes of the two responses: the amplitudes of the second responses were 96 ± 7 % (n = 11), 104 ± 12 % (n = 11) and 95 ± 19 % (n = 10), respectively, of those of the first responses.

More than a half of SFO neurons (70 %) also responded to BzATP (100 μM), but the average $\Delta[Ca^{2+}]_i$ was 182 ± 25 nM (n = 47), which was significantly smaller than that recorded from SFO glial cells (493 ± 181 nM, n = 27). A minority of glial cells showed $[Ca^{2+}]_i$ responses to glutamate, AVP, CCh and AII (Fig. 2B, insets). The largest difference in the response rate between neurons and glia was found in the responses to glutamate: only 7 % of glial cells responded to glutamate.

How individual neurons and glia responded to the multiple ligands is shown by Venn diagrams in Fig. 2C. In neurons, there was extensive overlap in the responses to AII, CCh and AVP: 96 % of the AII-responsive neurons showed responses to either CCh or AVP

or to both, and 54 % of the AII-responsive neurons showed responses to both CCh and AVP. In glial cells, there was less overlap: approximately 66 % of AII-responsive glia showed responses to either of the other two.

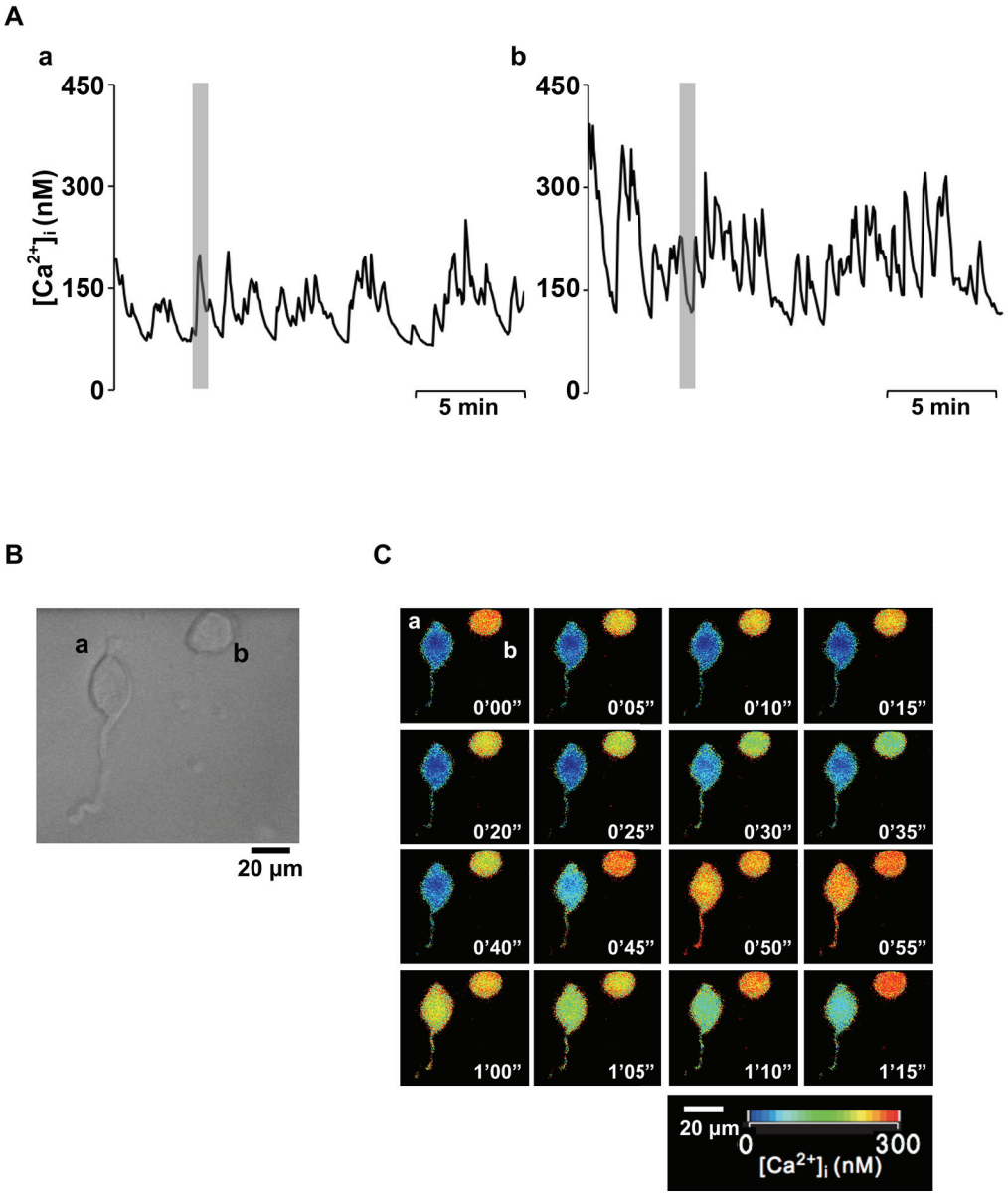

Fig. 1 Spontaneous oscillations in $[Ca^{2+}]_i$ observed in dissociated SFO neurons. **A**, time courses of spontaneous $[Ca^{2+}]_i$ oscillations obtained from cells a & b shown in B. **B**, bright-field images of the two SFO neurons that exhibited spontaneous $[Ca^{2+}]_i$ oscillations. **C**, pseudocolor images of spontaneous $[Ca^{2+}]_i$ oscillations over 75 sec shown by gray bars in A. Note that in cell 'a', $[Ca^{2+}]_i$ reached a high level throughout the entire cell, including its dendrite.

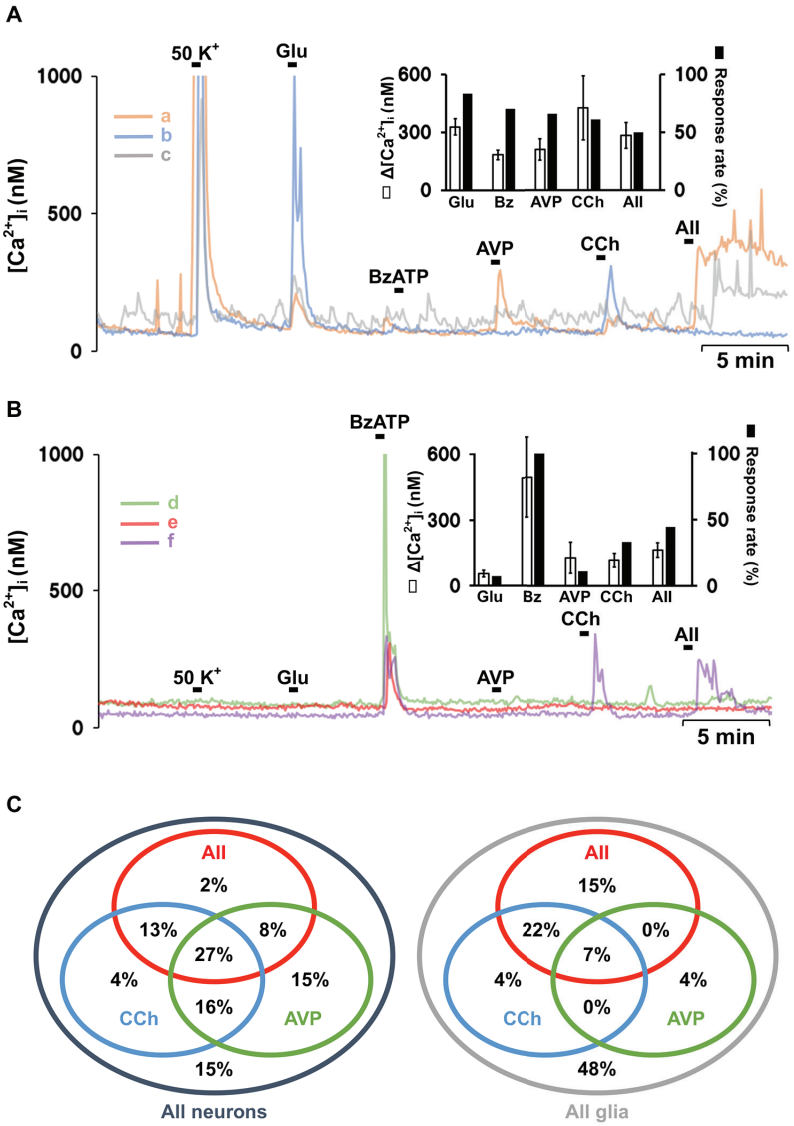

Fig. 2 Representative time courses of basal $[Ca^{2+}]_i$ and $[Ca^{2+}]_i$ responses to various treatments of acutely dissociated SFO cells. **A**, time courses of cells that exhibited a sharp and large $[Ca^{2+}]_i$ rise in response to high K^+ (50 mM K^+). Cells were treated with high K^+ (50 K^+) first and then 100 μM glutamate (Glu), 100 μM BzATP, 100 nM arginine vasopressin (AVP), 100 μM carbachol (CCh), and 100 nM angiotensin II (AII). Note that prior to any treatments, spontaneous Ca^{2+} oscillations were observed in cells a & c. **A inset**, summarized data for the amplitude (open bar) and response rate (closed bar) of the $[Ca^{2+}]_i$ responses in high-K^+-responsive cells (n = 67). **B**, time courses of cells that exhibited no $[Ca^{2+}]_i$ rise in response to high K^+ (50 mM K^+). Note that there was little or no basal $[Ca^{2+}]_i$ activity, and a sharp and large $[Ca^{2+}]_i$ rise in response to BzATP was consistently observed in these cells. **B inset**, summary data for the amplitude (open bar) and response rate (closed bar) of the $[Ca^{2+}]_i$ responses in cells that showed no $[Ca^{2+}]_i$ response to high K^+ and a marked $[Ca^{2+}]_i$ response to BzATP (n = 27). The amplitude of the $[Ca^{2+}]_i$ response was expressed by the peak $\Delta[Ca^{2+}]_i$ value (calculated by subtracting the basal $[Ca^{2+}]_i$ from the peak $[Ca^{2+}]_i$ during each treatment). **C**, Venn diagrams showing overlap of the responsiveness to the three ligands AII, CCh and AVP of individual neurons (n = 67) and glia (n = 27) of the SFO.

2.2 Spontaneous Ca^{2+} oscillations in SFO neurons

There was a clear difference in the basal $[Ca^{2+}]_i$ activity between SFO neurons and glial cells: in 174/307 (56.7 %) of neurons tested, spontaneous repeated elevations of $[Ca^{2+}]_i$ (Ca^{2+} oscillations) were observed. However, none of the glial cells examined showed such spontaneous $[Ca^{2+}]_i$. Examples of the time course of spontaneous Ca^{2+} oscillations are shown in Fig. 1A. The mean amplitude and frequency of spontaneous Ca^{2+} oscillations calculated from 37 cells showing relatively regular oscillations ranged from 31 to 313 nM (average; 93 ± 10 nM) and from 0.4 to 1.8 min^{-1} (average; 0.96 ± 0.06 min^{-1}), respectively. The frequency distribution was as follows: less frequent than 0.5 min^{-1}, 4 cells (11 %); 0.5 to less than 1.0 min^{-1}, 15 cells (40 %); 1.0 to less than 1.5 min^{-1}, 14 cells (38 %); and more frequent than 1.5 min^{-1}, 4 cells (11 %). Fig. 1C shows pseudocolored $[Ca^{2+}]_i$ images of two neighboring neurons (cell 'a' with a long dendrite like process and cell 'b' with no process emanating from the cell body) exhibiting spontaneous Ca^{2+} oscillations with distinct frequencies. At the peak of Ca^{2+} oscillations, $[Ca^{2+}]_i$ reached a high level throughout the cytosolic space, including the dendrite (Fig. 1C, cell 'a'). There was no obvious correlation between the occurrence of spontaneous Ca^{2+} oscillations and the appearance of the cell (cell size or whether it had a dendritic-like process attached).

2.3 Ca^{2+} oscillations induced by low concentrations of AII and glutamate and by modest increases in extracellular K^+

In SFO neurons not showing spontaneous Ca^{2+} oscillations (silent neurons), AII and glutamate at low concentrations (AII at as low as 1 to 100 pM and glutamate at 1 to 10 μM) induced Ca^{2+} oscillations. AII (1 to 100 pM) and glutamate (1 to 10 μM) initiated

Ca^{2+} oscillations in 32/73 and 8/12 silent neurons, respectively. Examples of such induction are shown in Fig. 3A-B and Fig. 4. Interestingly, a modest increase in the extracellular K^+ concentration from 5 mM to 8 mM also induced Ca^{2+} oscillations in 8/8 silent neurons. One such example is shown in Fig. 3C. The induced Ca^{2+} oscillations tended to persist for some time after the treatments were ceased. When AII, glutamate, or K^+ was given at a higher concentration, the $[Ca^{2+}]_i$ response became larger followed by a decreasing trend (Fig. 3A-C, insets), from which repetitive increases in $[Ca^{2+}]_i$ occasionally arose.

2.4 Concentration dependency of AII-induced Ca^{2+} oscillations

A more detailed concentration-response relation of the AII-induced $[Ca^{2+}]_i$ increase was examined with AII at concentrations ranging from 1 pM to 100 nM. Of 21 AII-responsive neurons examined in this series of experiments, 11 were silent and 10 were spontaneously oscillating. In the 11 silent neurons, Ca^{2+} oscillation was initiated in 8 neurons by AII (1 pM) and in 3 neurons by AII (3 pM). As shown in Fig. 4A, in cell 'a', where basal $[Ca^{2+}]_i$ was stable at the beginning, application of AII (1 pM) induced Ca^{2+} oscillations, and the amplitude and frequency of Ca^{2+} oscillations increased as AII concentration increased. Another neuron in Fig. 4A, cell 'b', showing spontaneous Ca^{2+} oscillations also responded to the increasing concentrations of AII with increased amplitude and frequency of Ca^{2+} oscillations. In all of the 21 neurons examined, the pattern of the response to AII at the low concentrations was Ca^{2+} oscillations, but not a large $[Ca^{2+}]_i$ peak followed by a sustained plateau as seen in the response to AII (100 nM) in Fig. 2A. The concentration dependency of AII-induced increases in the amplitude and frequency of Ca^{2+} oscillations was analyzed in each group (Fig. 4B and C). In both types

of neurons, the amplitude and the frequency of Ca^{2+} oscillations increased in response to increasing concentrations of AII. The frequency increase was most evident at the higher AII concentration range; statistical significance was confirmed in the frequency increase in response to the AII concentration increase from 10 pM to 30 pM and from 30 pM to 100 pM (Fig. 4B and C). In silent neurons, the amplitude and frequency of Ca^{2+} oscillation during stimulation by AII at 100 pM were 393 ± 75 nM and 2.1 ± 0.2 min^{-1} (n = 11), respectively, were similar to the values in spontaneously oscillating neurons (amplitude, 381 ± 173 nM; frequency, 2.1 ± 0.3 min^{-1}, n = 10). Thus, the amplitude and frequency of Ca^{2+} oscillations during stimulation by AII at 100 pM were approximately 3.0- and 2.5-fold higher, respectively, than the values of spontaneous oscillations.

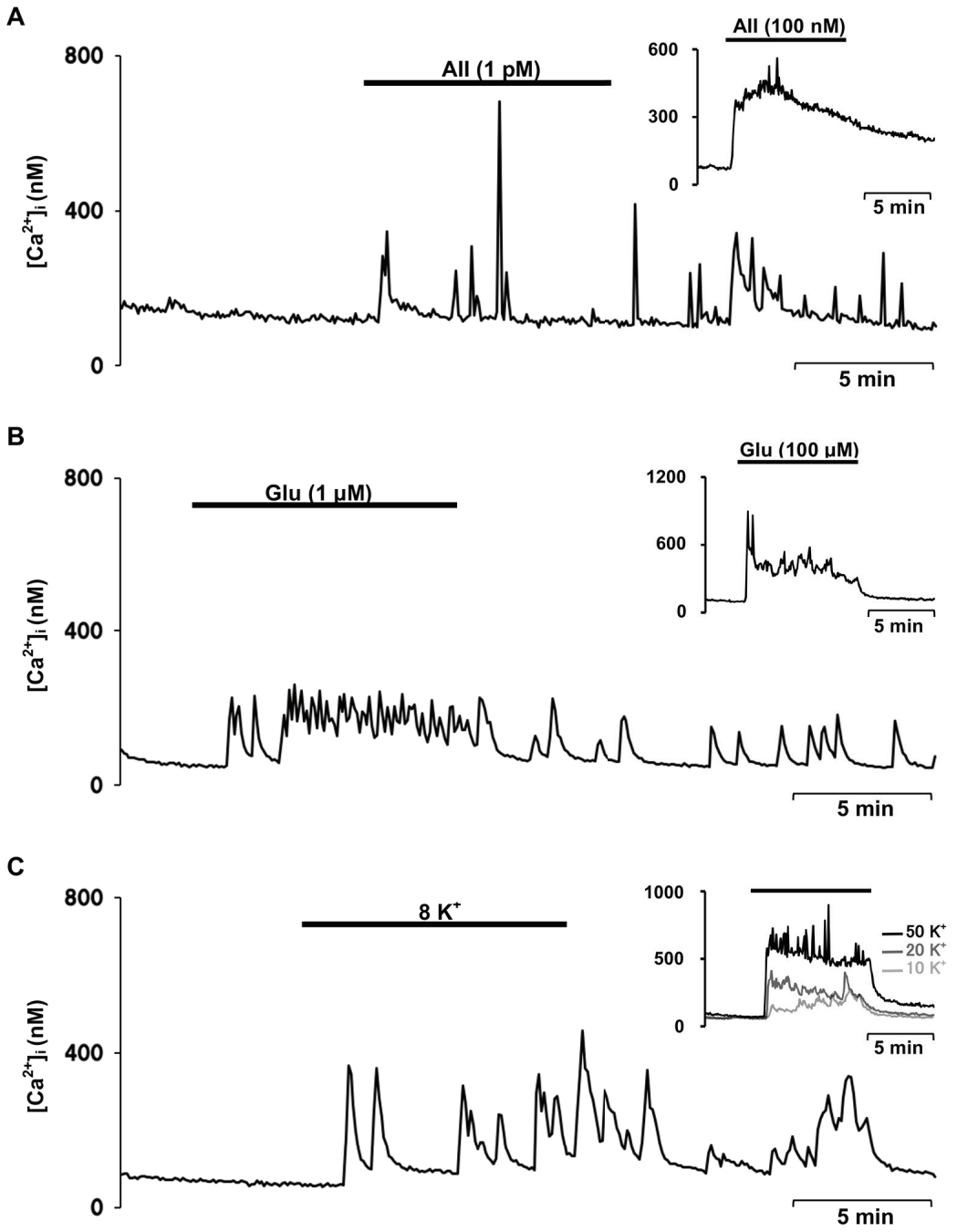

Fig. 3 Induction of Ca^{2+} oscillations in silent SFO neurons. Ca^{2+} oscillations were induced by a very low concentration (1 pM) of AII (**A**), 1 µM glutamate (**B**), and 8 mM K^+ (**C**). At higher concentrations, AII (100 nM), glutamate (100 µM) and K^+ (10, 20 and 50 mM) caused a larger $[Ca^{2+}]_i$ peak followed by a declining plateau phase (A-C, inset).

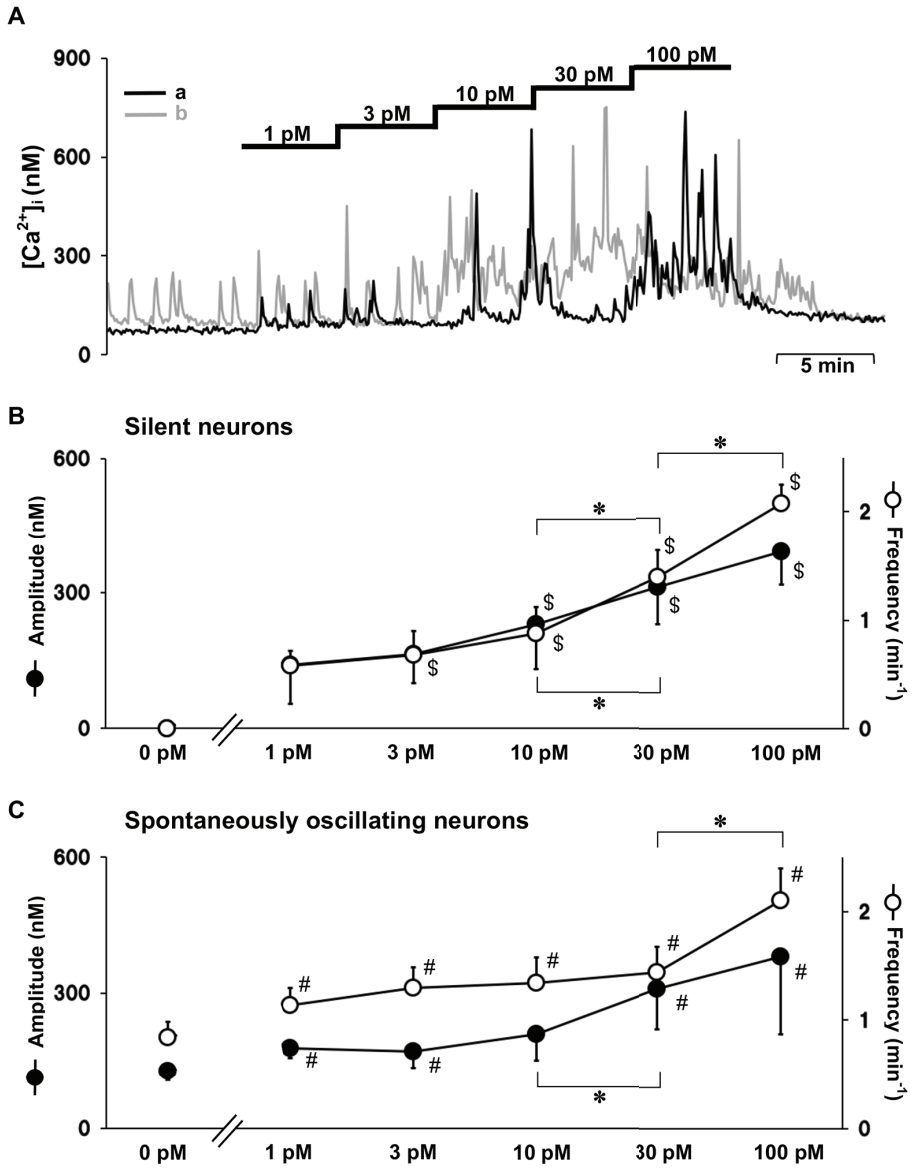

Fig. 4 Concentration-response analysis of AII-induced Ca^{2+} oscillations. **A**, representative Ca^{2+} traces showing concentration-dependent increases in the amplitude and frequency of Ca^{2+} oscillations. The lines (a & b) represent records obtained from a silent cell and a spontaneously oscillating cell, respectively. The concentration of AII was increased from 1 to 100 pM in a stepwise manner, as indicated. **B**, concentration-dependent increases in the amplitude and frequency of Ca^{2+} oscillations in silent cells (n = 11). **C**, concentration-dependent increases in the amplitude and frequency of Ca^{2+} oscillations in spontaneously oscillating cells (n = 10). $ represents statistical significance ($p < 0.05$) between the amplitude and frequency of Ca^{2+} oscillations induced by AII at 1 pM and those in the presence of various concentrations of AII. The asterisks represent statistical significance between the values indicated with the lines ($p<0.05$). # represents statistical significance ($p < 0.05$) between the amplitude and frequency of spontaneous Ca^{2+} oscillations and those in the presence of various concentrations of AII.

2.5 Mechanisms of Ca^{2+} oscillations

The mechanism of Ca^{2+} oscillations was studied by changing extracellular Ca^{2+} and Na^{+} concentrations, by applying a blocker of voltage-gated Na^{+} channels, and by applying a selective inhibitor of sarco/endoplasmic reticulum Ca^{2+} ATPase (SERCA), cyclopiazonic acid (CPA) to the SFO cells. CPA consistently evoked a transient rise in $[Ca^{2+}]_i$ (84 ± 48 nM, n = 21), indicating that SFO neurons possess intracellular Ca^{2+} stores in the somatodendritic region. However, CPA did not apparently affect the amplitude and frequency of spontaneous Ca^{2+} oscillations (Fig. 5A). Moreover, CPA did not affect Ca^{2+} oscillations enhanced by AII (n = 21). One such example is shown in Fig. 5A cell 'a'.

Spontaneous Ca^{2+} oscillations were arrested by removal of extracellular Ca^{2+} and strongly inhibited by replacement of extracellular Na^{+} with NMDG (Fig. 5B). The effects of the blocker of voltage-gated Na^{+} channels (VGSCs) tetrodotoxin (TTX, 1 μM) on Ca^{2+} oscillations were examined in 26 neurons. The patterns of the effects of TTX could be classified into two groups: (a) in 13 neurons Ca^{2+} oscillations were virtually arrested, and (b) in the other 13 neurons the amplitude and frequency of Ca^{2+} oscillations were decreased, but oscillations persisted in the presence of TTX. Two representative examples of the TTX effects are shown in Fig. 5C. Such relative TTX resistance was unlikely to be due to incomplete block of VGSCs, as in most of the group b neurons (n = 8), Ca^{2+} oscillations persisted even when the TTX concentration was increased from 1 to 5 μM. The inhibitory effects on spontaneous Ca^{2+} oscillations as well as on AII-enhanced Ca^{2+} oscillations observed in the three treatments are summarized in Fig. 5D-E. The effects in Fig 5D-E are expressed as average $\Delta[Ca^{2+}]_i$ during each treatment normalized by the control value obtained just before the treatment. Not only Ca^{2+} free and Na^{+} free, but also TTX significantly inhibited spontaneous Ca^{2+} oscillations and Ca^{2+} oscillations

enhanced by AII.

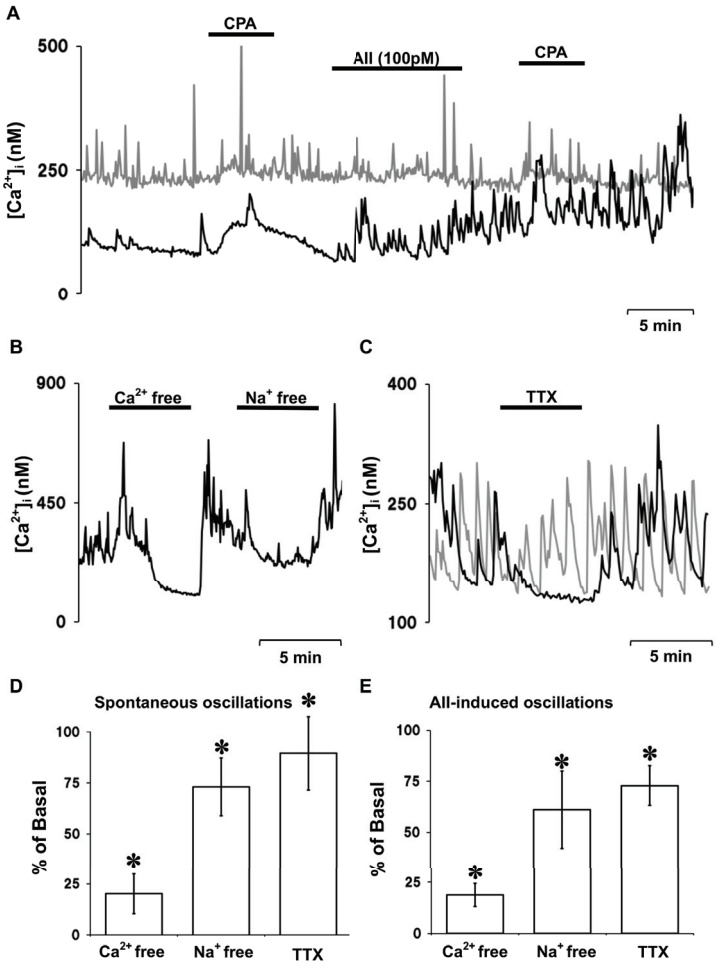

Fig. 5 Effects of a Ca^{2+}-ATPase inhibitor, a voltage-gated Na^+ channel blocker, extracellular Ca^{2+} free, and extracellular Na^+ free on spontaneous Ca^{2+} oscillations. **A**, two examples showing that spontaneous Ca^{2+} oscillations persisted after application of the inhibitor of the Ca^{2+}-dependent ATPase cyclopiazonic acid (CPA at 10 μM). In both cells, CPA caused a transient Ca^{2+} increase without obviously affecting Ca^{2+} oscillations. In cell 'a', Ca^{2+} oscillations enhanced by AII (100 pM) also persisted upon CPA application. **B**, spontaneous Ca^{2+} oscillations were arrested when extracellular Ca^{2+} was omitted and strongly inhibited when extracellular Na^+ was replaced with NMDG. **C**, spontaneous Ca^{2+} oscillations were either arrested (a) or only partially inhibited (b) by TTX (1 μM). **D**, summary data for the effects of Ca^{2+} free, Na^+ free, and TTX on spontaneous Ca^{2+} oscillations. The effects are expressed by the average $\Delta[Ca^{2+}]_i$ value (calculated by subtracting the basal $[Ca^{2+}]_i$ from the $[Ca^{2+}]_i$ averaged for 3 min at the end of each treatment) normalized by the $\Delta[Ca^{2+}]_i$ value obtained just before each treatment. The total number of neurons analyzed was 23 (Ca^{2+} free), 8 (Na^+ free), and 37 (TTX). The asterisks represent statistical significance between the $\Delta[Ca^{2+}]_i$ values before and during each treatment ($p < 0.05$). **E**, summary data for the effects of Ca^{2+} free, Na^+ free, and TTX on Ca^{2+} oscillations induced by AII (100 pM). The effects are expressed by the average $\Delta[Ca^{2+}]_i$ value (calculated by subtracting the basal $[Ca^{2+}]_i$ from the $[Ca^{2+}]_i$ averaged for 3 min at the end of each treatment) normalized by the $\Delta[Ca^{2+}]_i$ value obtained just before each treatment. The total number of neurons analyzed was 25 (Ca^{2+} free), 13 (Na^+ free), and 11 (TTX). The asterisks represent statistical significance between the $\Delta[Ca^{2+}]_i$ values before and during each treatment ($p < 0.05$).

2.6 Involvement of Ca^{2+} channels

To identify Ca^{2+} channels responsible for the Ca^{2+} entry, several Ca^{2+} channel blockers were tested in total 81 SFO neurons (Fig. 6). Spontaneous Ca^{2+} oscillations were strongly and consistently inhibited by the high-voltage-activated Ca^{2+} channel blocker Cd^{2+} (50 μM, n = 16) and the L-type Ca^{2+} channel blocker nicardipine (10 μM, n = 17). The T-type Ca^{2+} channel blocker Ni^{2+} (50 μM, n = 17), the N-type Ca^{2+} channel blocker ω-conotoxin GVIA (1 μM, n = 20), and the P/Q-type Ca^{2+} channel blocker ω-agatoxin IVA (100 nM, n = 11) had little or no effect on Ca^{2+} oscillations. Addition of ω-conotoxin MVIIC (1 μM), another blocker of P/Q-type channels, on top of ω-agatoxin IVA (100 nM) did not inhibit Ca^{2+} oscillations (n = 8). The effects of the Ca^{2+} channel blockers on spontaneous Ca^{2+} oscillations are summarized in Fig. 6B. The effects of the Ca^{2+} channel blockers are expressed as average $\Delta[Ca^{2+}]_i$ normalized by the control value. Only Cd^{2+} and nicardipine caused significant inhibition of spontaneous Ca^{2+} oscillations.

2.7 Effects of GABA on spontaneous Ca^{2+} oscillations

Lastly, whether spontaneous Ca^{2+} oscillations are affected by GABA, the major inhibitory neurotransmitter in the SFO (Honda et al., 2001; Osaka et al., 1992b), was also examined.

Application of GABA at 10 μM, promptly arrested spontaneous Ca^{2+} oscillations. Shortly after the removal of GABA, Ca^{2+} oscillations reappeared in all 6 SFO neurons examined. An example of the GABA-induced arrest of Ca^{2+} oscillations is shown in Fig. 7.

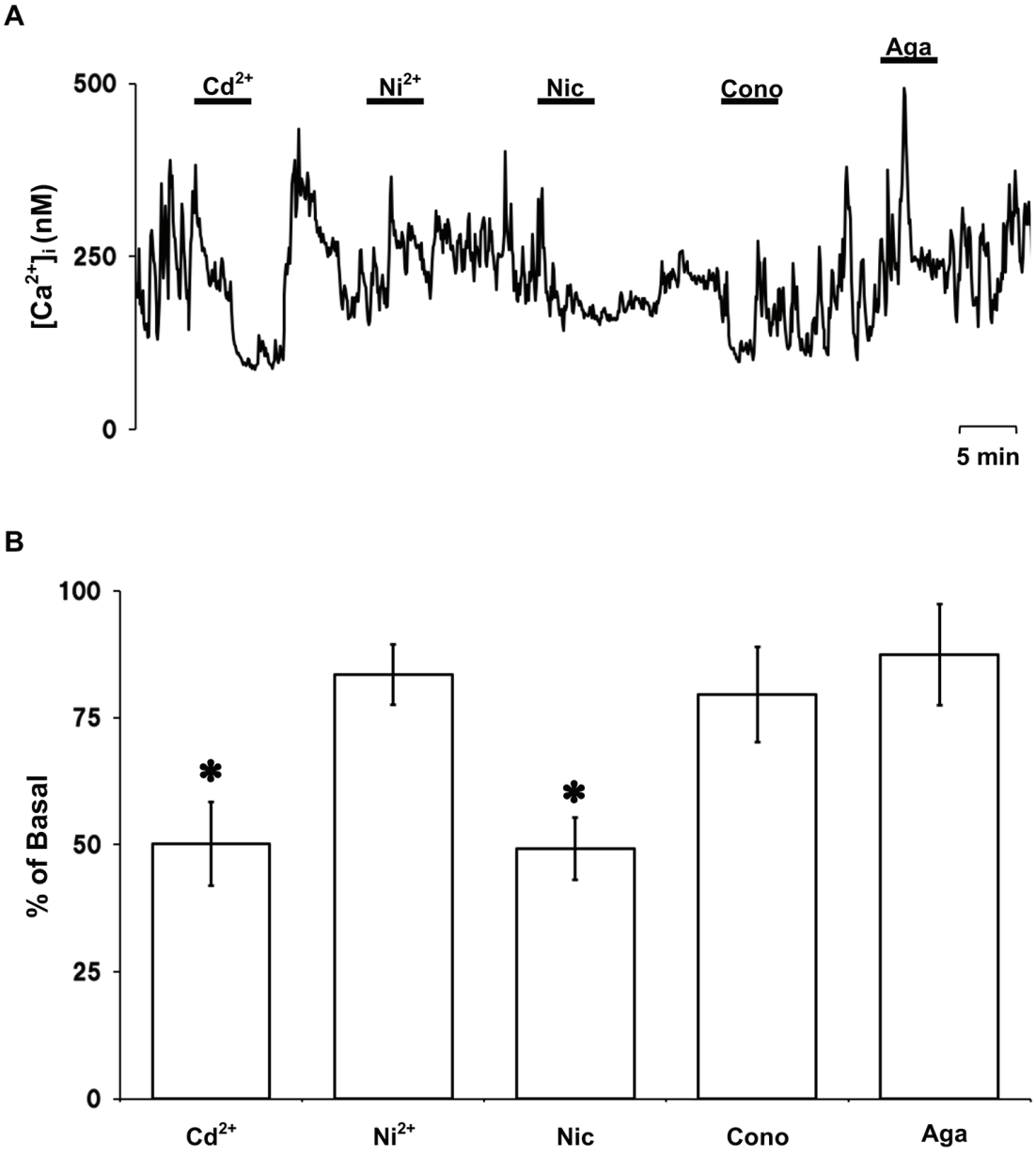

Fig. 6 Effects of Ca^{2+}-channel blockers on spontaneous Ca^{2+} oscillations. **A**, spontaneous Ca^{2+} oscillations were arrested by application of the high-voltage-activated Ca^{2+}-channel blocker Cd^{2+} (50 μM) or the L-type Ca^{2+}-channel blocker nicardipine (Nic, 10 μM). The selective low-voltage-activated Ca^{2+}-channel blocker Ni^{2+} (50 μM), the N-type Ca^{2+}-channel blocker ω-conotoxin GVIA (Cono, 1 μM) and the P/Q-type Ca^{2+}-channel blocker ω-agatoxin IVA (Aga, 1 μM) had little effects. **B**, summary data for the effects of Ca^{2+}-channel blockers. The effects are expressed by relative $\Delta[Ca^{2+}]_i$ values to the basal $[Ca^{2+}]_i$ in 16 (Cd^{2+}), 17 (Ni^{2+}), 17 (nicardipine), 20 (ω-conotoxin GVIA), and 11 (ω-agatoxin IVA) cells. The asterisks represent statistical significance between the $\Delta[Ca^{2+}]_i$ values before and during each treatment ($p < 0.05$).

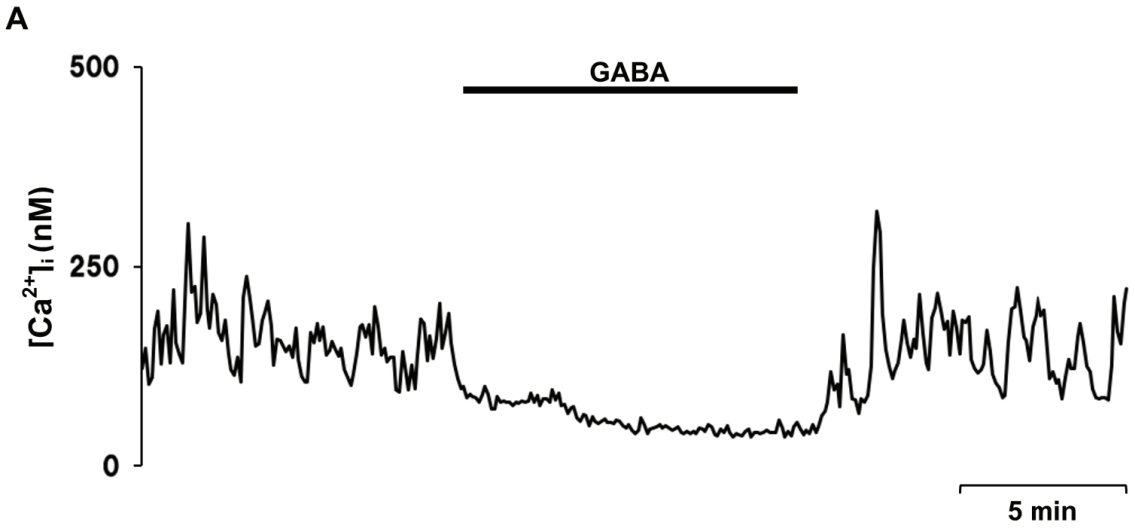

Fig. 7 Effects of GABA on spontaneous Ca^{2+} oscillations. Spontaneous Ca^{2+} oscillations were promptly arrested by application of GABA at 10 μM. Similar responses were observed in five other SFO neurons.

3. Discussion

3.1 Acutely dissociated single SFO neurons

The focus of this study was to characterize the properties of Ca^{2+} signals in SFO neurons. As the SFO is comprised of neuronal perikarya, neuropil, and glial cells (Dellmann, 1998), neurons were first distinguished from glial cells in acutely dissociated preparations following enzyme digestion using immunohistochemistry. SFO cells that did not stain for GFAP were classified as neurons. Second, using $[Ca^{2+}]_i$ measurements, sharp, large rises in $[Ca^{2+}]_i$ were consistently observed in response to high K^+ from the majority of SFO cells, regardless of the cell size and whether dendritic-like processes were attached. Therefore, in the present study, I used the responsiveness to high K^+ with a large (>100 nM) and sharp $[Ca^{2+}]_i$ rise, which is indicative of the presence of VGCCs, as an additional marker of neurons. This latter method to distinguish neurons and glia has been used in many previous studies using acutely dissociated preparations containing neurons and glia (Quallo et al., 2015; Vandewauw et al., 2018). In fact, multiple types of VGCCs carrying large currents function in SFO neurons (Wang et al., 2013; Washburn and Ferguson, 2001). Third, the large $[Ca^{2+}]_i$ response to glutamate, the major excitatory transmitter in the SFO (Gutman et al., 1985; Osaka et al., 1992a; Schmid, 1998; Weindl et al., 1992), observed in such high-K^+-responsive cells provided another piece of evidence that these cells were neuronal cells. Fourth, the finding that cells that showed no response to high K^+ responded to BzATP with large increases in $[Ca^{2+}]_i$ suggested that these cells were glia. Astrocytes, oligodendrocytes and microglia express high levels of the P2X7 receptor (Illes et al., 2017), to which BzATP has a higher affinity than ATP (Donnelly-Roberts and Jarvis, 2007). BzATP was previously used to distinguish $[Ca^{2+}]_i$ responses from neurons and glial cells in acutely dissociated neurons of hypothalamic

supraoptic neurons (Shibuya et al., 1999). The SFO cells were round with no processes in our preparations, which is in sharp contrast with the morphology of SFO glial cells found in culture, which possess flat cytosol and multiple processes (Gebke et al., 1998). The difference in the appearance of glial cells may be due to morphological changes during culture as it has been shown that glial cells can undergo drastic changes in their morphology when they are maintained in culture. (Caldeira et al., 2014; Georgieva et al., 2018)

3.2 Spontaneous Ca^{2+} oscillations

Two distinct patterns were observed in the basal $[Ca^{2+}]_i$ behavior of SFO neurons, namely, either little spontaneous activity or spontaneous Ca^{2+} oscillations. This is the first demonstration of spontaneous Ca^{2+} oscillations in SFO neurons, although the occurrence of AII induced Ca^{2+} oscillations in about 3 % of SFO neurons has been previously reported (Gebke et al., 1998). Ca^{2+} oscillations have been ubiquitously observed in various types of cells, including neurons, more commonly in response to membrane receptor activation, and spontaneously in certain types of cells (Berridge, 1990; Smedler and Uhlen, 2014). In the present study, spontaneous Ca^{2+} oscillations were observed in most of the SFO neurons. Moreover, the physiological ligands frequently induced Ca^{2+} oscillations in silent neurons, suggesting that Ca^{2+} oscillations are a feature common to most SFO neurons. The Ca^{2+} rise and fall during spontaneous Ca^{2+} oscillations occurred at the slow rate of about once per minute and with an average amplitude of approximately 100 nM. The average amplitude is nearly half of the amplitude of the responses to the neuropeptides AII and AVP administered at their maximal concentrations, indicating the peak $[Ca^{2+}]_i$ reached during spontaneous Ca^{2+} oscillations was of considerable level.

Furthermore, during the peak of Ca^{2+} oscillations, $[Ca^{2+}]_i$ in the entire cytosolic space reached an equally high level, suggesting that most enzymes and organelles in the cytosol may receive the signal. As $[Ca^{2+}]_i$ is the key signal to various important cellular events, spontaneous Ca^{2+} oscillations in SFO neurons may play an important role in maintaining the basal activities of these neurons.

3.3 The mechanism of Ca^{2+} oscillations

Analyses of $[Ca^{2+}]_i$ following the use of several ion channel blockers, as well as changes in the extracellular ionic concentrations provided evidence for the mechanisms by which the oscillations occur. The lack of effect of CPA, a selective inhibitor of SERCA, indicates that spontaneous Ca^{2+} oscillations in SFO neurons are independent of intracellular Ca^{2+} stores, indicating that they are not 'store' oscillations, but 'membrane' oscillations (Berridge, 1990; Smedler and Uhlen, 2014). Thus, our data suggest that spontaneous Ca^{2+} oscillations are a result of periodic increases in Ca^{2+} entry followed by Ca^{2+} pumping out of the cell, and they could be the mechanism by which SFO neurons maintain the basal $[Ca^{2+}]_i$.

The prompt arrest of spontaneous Ca^{2+} oscillations by Ca^{2+} removal and the potent inhibition by Na^+ replacement indicate that the spontaneous Ca^{2+} oscillations occur due to phasic increases of Ca^{2+} entry, which depends, at least in part, on Na^+ entry via either voltage-gated Na^+ channels or cation channels. The heterogeneity in the TTX sensitivity suggests that in some neurons, Ca^{2+} entry occurs during spontaneous Na^+ action potentials, and in others, it occurs during a process independent of Na^+ spikes. It has been reported in electrophysiological studies that 53 % of isolated SFO neurons exhibited bursting activity (Washburn et al., 2000), and such electrical activity may underlie the

spontaneous Ca^{2+} oscillations that were arrested by TTX. For the Ca^{2+} oscillations that were only partially inhibited by TTX, it may be of note that in hypothalamic median preoptic nucleus neurons, Ca^{2+}-dependent regenerative auto-excitation that is resistant to TTX inhibition but susceptible to blockage by divalent cation Ca^{2+} channel blockers has been reported (Spanswick and Renaud, 2005). Further electrophysiological studies are needed to elucidate whether SFO neurons exhibit a similar Ca^{2+}-dependent regenerative activity.

The significant blockade of Ca^{2+} oscillations by Cd^{2+} and nicardipine, and the lack of effect by Ni^{2+}, ω-conotoxin GVIA and ω-agatoxin IVA indicate that L-type Ca^{2+} channels are the major source for the $[Ca^{2+}]_i$ increases during Ca^{2+} oscillations. There are four types of high-voltage-activated VGCCs, the L-, N-, P/Q-, and R-types (Ertel et al., 2000). Electrophysiological studies in SFO neurons have reported that these neurons possess VGCCs of N- and L-types (Wang et al., 2013; Washburn and Ferguson, 2001) and that N-type Ca^{2+} channels were the largest component (65 %) (Washburn and Ferguson, 2001). Even though N-type Ca^{2+} channels in SFO neurons are relatively insensitive to voltage-dependent inactivation (Washburn and Ferguson, 2001), Ca^{2+} entry during sustained depolarization, such as the $[Ca^{2+}]_i$-rising phase of Ca^{2+} oscillations, could extensively depend on L-type Ca^{2+} channels, which show very slow inactivation (Dolphin, 2009).

3.4 Ca^{2+} oscillations induced by AII and the other stimulants

The cells that showed little basal activity were likely to be electrically and/or metabolically quiescent SFO neurons. However, these cells became active during AII exposure, because AII given at picomolar concentrations consistently initiated Ca^{2+}

oscillations. In general, intrinsic electrophysiological properties of single neuronal cells and recurrent circuits in the neuronal network are thought to generate spontaneous activity (Malmersjo et al., 2013). Because acutely isolated SFO neurons were used in this study, the results of AII-initiated Ca^{2+} oscillations suggest that AII affected some intrinsic properties of these neurons that regulate their spontaneous activity. The receptor subtype mediating the $[Ca^{2+}]_i$-raising effects of AII is AT1 (Gebke et al., 1998). The time course of AII-induced $[Ca^{2+}]_i$ oscillations was often slower in onset and recovery than that of $[Ca^{2+}]_i$ increases in response to glutamate and high K^+, suggesting that some metabotropic process and second messenger systems are involved in the $[Ca^{2+}]_i$ response. AT1 receptors couple with phospholipase C and IP_3 to cause Ca^{2+} release from intracellular Ca^{2+} stores in CNS neurons (Seltzer et al., 1995) as well as in various peripheral tissues. However, the result that extracellular Ca^{2+} removal inhibited AII-induced Ca^{2+} increases clearly indicates that voltage-dependent Ca^{2+} entry is the major source of the $[Ca^{2+}]_i$ increase in response to AII in SFO neurons. AII can activate voltage-dependent Ca^{2+} entry in two ways: activation of non-selective cation channels (Ono et al., 2001) and inhibition of the outwardly rectifying K^+ currents (Ferguson and Li, 1996).

The findings that AII-induced Ca^{2+} oscillations were susceptible to inhibition by Ca^{2+} removal, Na^+ replacement, and TTX, as were spontaneous Ca^{2+} oscillations, suggest that a common mechanism underlies the two Ca^{2+} oscillations. Moreover, the results that Ca^{2+} oscillations could be induced by the two other stimulants, application of glutamate at low concentrations and the modest increase in extracellular K^+ to 8 mM, suggest that a slight depolarization of the membrane potential may be enough to switch on an intrinsic mechanism of SFO neurons to initiate Ca^{2+} oscillations. The present result that spontaneous Ca^{2+} oscillations were promptly and reversibly arrested by GABA could be

interpreted to mean that GABA hyperpolarized the membrane potential via $GABA_A$ receptors and suppressed the intrinsic mechanism. The observation that the stronger stimuli of higher concentrations of the ligands or extracellular K^+ induced a larger $[Ca^{2+}]_i$ peak followed by a sustained or gradually declining plateau suggest that when Ca^{2+} entry via VGCCs was enhanced to a certain level, the intrinsic mechanism of Ca^{2+} oscillations was overridden. However, additional studies are needed to elucidate the precise cellular mechanism of Ca^{2+} oscillations in SFO neurons.

3.5 Physiological significance of Ca^{2+} oscillations

In general, it has been suggested that Ca^{2+} oscillations are a common Ca^{2+}-signaling mechanism to control cellular functions without harming the cell itself (Berridge et al., 1998). An advantage of encoding Ca^{2+} signals with Ca^{2+} oscillations is that the signal can be modulated by changing both the amplitude and frequency of oscillations. The frequency modulation of Ca^{2+} oscillations leads to activation of mitochondrial metabolism, formation of transcription factors, and various other cellular events (Smedler and Uhlen, 2014).

In the present study, it was observed that the majority of SFO neurons exhibited spontaneous Ca^{2+} oscillations and moreover exposure of these SFO neurons to AII at picomolar concentrations either initiated Ca^{2+} oscillations in silent neurons or potentiated Ca^{2+} oscillations in neurons showing spontaneous Ca^{2+} oscillations. The plasma concentrations of AII in normal rats is approximately 5 pM, which increases in renal hypertensive rats and in rats in a Na^+-depleted condition to approximately 66 pM and 72 pM, respectively (Bunkenburg et al., 1991). These AII concentrations are the concentrations at which AII significantly modulated both the amplitude and frequency of

Ca^{2+} oscillations in the present study. Thus, the amplitude and frequency of Ca^{2+} oscillations might encode the AII concentrations being transmitted to cellular events in SFO neurons. At the highest AII concentration tested in the concentration-dependency experiment (100 pM), both the amplitude and frequency of Ca^{2+} oscillations increased approximately 3-fold. If both of these parameters were increased 3-fold, it could potently modulate various Ca^{2+}-dependent processes, such as gene expression and exocytotic events in the cytosol. The L-type Ca^{2+} channel, the importance of which in the spontaneous Ca^{2+} oscillations was revealed in the present study, plays a major role in sending the signal from the plasma membrane to the nucleus (Deisseroth et al., 2003). Exocytotic events occur, even in the somatodendritic region of CNS neurons. Although there is no report for somatodendritic release in the SFO, Ca^{2+}-dependent increases in the somatodendritic release regulate functions of hypothalamic supraoptic neurons in response to excitatory stimuli (Ludwig et al., 2002; Shibuya et al., 1998).

In any event, because cytosolic Ca^{2+} has been implicated in various cellular functions, such as transmitter release, synaptic plasticity, regulation of ion channels, gene expression, and cell survival (Augustine et al., 2003), the present findings that the basal $[Ca^{2+}]_i$ behavior in SFO neurons is modulated positively by AII at physiologically relevant low concentrations, and negatively by GABA, which is the major inhibitory synaptic input to the SFO (Honda et al., 2001; Osaka et al., 1992b), seem to be of physiological and/or pathophysiological importance.

3.6 Responsiveness of single SFO neurons to various ligands

The results obtained using dissociated and cultured preparations of SFO neurons have provided several lines of evidence that these neurons possess multiple receptors, such as

AT1, V1a, and muscarinic M_1 receptors that are linked to Ca^{2+} signaling pathways (Gebke et al., 1998; Johnson et al., 2001; Jurzak et al., 1994; Jurzak et al., 1995a; Jurzak et al., 1995b). In the present study, I tested glutamate, BzATP, AVP, CCh and AII in acutely dissociated SFO neurons and found that most AII-responsive neurons responded to either AVP or CCh or to both. This extensive overlap suggests that a single SFO neuron can sense multiple stimulatory signals, all of which are related to the water/electrolyte balance and cardiovascular control. This overlap may represent how these signals converge at the level of the SFO or could be a sort of fault-tolerant mechanism in the homeostatic response of SFO neurons. By using electrophysiology in single SFO neurons, Pullman *et al*. (Pulman et al., 2006) have reported that no SFO neuron responded to both ghrelin and amylin, the signaling peptides for the hunger and satiety, respectively, indicating that the two peptides influence separate subpopulations of SFO neurons. Because SFO neurons regulate multiple functions, such as water and salt intake, feeding, or immune response, it would be of interest to analyze how $[Ca^{2+}]_i$ responses to ligands with different physiological functions overlap in SFO neurons. Additionally, as SFO neurons project to many brain regions (Dellmann, 1998), it would be also intriguing to understand the projection-dependency of responsiveness to the ligands.

There is no report on purinergic receptors in SFO neurons. The result that the majority of SFO neurons responded to BzATP, a P2X7 receptor agonist, suggests that these neurons may possess this type of ionotropic purinergic receptor. However, whether P2X7 receptors play a role in neuronal cells is controversial (Illes et al., 2017). Moreover, the present result that the response to BzATP observed in neurons was significantly smaller than that in glia could be interpreted to mean that the response in neurons is mediated by other types of P2X receptors, as BzATP is the most potent agonist but not a selective

agonist for the P2X7 receptor (Donnelly-Roberts and Jarvis, 2007).

3.7 Differences between the present results and previous results obtained in cultured SFO neurons

In the present study, 50 % of dissociated SFO neurons responded to AII, which is in clear contrast with the results obtained from cultured rat SFO neurons, where less than approximately 20 % of neurons responded to AII (Gebke et al., 1998). Moreover, the minimally effective concentration of AII to evoke $[Ca^{2+}]_i$ increases in this study was as low as 1 pM, which is nearly three orders of magnitude smaller than the threshold AII concentration reported in cultured SFO neurons (Gebke et al., 1998). Additionally, there was a clear difference in the pattern of responses to repeated applications of AII between the present results and the results obtained in cultured SFO neurons. The amplitude of the $[Ca^{2+}]_i$ increases in response to the second application of AII was found in the present studies to be identical (>95 %) to that to the first application of AII. In contrast, cultured neurons sometimes did not respond at all to the second AII (Gebke et al., 1998). The differences in the results between acutely dissociated neurons and neurons maintained in culture could be due to some changes in AII receptors and their downstream signaling mechanisms that might have occurred during culture. Furthermore, the response rate to AII found in our study is close to that reported in electrophysiological studies in brain slices or *in vivo* (Felix and Akert, 1974; Gutman et al., 1988; Li and Ferguson, 1993; Okuya et al., 1987; Schmid and Simon, 1992; Tanaka et al., 1987). Taken together, our findings with those of electrophysiological studies suggest that acutely dissociated preparations may better reflect physiological conditions of SFO neurons *in vivo*. There are reports showing acutely dissociated preparations from CNS neurons exhibit behaviors

that match their *in vivo* physiological properties. For example, using the Ca^{2+} imaging technique in acutely dissociated hypothalamic supraoptic neurons, Kortus *et al*. (Kortus et al., 2016) reported that vasopressin and oxytocin neurons exhibited spontaneous Ca^{2+} oscillations and that the Ca^{2+} oscillations of these two types of neurons were enhanced during dehydration and lactation, respectively.

In the present study, $[Ca^{2+}]_i$ increased by similar amplitudes in response to AII, high K^+, and glutamate. It appears that acutely dissociated preparations of SFO neurons provide a useful tool to observe the effects of drugs by comparing responses to repeated stimuli and to investigate the property of SFO neurons at the single-cell level. Because *in vitro* preparations such as cultured SFO cells or SFO cells in brain slices may have synaptic inputs or other cell-to-cell communication influences from surrounding cells via paracrine secretion or gap junctions, actions through such indirect pathways cannot be excluded. Therefore, acutely dissociated preparations of neurons and glia from SFO tissues may also be beneficial to examine direct actions of various neurotransmitters or blood-borne signaling molecules and to analyze the cellular mechanisms that are intrinsic to SFO cells in an isolated condition.

3.8 Conclusions

The present study revealed that the majority of acutely isolated SFO neurons exhibited spontaneous Ca^{2+} oscillations that are dependent on Ca^{2+} entry in part through voltage-gated Ca^{2+} channels of L-type. The primary blood-borne excitatory input to SFO, AII, increased the amplitude and frequency of Ca^{2+} oscillations at concentrations from 1 to 100 pM, and the primary inhibitory neurotransmitter in SFO, GABA, abolished Ca^{2+} oscillations in a quickly reversible manner, suggesting that Ca^{2+} oscillations may play a

role in the regulation of functions of SFO neurons. Moreover, in silent SFO neurons, Ca^{2+} oscillations could be induced by the picomolar concentrations of AII, low micromolar concentrations of glutamate, and increasing the extracellular K^+ concentration to 8 or 10 mM, indicating that Ca^{2+} oscillations may be a common feature for SFO neurons. Acutely dissociated preparations from SFO tissues may provide a useful tool to examine intrinsic regulatory mechanisms of SFO neurons and glial cells.

4. Graphical abstract

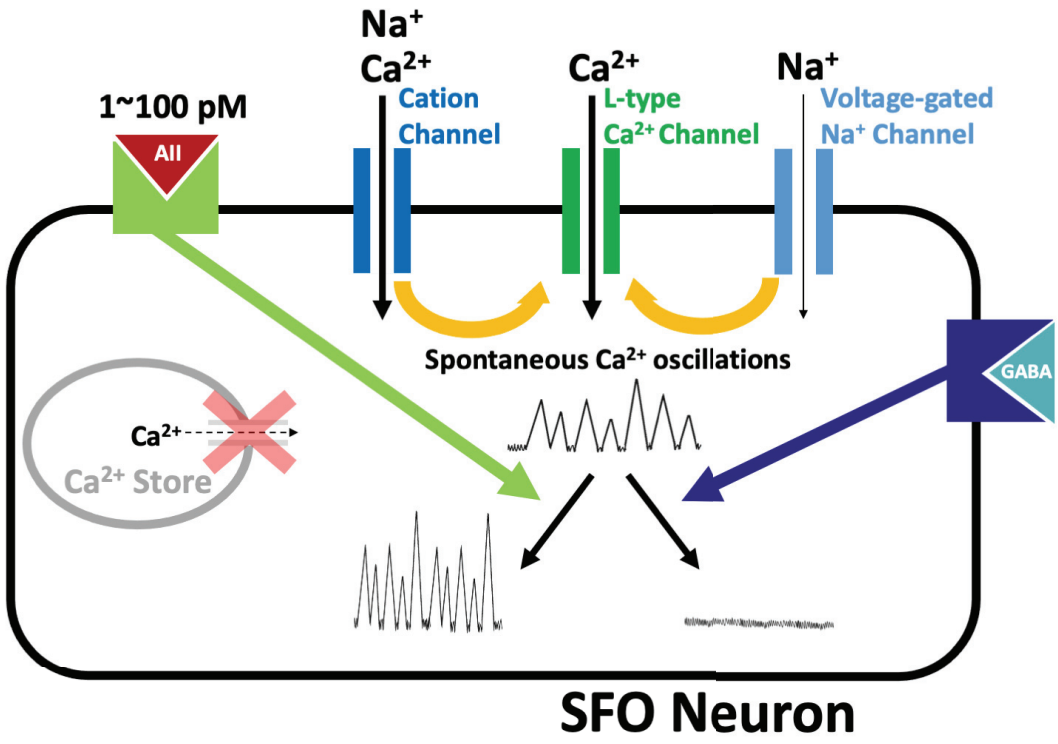

5. Experiment procedure

5.1 Solution

The solution used for making slices was a modified Krebs-Henseleit solution (KHB) containing (mM) NaCl, 124; KCl, 5; $MgSO_4$, 1.3; KH_2PO_4, 1.24; $CaCl_2$, 2; $NaHCO_3$, 25.9; and glucose, 10. It was continuously oxygenated with a mixture of 95 % O_2 and 5 % CO_2. The standard solution used for dissociation and perfusion of SFO neurons was HEPES-buffered solution (HBS) containing (mM) NaCl, 140; KCl, 5; $CaCl_2$, 2; $MgCl_2$,1; glucose, 10 and HEPES, 10 (pH adjusted to 7.4 with Tris). It was continuously oxygenated with 100 % O_2 gas. For extracellular Ca^{2+}-free experiments, HBS without adding $CaCl_2$ was used, and for extracellular Na^+-free experiments, Na^+ was replaced with equimolar N-methyl-D-glucamine.

5.2 Dissociation of SFO neurons

SFO neurons were dissociated by an enzymatic digestion method described elsewhere (Shibuya et al., 1998). All experiments were carried out under the control of the Ethics Committee of Animal Care and Experimentation, Tottori University, Japan. In brief, young male Wistar rats (three to four weeks of age) were deeply anesthetized with isoflurane, and SFO tissues were cut from the brain. In initial experiments, a block of brain tissue containing the SFO was cut on a vibratome-type slicer (DSK-2000; DSK, Kyoto, Japan), the SFO was identified anatomically, and removed using a circular punch (i.d. 0.6 mm). The SFO tissues were incubated in HBS containing pronase (Sigma, 0.5 mg/10 ml) for 25 min and then in a solution containing thermolysin (Sigma, 1 mg/10 ml) for 20 min, at 32 °C. The tissues were then transferred to an enzyme-free HBS and mechanically dissociated by trituration with fire-polished glass pipettes. The dissociated

cells were incubated in oxygenated HBS solution for 40 min at room temperature (~23 °C) before loading with fura-2.

After dissociation, immunohistochemical analysis was performed using an antibody against the astrocyte marker glial fibrillary acidic protein (GFAP, Incstar, MN, USA), according to a method described elsewhere (Ison et al., 1993) to identify neuronal and glial cell populations.

5.3 $[Ca^{2+}]_i$ measurement

For fura-2 loading, dissociated SFO cells were incubated in HBS with the addition of acetoxymethyl esters of fura-2 (fura-2/AM, 1 μM) for 60 min at room temperature. The cells were then washed by perfusing with dye-free HBS before measurements of $[Ca^{2+}]_i$.

The arrangements for measuring fluorescence have been described previously (Moriya et al., 2015; Shibuya et al., 1998). In brief, cells were continuously perfused with HBS in a small volume chamber (approximately 200 μl) that had a glass coverslip bottom and that was positioned on the stage of an inverted microscope (TMD-300; Nikon, Tokyo, Japan). A complete change of the solution in the chamber in a few seconds at a perfusion rate of 1.5 ml/min. Fluorescence images with excitation at 340 and 380 nm were recorded at 5 s intervals with CCD camera systems (AquaCosmos, Hamamatsu Photonics, Hamamatsu, Japan or QuantiCell 700, JEOL, Tokyo, Japan). The ratio of fluorescence for each pixel obtained with excitation at 340 and 380 nm (F340/F380) was used to calculate $[Ca^{2+}]_i$. A calibration curve of $[Ca^{2+}]_i$ for F340/F380 was determined using a regression curve obtained from measurements with free-acid fura-2 dissolved in series of Ca^{2+}-buffered solutions containing 0, 17, 38, 65, 100, 150, 225, 351, 602, 1350, and 39000 nM free Ca^{2+} (Life technologies, Carlsbad, CA, USA). To estimate $[Ca^{2+}]_i$ in

individual cells, regions of interest (ROIs) were chosen to include the soma of each SFO cell, and average values of $[Ca^{2+}]_i$ in pixels contained in each ROI were calculated. All experiments were performed at room temperature (~23 °C).

The baseline $[Ca^{2+}]_i$ in each cell was determined by calculating the average $[Ca^{2+}]_i$ at the beginning of measurement in cells showing little or no spontaneous activity and by calculating the lowest $[Ca^{2+}]_i$ value during inter-oscillation periods in cells showing spontaneous Ca^{2+} oscillations. Cells showing $[Ca^{2+}]_i$ responses larger than 100 nM from the baseline were regarded as healthy neurons and were used for further analysis. An increase in $[Ca^{2+}]_i$ larger than 30 nM was regarded as a meaningful response, to exclude interference from the noise of the fluorescence signal. Repeated $[Ca^{2+}]_i$ elevations larger than 30 nM were regarded as Ca^{2+} oscillations, and consequently the frequency was calculated by considering the $[Ca^{2+}]_i$ elevations larger than 30 nM as one peak during Ca^{2+} oscillations. The amplitude of $[Ca^{2+}]_i$ responses was expressed as $\Delta[Ca^{2+}]_i$, which was calculated by subtracting the average $[Ca^{2+}]_i$ before drug application from the peak $[Ca^{2+}]_i$ amplitude detected after the onset of drug application.

5.4 Drugs

Angiotensin II, arginine vasopressin (AVP), ω-conotoxin GVIA, ω-agatoxin IVA, and ω-conotoxin MVIIC were purchased from Peptide Institute (Osaka, Japan); TTX was from Nacalai Tesque (Kyoto, Japan); nicardipine was from Sigma-Aldrich (St. Louis, MO); fura-2/AM was from Dojindo (Kumamoto, Japan); isoflurane was from Pfizer (Tokyo, Japan); other drugs were of analytical grade from Fujifilm Wako Pure Chemical Co. (Osaka, Japan).

5.5 Statistics

All values are expressed as the mean ± SEM, and 'n' represents the number of neurons examined. A P value of < 0.05 using Student's t-test was considered statistically significant.

6. References

Augustine, G.J., Santamaria, F., Tanaka, K., 2003. Local calcium signaling in neurons. Neuron. 40**,** 331-346.

Berridge, M.J., 1990. Calcium oscillations. J Biol Chem. 265**,** 9583-9586.

Berridge, M.J., Bootman, M.D., Lipp, P., 1998. Calcium - a life and death signal. Nature. 395**,** 645-648.

Bunkenburg, B., Schnell, C., Baum, H.P., Cumin, F., Wood, J.M., 1991. Prolonged angiotensin-II antagonism in spontaneously hypertensive rats - hemodynamic and biochemical consequences. Hypertension. 18**,** 278-288.

Caldeira, C., Oliveira, A.F., Cunha, C., Vaz, A.R., Falcao, A.S., Fernandes, A., Brites, D., 2014. Microglia change from a reactive to an age-like phenotype with the time in culture. Front. Cell. Neurosci. 8, 152.

Cottrell, G.T., Ferguson, A.V., 2004. Sensory circumventricular organs: central roles in integrated autonomic regulation. Regul. Pept. 117**,** 11-23.

Deisseroth, K., Mermelstein, P.G., Xia, H., Tsien, R.W., 2003. Signaling from synapse to nucleus: the logic behind the mechanisms. Curr. Opin. Neurobiol. 13**,** 354-65.

Dellmann, H.D., Linner, J.G., 1979. Ultrastructure of the subfornical organ of the chicken (gallus-domesticus). Cell Tissue Res.197**,** 137-153.

Dellmann, H.D., 1998. Structure of the subfornical organ: A review. Microsc Res Tech. 41**,** 85-97.

Dolphin, A.C., 2009. Calcium channel diversity: multiple roles of calcium channel subunits. Curr. Opin. Neurobiol. 19**,** 237-244.

Donnelly-Roberts, D.L., Jarvis, M.F., 2007. Discovery of P2X7 receptor-selective antagonists offers new insights into P2X7 receptor function and indicates a role in chronic pain states. Br. J. Pharmacol. 151**,** 571-579.

Ertel, E.A., Campbell, K.P., Harpold, M.M., Hofmann, F., Mori, Y., Perez-Reyes, E., Schwartz, A., Snutch, T.P., Tanabe, T., Birnbaumer, L., Tsien, R.W., Catterall, W.A., 2000. Nomenclature of voltage-gated calcium channels. Neuron. 25**,** 533-535.

Felix, D., Akert, K., 1974. The effect of angiotensin II on neurones of the cat subfornical organ. Brain Res. 76**,** 350-353.

Ferguson, A.V., Bains, J.S., 1996. Electrophysiology of the circumventricular organs. Front Neuroendocrinol. 17**,** 440-475.

Ferguson, A.V., Li, Z.H., 1996. Whole cell patch recordings from forebrain slices demonstrate angiotensin II inhibits potassium currents in subfornical organ neurons. Regul. Pept. 66**,** 55-58.

Fitzsimons, J.T., 1998. Angiotensin, thirst, and sodium appetite. Physiol. Rev. 78**,** 583-686.

Gebke, E., Muller, A.R., Jurzak, M., Gerstberger, R., 1998. Angiotensin II-induced calcium signalling in neurons and astrocytes of rat circumventricular organs. Neuroscience. 85**,** 509-520.

Georgieva, M., Leeson-Payne, A., Dumitrascuta, M., Rajnicek, A., Malcangio, M., Huang, W.L., 2018. A refined rat primary neonatal microglial culture method that reduces time, cost and animal use. J. Neurosci. Methods 304**,** 92-102.

Gross, P.M., 1992. Circumventricular organ capillaries. Prog. Brain Res. 91**,** 219-233.

Gutman, M.B., Ciriello, J., Mogenson, G.J., 1985. Effect of paraventricular nucleus lesions on cardiovascular-responses elicited by stimulation of the subfornical organ in the rat. Physiol. Pharmacol. 63**,** 816-824.

Gutman, M.B., Ciriello, J., Mogenson, G.J., 1988. Effects of plasma Angiotensin II and hypernatremia on subfornical organ neurons. Am. J. Physiol. 254**,** R746-R754.

Honda, E., Xu, S., Ono, K., Ito, K., Inenaga, K., 2001. Spontaneously active GABAergic interneurons in the subfornical organ of rat slice preparations. Neurosci Lett. 306**,** 45-48.

Illes, P., Khan, T.M., Rubini, P., 2017. Neuronal P2X7 Receptors Revisited: Do They Really Exist? J. Neurosci. 37**,** 7049-7062.

Ison, A., Yuri, K., Ueta, Y., Leng, G., Koizumi, K., Yamashita, H., Kawata, M., 1993. Vasopressin-immunoreactive and oxytocin-immunoreactive hypothalamic neurons of inbred polydipsic mice. Brain Res. Bull. 31**,** 405-414.

Johnson, A.K., Gross, P.M., 1993. Sensory circumventricular organs and brain homeostatic pathways. FASEB J.7**,** 678-686.

Johnson, R.F., Beltz, T.G., Sharma, R.V., Xu, Z., Bhatty, R.A., Johnson, A.K., 2001. Agonist activation of cytosolic Ca^{2+} in subfornical organ cells projecting to the supraoptic nucleus. Am. J. Physiol. Regul. Integr. Comp. Physiol. 280**,** R1592-R1599.

Jurzak, M., Muller, A.R., Schmid, H.A., Gerstberger, R., 1994. Primary culture of circumventricular organs from the rat brain lamina terminalis. Brain Res. 662**,** 198-208.

Jurzak, M., Muller, A.R., Gerstberger, R., 1995a. Characterization of vasopressin receptors in cultured-cells derived from the region of rat-brain circumventricular organs. Neuroscience. 65**,** 1145-1159.

Jurzak, M., Muller, A.R., Gerstberger, R., 1995b. AVP-fragment peptides induce Ca^{2+} transients in cells cultured from rat circumventricular organs. Brain Res. 673**,** 349-355.

Kortus, S., Srinivasan, C., Forostyak, O., Ueta, Y., Sykova, E., Chvatal, A., Zapotocky, M., Verkhratsky, A., Dayanithi, G., 2016. Physiology of spontaneous $[Ca^{2+}]_i$ oscillations in the isolated vasopressin and oxytocin neurones of the rat supraoptic nucleus. Cell Calcium. 59**,** 280-288.

Li, Z., Ferguson, A.V., 1993. Angiotensin-II responsiveness of rat paraventricular and subfornical organ neurons in-vitro. Neuroscience. 55**,** 197-207.

Ludwig, M., Sabatier, N., Bull, P.M., Landgraf, R., Dayanithi, G., Leng, G., 2002. Intracellular calcium stores regulate activity-dependent neuropeptide release from dendrites. Nature. 418**,** 85-89.

Malmersjo, S., Rebellato, P., Smedler, E., Planert, H., Kanatani, S., Liste, I., Nanou, E., Sunner, H., Abdelhady, S., Zhang, S.B., Andang, M., El Manira, A., Silberberg, G., Arenas, E., Uhlen, P., 2013. Neural progenitors organize in small-world networks to promote cell proliferation. PNAS of USA. 110**,** E1524-E1532.

McKinley, M.J., Allen, A.M., Burns, P., Colvill, L.M., Oldfield, B.J., 1998. Interaction of circulating hormones with the brain: The roles of the subfornical organ and the organum vasculosum of the lamina terminalis. Clin. Exp. Pharmacol. Physiol. 25**,** S61-S67.

Mimee, A., Smith, P.M., Ferguson, A.V., 2013. Circumventricular organs: Targets for integration of circulating fluid and energy balance signals? Physiol. Behav. 121**,** 96-102.

Moriya, T., Shibasaki, R., Kayano, T., Takebuchi, N., Ichimura, M., Kitamura, N., Asano, A., Hosaka, Y.Z., Forostyak, O., Verkhratsky, A., Dayanithi, G., Shibuya, I., 2015. Full-length transient receptor potential vanilloid 1 channels mediate calcium signals and possibly contribute to osmoreception in vasopressin neurones in the rat supraoptic nucleus. Cell Calcium. 57**,** 25-37.

Okuya, S., Inenaga, K., Kaneko, T., Yamashita, H., 1987. Angiotensin II sensitive neurons in the supraoptic nucleus, subfornical organ and anteroventral third ventricle of rats in vitro. Brain Res. 402**,** 58-67.

Ono, K., Honda, E., Inenaga, K., 2001. Angiotensin II induces inward currents in subfornical organ neurones of rats. J. Neuroendocrinol. 13**,** 517-523.

Osaka, T., Yamashita, H., Koizumi, K., 1992a. Inhibitory inputs to the subfornical organ from the AV3V - involvement of GABA. Brain Res. Bull. 29**,** 581-587.

Pulman, K.J., Fry, W.M., Cottrell, G.T., Ferguson, A.V., 2006. The subfornical organ: A central target for circulating feeding signals. J. Neurosci. 26**,** 2022-2030.

Quallo, T., Vastani, N., Horridge, E., Gentry, C., Parra, A., Moss, S., Viana, F., Belmonte, C., Andersson, D.A., Bevan, S., 2015. TRPM8 is a neuronal osmosensor that regulates eye blinking in mice. Nat. Commun. 6.

Schmid, H.A., Simon, E., 1992. Effect of angiotensin II and atrial natriuretic factor on neurons in the subfornical organ of ducks and rats in vitro. Brain Res. 588**,** 324-8.

Schmid, H.A., 1998. Effect of glutamate and angiotensin II on whole cell currents and release of nitric oxide in the rat subfornical organ. Amino Acids. 14**,** 113-119.

Seltzer, A.M., Zorad, S., Saavedra, J.M., 1995. Stimulation of angiotensin II AT1 receptors in rat median eminence increases phosphoinositide hydrolysis. Brain Res. 705**,** 24-30.

Shibuya, I., Noguchi, J., Tanaka, K., Harayama, N., Inoue, Y., Kabashima, N., Ueta, Y., Hattori, Y., Yamashita, H., 1998. PACAP increases the cytosolic Ca^{2+} concentration and stimulates somatodendritic vasopressin release in rat supraoptic neurons. J. Neuroendocrinol. 10**,** 31-42.

Shibuya, I., Tanaka, K., Hattori, Y., Uezono, Y., Harayama, N., Noguchi, J., Ueta, Y., Izumi, F., Yamashita, H., 1999. Evidence that multiple P2X purinoceptors are functionally expressed in rat supraoptic neurones. J. Physiol. (Lond.) 514**,** 351-367.

Simpson, N.J., Ferguson, A.V., 2017. The proinflammatory cytokine tumor necrosis factor-alpha excites subfornical organ neurons. J Neurophysiol. 118**,** 1532-1541.

Simpson, N.J., Ferguson, A.V., 2018. Tumor necrosis factor alpha potentiates the effects of angiotensin II on subfornical organ neurons. Am J Physiol Regul Integr Comp Physiol.

Smedler, E., Uhlen, P., 2014. Frequency decoding of calcium oscillations. Biochim Biophys Acta Gen Subj. 1840**,** 964-969.

Smith, P.M., Ferguson, A.V., 2010. Circulating signals as critical regulators of autonomic state-central roles for the subfornical organ. Am. J. Physiol. Regul. Integr. Comp. Physiol. 299**,** R405-R415.

Spanswick, D., Renaud, L.P., 2005. Angiotensin II induces calcium-dependent rhythmic activity in a Subpopulation of rat hypothalamic median preoptic nucleus neurons. J. Neurophysiol. 93**,** 1970-1976.

Tanaka, J., Saito, H., Kaba, H., 1987. Subfornical organ and hypothalamic paraventricular nucleus connections with median preoptic nucleus neurons - an electrophysiological study in the rat. Exp Brain Res 68**,** 579-585.

Vandewauw, I., De Clercq, K., Mulier, M., Held, K., Pinto, S., Van Ranst, N., Segal, A., Voet, T., Vennekens, R., Zimmermann, K., Vriens, J., Voets, T., 2018. A TRP channel trio mediates acute noxious heat sensing. Nature. 555**,** 662-666.

Wang, G., Sarkar, P., Peterson, J.R., Anrather, J., Pierce, J.P., Moore, J.M., Feng, J., Zhou, P., Milner, T.A., Pickel, V.M., Iadecola, C., Davisson, R.L., 2013. COX-1-derived PGE_2 and PGE_2 type 1 receptors are vital for angiotensin II-induced formation of reactive oxygen species and Ca^{2+} influx in the subfornical organ. Am J Physiol Heart Circ Physiol. 305**,** H1451-61.

Washburn, D.L.S., Anderson, J.W., Ferguson, A.V., 2000. A subthreshold persistent sodium current mediates bursting in rat subfornical organ neurones. J. Physiol. (Lond.) 529**,** 359-371.

Washburn, D.L.S., Ferguson, A.V., 2001. Selective potentiation of N-type calcium channels by angiotensin II in rat subfornical organ neurones. J. Physiol. (Lond.) 536**,** 667-675.

Weindl, A., Bufler, J., Winkler, B., Arzberger, T., Hatt, H., 1992. Neurotransmitters and receptors in the subfornical organ - immunohistochemical and electrophysiological evidence. Prog. Brain Res. 91**,** 261-269.

Yu, Y., Wei, S.G., Weiss, R.M., Felder, R.B., 2018. Angiotensin II Type la Receptors in the Subfornical Organ Modulate Neuroinflammation in the Hypothalamic Paraventricular Nucleus in Heart Failure Rats. Neuroscience. 381, 46-58.

Chapter 2

Persistent cytosolic Ca^{2+} increase induced by angiotensin II at nanomolar concentrations in acutely dissociated subfornical organ (SFO) neurons of rats

Highlights

6. AII (≥1 nM) induced a persistent $[Ca^{2+}]_i$ increase in acutely dissociated SFO neurons
7. The persistent AII-induced $[Ca^{2+}]_i$ increase was maintained by Ca^{2+} entry
8. The Ca^{2+} entry was mediated in part by voltage-gated Ca^{2+} channels of L and P/Q types
9. CaMK and PKC were involved in the persistent $[Ca^{2+}]_i$ increase
10. GABA reversibly inhibited the persistent $[Ca^{2+}]_i$ increase

Abstract

Angiotensin II (AII) acts at subfornical organ (SFO) to elicit drinking behavior and alter arterial pressure. I have previously reported that low concentrations of AII induce Ca^{2+} oscillations and increase the amplitude and frequency of the spontaneous Ca^{2+} oscillations in acutely dissociated SFO neurons. In the present study I examined the effects on cytosolic Ca^{2+} in these neurons of AII concentrations observed in pathophysiological states using the Fura-2 Ca^{2+}-imaging technique. AII at nanomolar concentrations was found to induce an initial $[Ca^{2+}]_i$ peak followed by a persistent $[Ca^{2+}]_i$ increase lasting for longer than 1 hour. On the other hand, $[Ca^{2+}]_i$ responses to 50 mM K^+, and maximally effective concentrations of glutamate, carbachol, and vasopressin returned to the basal levels within 20 min. The AII-induced $[Ca^{2+}]_i$ increase was blocked by the specific AT1 antagonist losartan when applied prior to the AII, but had no effect when added during the persistent phase initiated by AII. The persistent phase was unaffected by inhibition of Ca^{2+} store Ca^{2+}ATPase, suppressed by extracellular Ca^{2+} removal, and significantly inhibited by L and P/Q type Ca^{2+} channel blockers. The persistent phase was also reversibly suppressed by GABA and inhibited by CaMK and PKC inhibitors. The results demonstrate that persistent $[Ca^{2+}]_i$ increase evoked by pathophysiological concentrations of AII was initiated by AT1 receptor activation and maintained by Ca^{2+} entry mechanisms in part through L and P/Q type Ca^{2+} channels, and with the involvement of CaMK and PKC. The persistent $[Ca^{2+}]_i$ increase induced by AII at high pathophysiological levels may have a significant role in altering SFO neuronal functions.

1. Introduction

Angiotensin II (AII) is a octapeptide that regulates body fluid homeostasis and drinking behaviors as well as cardiovascular and renal functions. In the central nervous system (CNS), AII is believed to be sensed by the circumventricular organs (CVOs). The subfornical organ (SFO) is one of the CVOs that lacks the blood-brain barrier, allowing it to directly sense blood-borne molecules, including AII (Cottrell and Ferguson, 2004; Gross, 1992; McKinley et al., 1998; Smith and Ferguson, 2010). Then, the SFO sends efferent projections to other brain regions, such as the hypothalamic paraventricular and supraoptic nuclei, the medulla oblongata, and the spinal cord (Dellmann, 1998) to modulate the brain function. It is proposed that the SFO serves as a target of circulatory molecules involved in body fluid homeostasis (Cottrell and Ferguson, 2004; Fitzsimons, 1998; Simpson and Ferguson, 2017; Simpson and Ferguson, 2018; Yu et al., 2018). One of the best-characterized functions of the SFO is an increase in water intake in response to blood-borne AII (Fitzsimons, 1998).

The mechanism of SFO neurons by which AII activates various cellular events has been studied at the single-cell level with electrophysiology (Felix and Akert, 1974; Gutman et al., 1988; Li and Ferguson, 1993; Okuya et al., 1987; Schmid and Simon, 1992; Tanaka et al., 1987) or the imaging technique for the intracellular Ca^{2+} concentration ($[Ca^{2+}]_i$) in SFO slices or dissociated SFO neurons (Gebke et al., 1998; Johnson et al., 2001; Jurzak et al., 1995b; Pulman et al., 2006; Simpson and Ferguson, 2018). Previously, I have reported that acutely dissociated SFO neurons responded to high K^+, glutamate, BzATP, carbachol (CCh), arginine vasopressin (AVP), and to AII with marked increases in $[Ca^{2+}]_i$ (Izumisawa et al., 2018) . In the study, I found that AII at picomolar concentrations (1 to 100 pM) induced Ca^{2+} oscillations in SFO neurons

showing little $[Ca^{2+}]_i$ spontaneous activity, and increased the amplitude and frequency of Ca^{2+} oscillations in spontaneously oscillating neurons.

In the present study, I used AII at nanomolar concentrations, which would be close to the concentrations during pathophysiological conditions, and found that AII at nanomolar concentrations caused long-lasting increases in $[Ca^{2+}]_i$, while the other stimuli such as high K^+ or glutamate caused transient $[Ca^{2+}]_i$ responses. I also analyzed cellular mechanisms involved in the persistent $[Ca^{2+}]_i$ increase induced by AII, and found that the persistent phase was maintained by an increased Ca^{2+} entry due to phosphorylation by calcium-calmodulin-dependent kinase (CaMK) and protein kinase C (PKC).

2. Results

2.1 Comparison of $[Ca^{2+}]_i$ responses to angiotensin II and various other stimuli in acutely dissociated SFO neurons

SFO neurons, judged by their marked $[Ca^{2+}]_i$ responses to high K^+ (50 mM) (Izumisawa et al., 2018), responded to AII (100 nM) with an initial peak followed by a persistent $[Ca^{2+}]_i$ rise, which lasted for more than 20 min after washout (Fig. 1A). This is in a sharp contrast with $[Ca^{2+}]_i$ responses to high K^+, which were transient. The pattern of the $[Ca^{2+}]_i$ response in pseudocolored images showed that although the $[Ca^{2+}]_i$ level in the whole cytosol came back to the pre-stimulus level 20 min after washout in the response to high K^+, it remained a high level for 20 min or more in the response to AII. There were three patterns in the AII-induced $[Ca^{2+}]_i$ responses: first pattern was long-lasting but oscillatory $[Ca^{2+}]_i$ increase (as seen in Fig. 1A and Fig. 3A; repeated $[Ca^{2+}]_i$ elevations larger than 30 nM of amplitude were regarded as Ca^{2+} oscillations (Izumisawa et al., 2018)), second pattern was persistent plateau which did not return to the basal level for 20 min or more after washout of AII (as seen in Fig. 1B and Fig. 3B), and third was a gradual decline to finally reach the level below 10 % of the peak $[Ca^{2+}]_i$ within 20 min after washout. The most common pattern was the persistent plateau, which was observed in 25/43 (58%) of AII-responding SFO neurons. The long-lasting oscillatory response was observed in 16/43 (37%) neurons, and the third pattern was least frequent, seen only in 2/43 (5%) neurons. In 8 out of 10 neurons where the observation was continued for longer than 1 hour after AII washout, the persistent $[Ca^{2+}]_i$ response lasted throughout the observation. One such example is shown in Fig. 1D.

The pattern of $[Ca^{2+}]_i$ responses were examined with the three other ligands known to act on G-protein-coupled receptors (GPCRs), glutamate, CCh, and AVP, all of which are

reported to evoke a $[Ca^{2+}]_i$ increase in SFO neurons (Izumisawa et al., 2018; Johnson et al., 2001; Jurzak et al., 1995a). As shown in Fig. 1B, $[Ca^{2+}]_i$ responses to all three given at their maximally effective concentrations were transient, and the $[Ca^{2+}]_i$ level returned to the level below 10 % of the peak $[Ca^{2+}]_i$ level within a few to several min after washout. As the amplitude of the $[Ca^{2+}]_i$ increase in response to the five stimuli differed largely from cells to cells, the persistence of the $[Ca^{2+}]_i$ responses was expressed by taking the ratio between the $[Ca^{2+}]_i$ rise above the baseline ($\Delta[Ca^{2+}]_i$) recorded 20 min after washout and $\Delta[Ca^{2+}]_i$ at the peak (Fig. 1C). The ratio of the $[Ca^{2+}]_i$ responses to AII, high K^+, glutamate, CCh and AVP were 0.33 ± 0.06 (n = 11), −008 ± 0.03 (n = 16), 0.05 ± 0.05 (n = 9), −0.04 ± 0.04 (n = 20), and 0.00 ± 0.07 (n = 8), respectively. From these results, it was obvious that only AII caused the persistent $[Ca^{2+}]_i$ response.

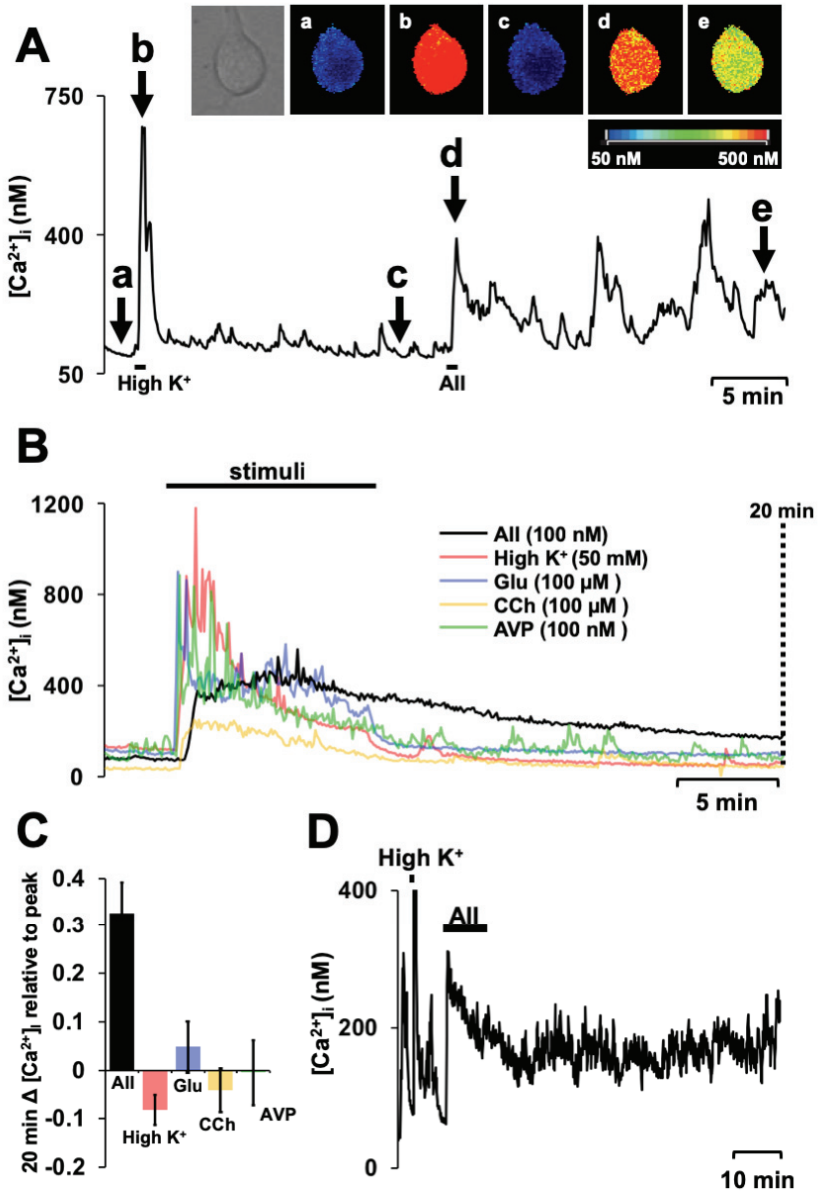

Fig. 1 $[Ca^{2+}]_i$ responses to various stimulus, 100 nM angiotensin II (AII), 50 mM K^+ (high K^+), 100 μM glutamate (Glu), 100 μM carbachol (CCh) and 100 nM arginine vasopressin (AVP), observed in dissociated SFO neurons. **A**, a time course of $[Ca^{2+}]_i$ responses to 50 mM K^+ and AII (100 nM) obtained in a single SFO neuron, with pseudocolor images of the neuron obtained at the timing shown by arrows (a-e). The bright field image of the neuron was shown at leftmost. Pseudocolors represent $[Ca^{2+}]_i$ shown by the color scale bar. Note that in this neuron, $[Ca^{2+}]_i$ came back to the pre-stimulus level quickly after high K^+, but remained high (in this experiment, large oscillations in $[Ca^{2+}]_i$ were observed) for more than 20 min after AII was washed out. **B**, representative examples of $[Ca^{2+}]_i$ responses to the various stimuli. Note that the $[Ca^{2+}]_i$ response to AII was persistent after washout, but that to the other stimuli returned to the basal level after the other simulants were washed out. **C**, summary data for the average of the normalized $\Delta[Ca^{2+}]_i$ recorded 20 min after washout, which was calculated by dividing the $\Delta[Ca^{2+}]_i$ value recorded 20 min after AII washout by the peak $\Delta[Ca^{2+}]_i$ recorded immediately after AII application. The numbers of experiments were 11 (AII), 16 (high K^+), 9 (glu), 20 (CCh), and 8 (AVP). D, representative example of the persistent $[Ca^{2+}]_i$ increase lasted longer than 1h after AII washout.

2.2 Concentration- and exposure-time-dependence of the persistent $[Ca^{2+}]_i$ responses to AII

To examine whether there was concentration-dependency in the persistence of the AII-induced $[Ca^{2+}]_i$ response, AII was administered at concentrations from 10 pM to 100 nM (Fig. 2A). Exposure to 10 pM or 100 pM AII initiated Ca^{2+} oscillations as I have previously reported (Izumisawa et al., 2018), and the amplitude and frequency of the induced oscillations gradually decreased after washout of AII. By contrast, AII at 1, 10 or 100 nM induced rapid and large $[Ca^{2+}]_i$ peak followed by the persistent $[Ca^{2+}]_i$ increase. The ratios of $\Delta[Ca^{2+}]_i$ recorded 20 min after washout and $\Delta[Ca^{2+}]_i$ at the peak measured with the five different concentrations of AII are shown in Fig. 2B. The results indicate that AII given at 1 nM or higher induced the persistent $[Ca^{2+}]_i$ increase.

To examine whether there was exposure-time-dependency in the persistence of the AII-induced $[Ca^{2+}]_i$ response, AII (100 nM) was administered for 30 sec, 1, 3 or 9 min (Fig. 2C). AII administered for as short as 30 sec induced the persistent increase, just as AII given for the longer exposure time. There was no significant difference between the ratios of $\Delta[Ca^{2+}]_i$ recorded 20 min after washout and $\Delta[Ca^{2+}]_i$ at the peak measured with the four different exposure time of AII (Fig. 2D), indicating that 30 sec is long enough to induce the persistent $[Ca^{2+}]_i$ response.

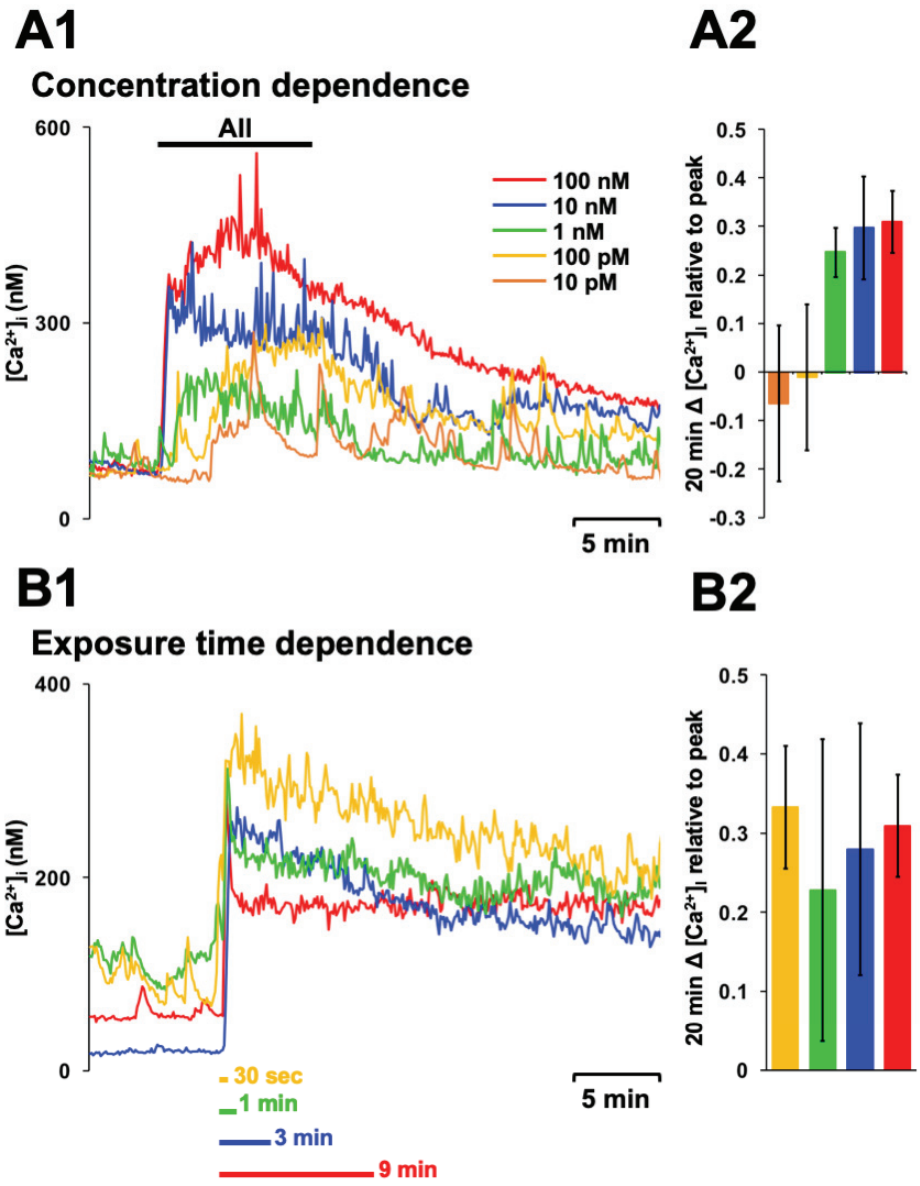

Fig. 2 Concentration- and exposure-time-dependence of the persistent $[Ca^{2+}]_i$ increase induced by AII. **A1**, representative time courses of $[Ca^{2+}]_i$ increases induced by AII at the concentration of 10 pM to 100 nM. **A2**, summary data for the averaged $\Delta[Ca^{2+}]_i$ recorded 20 min after wash out normalized to their peak $[Ca^{2+}]_i$ value. The numbers of experiments were 15 (10 pM), 23 (100 pM), 18 (1 nM), 17 (10 nM), and 11 (100 nM). Note that the persistent $[Ca^{2+}]_i$ increase became obvious with AII at concentrations of 1 nM or higher. **B1**, representative time courses of $[Ca^{2+}]_i$ increases induced by AII (100 nM) administered for 30 sec, 1, 3, and 9 min. **B2**, summary data for the average of the $\Delta[Ca^{2+}]_i$ recorded 20 min after washout normalized to the peak $[Ca^{2+}]_i$ value. The numbers of experiments were 14 (30 sec), 8 (1 min), 14 (3 min), and 11 (9 min). Note that the persistent $[Ca^{2+}]_i$ increase was observed even when AII was administered for 30 sec.

2.3 AII receptor subtype responsible for the persistent $[Ca^{2+}]_i$ response

The subtype of AII receptors responsible for the AII-induced $[Ca^{2+}]_i$ response was examined using the selective antagonists for AT1 and AT2 receptors, losartan and PD123319, respectively (Gebke et al., 1998). Losartan (10 μM) virtually abolished the AII (100 nM)-induced $[Ca^{2+}]_i$ response, and when losartan was removed, a large $[Ca^{2+}]_i$ peak followed by a persistent $[Ca^{2+}]_i$ increase appeared (Fig. 3A1). The peak $\Delta[Ca^{2+}]_i$ values recorded in response to AII (100 nM) in the presence of losartan and after washout of losartan were 35 ± 16 nM and 232 ± 22 nM (n = 8), respectively. Surprisingly, losartan (10 μM) administered during the persistent phase of AII-induced $[Ca^{2+}]_i$ response did not show a significant inhibitory effect: $\Delta[Ca^{2+}]_i$ before ('a' in Fig. 3A1), during ('b' in Fig. 3A1), and after ('c' in Fig. 3A1) the losartan administration were 113 ± 16, 91 ± 15, and 91 ± 14 nM, respectively (n = 8) (Fig. 3A2).

AII (100 nM) administered in the presence of PD123319 (10 μM) induced $\Delta[Ca^{2+}]_i$ peak (135 ± 20 nM, n = 18) followed by a persistent increase (Fig. 3B1). There was no discernible increase upon the removal of PD123319 (n = 18). Moreover, PD123319 (10 μM) administered during the persistent phase of AII-induced $[Ca^{2+}]_i$ response did not cause a significant inhibitory effect: $\Delta[Ca^{2+}]_i$ before ('d' in Fig. 3B1), during ('e' in Fig. 3B1), and after ('f' in Fig. 3B1) the PD123319 administration were 92 ± 12, 85 ± 20, and 97 ± 12 nM, respectively (n = 18) (Fig. 3B2).

2.4 Analysis of the source of Ca^{2+} involved in the persistent $[Ca^{2+}]_i$ increase induced by AII

I and others have reported that the major pathway of the AII-induced $[Ca^{2+}]_i$ response was Ca^{2+} entry though membrane ion channels, but not Ca^{2+} release from intracellular

stores (Gebke et al., 1998; Izumisawa et al., 2018). In this series of experiments, I analyzed the pathway of the persistent $[Ca^{2+}]_i$ increase induced by AII. Extracellular Ca^{2+} removal itself caused no change in the basal $[Ca^{2+}]_i$ of silent neurons but totally abolished AII (100 nM)-induced $[Ca^{2+}]_i$ increase (Fig. 4A). Immediately after Ca^{2+} was restored, $[Ca^{2+}]_i$ quickly increased and maintained a high level. The $\Delta[Ca^{2+}]_i$ in response to AII in the Ca^{2+}-free solution ('a' in Fig. 4A) was 14 ± 59 nM, and the $\Delta[Ca^{2+}]_i$ averaged for 2 min after Ca^{2+} was restored ('b' in Fig. 4A) was 116 ± 80 nM (n = 10). Moreover, extracellular Ca^{2+} removal during the persistent phase of the AII-induced $[Ca^{2+}]_i$ increase profoundly decreased $[Ca^{2+}]_i$ in a reversible manner (Fig. 4B).

The involvement of intracellular Ca^{2+} stores in the persistent $[Ca^{2+}]_i$ increase induced by AII was studied by applying the selective inhibitor of sarco/endoplasmic reticulum Ca^{2+} ATPase (SERCA), cyclopiazonic acid (CPA) to SFO neurons. As reported previously (Izumisawa et al., 2018), CPA (10 μM) caused a consistent increase in the basal $[Ca^{2+}]_i$, but did not inhibit the initial peak nor the persistent $[Ca^{2+}]_i$ increase induced by AII (Fig. 4C1). The initial $[Ca^{2+}]_i$ peak value in the response to AII obtained in the presence of CPA was 511 ± 187 nM (n = 9). The average was nearly two fold larger than that obtained in the absence of CPA, but there was no significant difference. The ratio of $\Delta[Ca^{2+}]_i$ recorded 20 min after washout of AII and $\Delta[Ca^{2+}]_i$ at the peak measured in the presence of CPA was 0.30 ± 0.11 (n = 9) and there was no significant difference between this value and the ratio recorded in the absence of CPA (Fig. 4C2). These results indicate that the Ca^{2+} source for the persistent $[Ca^{2+}]_i$ increase induced by AII was extracellular fluid but not intracellular Ca^{2+} stores.

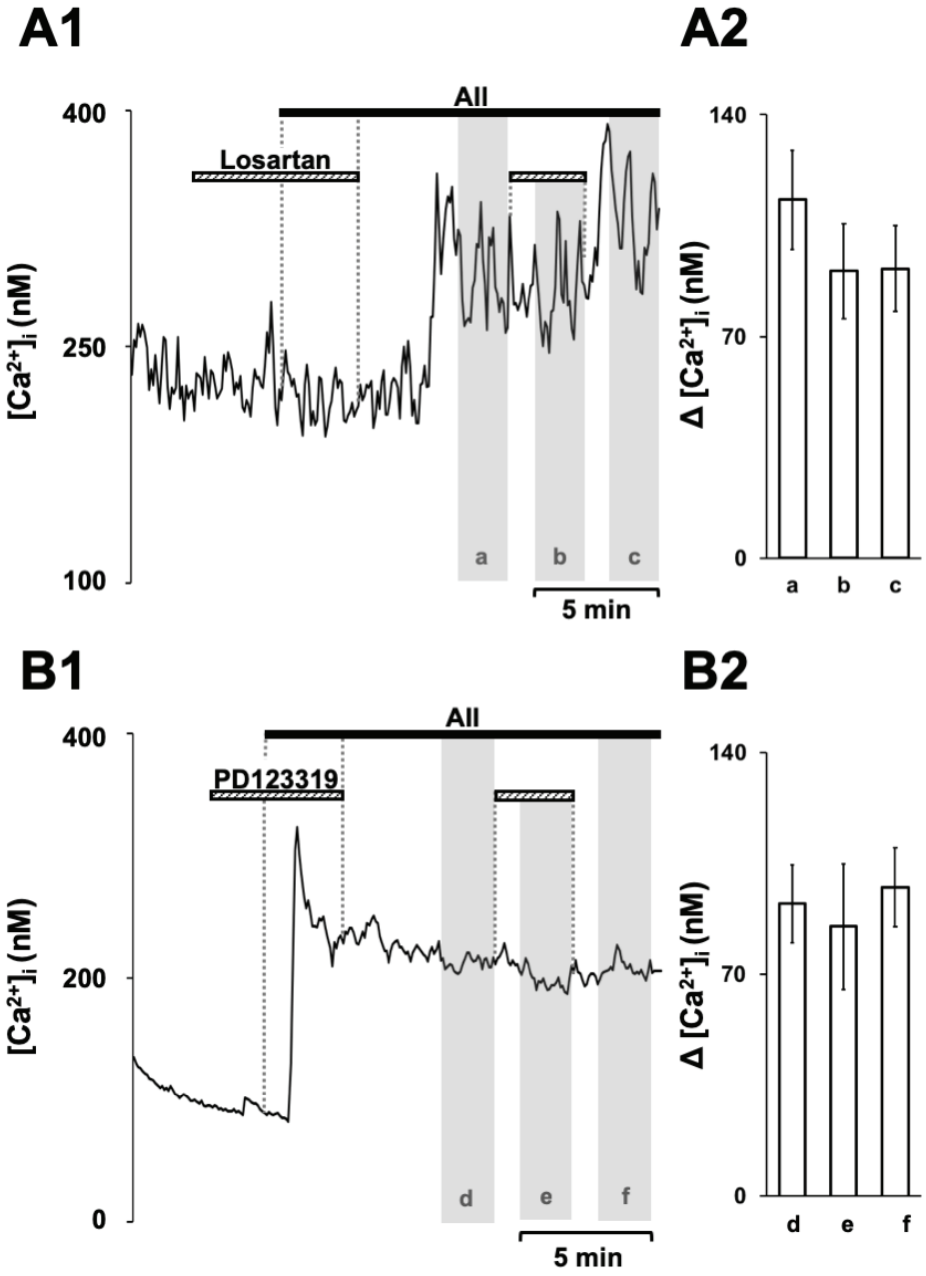

Fig. 3 Effects of selective antagonists for the two angiotensin II receptors, AT1 and AT2, on the AII-induced $[Ca^{2+}]_i$ increase. **A1**, representative time courses of $[Ca^{2+}]_i$ increases induced by AII (100 nM) in the presence of the selective AT1 antagonist, losartan (10 μM). Note that the $[Ca^{2+}]_i$ increases by AII was strongly suppressed in the presence of losartan, and appeared after its washout. Note also that losartan had no effect once the persistent $[Ca^{2+}]_i$ increase was initiated by AII. **A2**, summary data for the $\Delta[Ca^{2+}]_i$ before ('a' in Fig. 3A1), during ('b' in Fig. 3A1), and after ('c' in Fig. 3A1) the losartan administration (n = 8). **B1**, representative time courses of $[Ca^{2+}]_i$ increases induced by AII (100 nM) in the presence of the selective AT_2 antagonist, PD123319 (10 μM). PD123319 had no effect on the AII-induced $[Ca^{2+}]_i$ increase. **B2,** summary data for the $\Delta[Ca^{2+}]_i$ before ('d' in Fig. 3B1), during ('e' in Fig. 3B1), and after ('f' in Fig. 3B1) the PD123319 administration (n = 18).

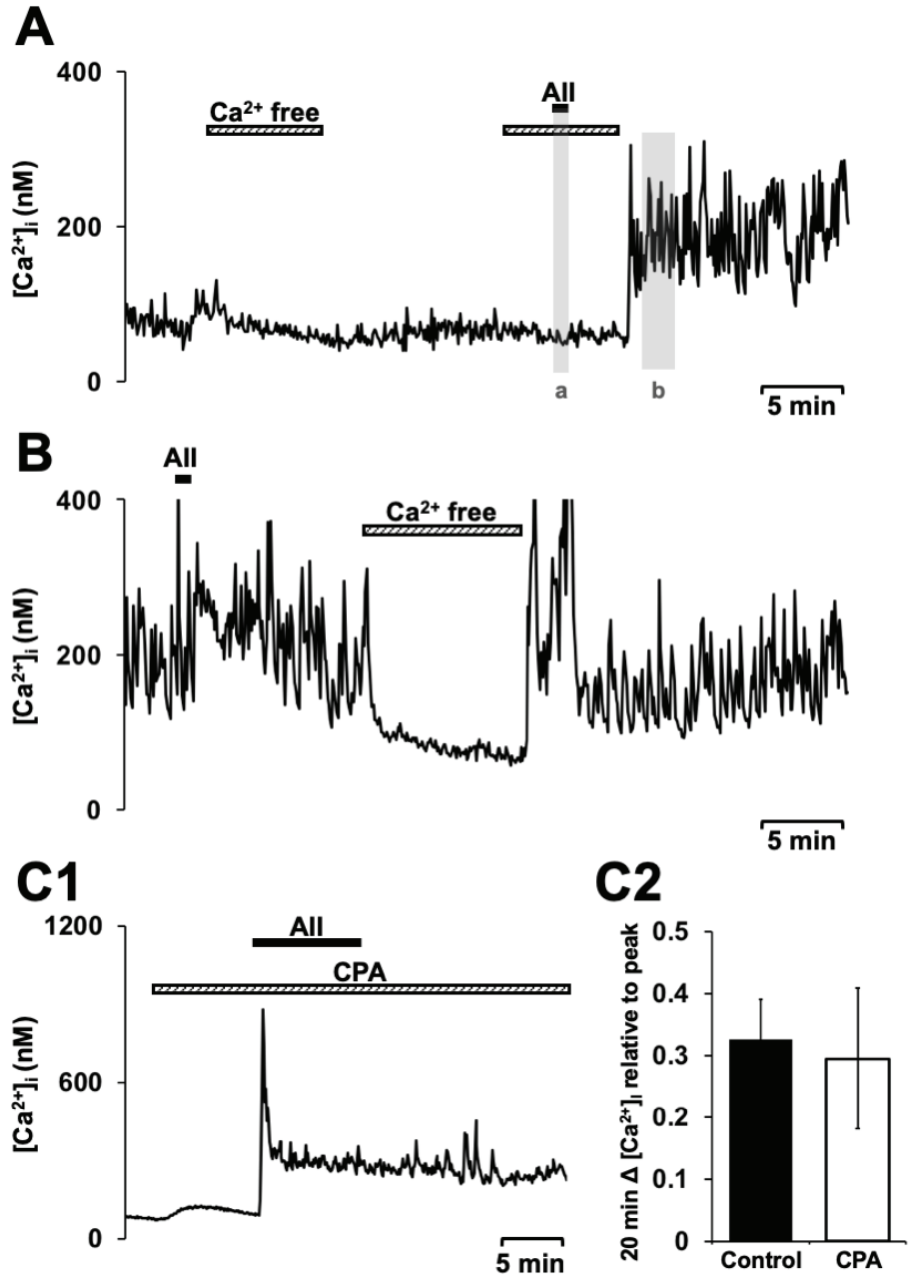

Fig. 4 Effects of extracellular Ca^{2+} removal and inhibition of Ca^{2+} release on the AII-induced $[Ca^{2+}]_i$ increase. **A**, a representative $[Ca^{2+}]_i$ trace showing the effects of extracellular Ca^{2+} removal (nominally Ca^{2+} free) on the basal $[Ca^{2+}]_i$ and AII-induced $[Ca^{2+}]_i$ increase. Extracellular Ca^{2+} removal itself had almost no effect on the basal $[Ca^{2+}]_i$. Note that the AII-induced $[Ca^{2+}]_i$ increase was not observed in the nominally Ca^{2+} free condition, but appeared quickly after extracellular Ca^{2+} was restored. **B**, a representative $[Ca^{2+}]_i$ trace showing the effects of extracellular Ca^{2+} removal on the persistent phase of the AII-induced $[Ca^{2+}]_i$ increase. **C1**, a representative $[Ca^{2+}]_i$ trace showing the effects of the inhibitor of Ca^{2+}-ATPase in the endoplasmic reticulum, cyclopiazonic acid (CPA). CPA caused virtually no effect on the AII-induced $[Ca^{2+}]_i$ increase. **C2**, summary data for the averaged $\Delta[Ca^{2+}]_i$ recorded 20 min after wash out normalized to their peak $[Ca^{2+}]_i$ value with and without CPA. The number of experiments were 9 (CPA). The control bar graph was from Fig. 1C.

2.5 Analysis of membrane ion channels mediating the persistent $[Ca^{2+}]_i$ increase induced by AII

The ionic mechanism of the persistent $[Ca^{2+}]_i$ increase was studied by changing extracellular Ca^{2+} and Na^+ concentrations, and by applying blockers of voltage-gated Na^+ and Ca^{2+} channels to SFO neurons. To minimize an error occurring when I examined effects of these treatments on the persistent phase of the $[Ca^{2+}]_i$ response, which sometimes decayed gradually and the extent and the rate of the decay differed from cell to cell, I used a protocol shown in Fig. 5A, where AII (100 nM) was added twice to a neuron. The second addition of AII induced a similar $[Ca^{2+}]_i$ response to the response to the first AII and there was no obvious desensitization of the $[Ca^{2+}]_i$ response. The averaged $\Delta[Ca^{2+}]_i$ during 3 min (from 3 min to 6 min after washout of AII) in the first ('a' in Fig. 5A) and second ('b' in Fig. 5A) AII were 100 ± 16 nM and 113 ± 20 nM, respectively (n = 6). There was no significant difference between the two values. The effect of each treatment of this series of experiment was examined during this three min period in the second AII application, and the magnitude of inhibition by each treatment was expressed as the relative $\Delta[Ca^{2+}]_i$ value to the first AII response.

Extracellular Na^+ replacement with NMDG profoundly decreased $[Ca^{2+}]_i$ in the persistent phase of the AII-induced $[Ca^{2+}]_i$ response (Fig. 5C), whereas the blocker of voltage-gated Na^+ channels, TTX, had a minor insignificant effect (Fig. 5B).

To identify voltage-gated Ca^{2+} channels responsible for the persistent $[Ca^{2+}]_i$ increase, effects of the selective blockers of voltage-gated Ca^{2+} channels of T-, L-, P/Q- and N-types, Ni^{2+}, nicardipine, ω-agatoxin IVA, and ω-conotoxin GVIA, respectively, and the non-selective blocker, Cd^{2+}, were examined. Nicardipine (10 μM) and ω-agatoxin IVA (100 nM) caused significant effects on $[Ca^{2+}]_i$ in the persistent phase of the AII-induced

$[Ca^{2+}]_i$ response (Fig. 5D). ω-Conotoxin GVIA (1 μM) tended to decrease the $[Ca^{2+}]_i$ level, but the effect was insignificant. Among them, nicardipine caused the largest inhibition (to 51 ± 10 %, n = 33) when applied alone. The cocktail of the three selective blockers inhibited the persistent phase to 34 ± 15 % (n = 38). Cd^{2+} (50 μM) also caused significant effects (Fig. 5E), but Ni^{2+} (50 μM) was without an effect. Fig. 5F summarizes the effects of the blockers and Na^+ replacement.

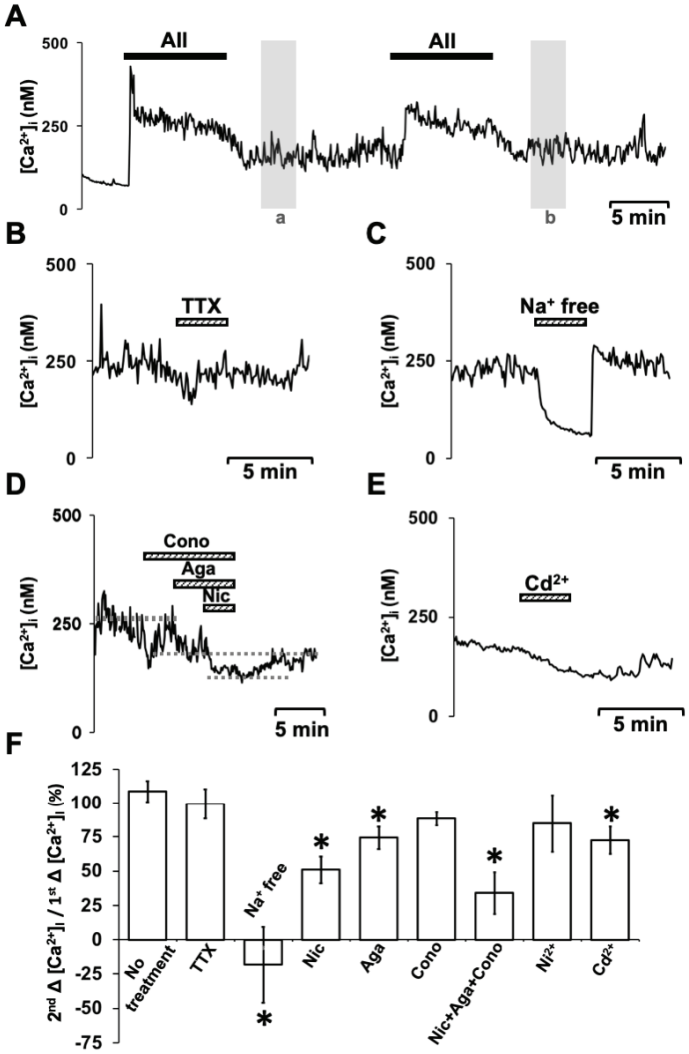

Fig. 5 Effects of blockers of voltage-gated Ca^{2+} and Na^+ channels, and of extracellular Na^+ replacement on the persistent phase of the AII-induced $[Ca^{2+}]_i$ increase. **A**, a representative $[Ca^{2+}]_i$ trace showing $[Ca^{2+}]_i$ responses to repeated exposure to AII (100 nM) for 9 min. Note that the time courses of the AII-induced persistent $[Ca^{2+}]_i$ increase were almost identical between the two responses. In this series of experiment, this protocol was used to examine the effects of the blockers or Na^+ replacement. The effect of each treatment was examined on the second response to AII ('b'), and the inhibition was expressed by the relative value to the first AII response ('a'). **B-E**, representative $[Ca^{2+}]_i$ traces showing effects of the voltage-gated Na^+ channel blocker, TTX (1 μM, **B**), extracellular Na^+ replacement with NMDG (**C**), a cocktail of blockers of voltage-gated Ca^{2+} channels (L, P/Q, and N types, **D**), and the non-selective Ca^{2+} channel blocker, Cd^{2+} (50 μM, **E**). The cocktail of the Ca^{2+} channel blockers contained 10 μM nicardipine (L), 100 nM ω-agatoxin IVA (P/Q), and 1 μM ω-conotoxin GVIA (N). **F**, summary data for the inhibition by Na^+ replacement or the channel blockers on the persistent phase of AII-induced $[Ca^{2+}]_i$ increase. The magnitude of the inhibition by each treatment was calculated by dividing the $\Delta[Ca^{2+}]_i$ during the last 1 min of each 3 min treatment (recorded in the second AII response, as in 'b') by the corresponding control $\Delta[Ca^{2+}]_i$ (recorded in the first AII response, as in 'a'). The total number of neurons analyzed was 6 (no treatment), 12 (TTX), 15 (Na^+ replacement), 33 (nicardipine alone), 14 (agatoxin alone), 13 (conotoxin alone), 38 (the cocktail), 6 (50 μM Ni^{2+}), and 8 (Cd^{2+}). The asterisks represent statistical significance ($p < 0.05$).

2.6 Analysis of intracellular mechanisms involved in the persistent $[Ca^{2+}]_i$ increase induced by AII

It has been reported in cultured hypothalamic neurons, AII activates two protein kinases, CaMK and PKC to modulate neuronal functions (Sumners et al., 2002; Wang et al., 2017; Wayman et al., 2008). In the present study, I analyzed whether these protein kinases were involved in the AII-induced persistent $[Ca^{2+}]_i$ response in SFO neurons. For this purpose, SFO neurons were exposed to the protein kinase inhibitors and then AII (100 nM) was applied in the presence of the inhibitors. KN93 alone did not cause significant changes on the basline $[Ca^{2+}]_i$ level (n = 8). The inhibitor of CaMK, KN93 (10 μM) potently inhibited the AII-induced $[Ca^{2+}]_i$ increase (Fig. 6A1), where the response to AII became transient in the presence of KN93, and when KN93 was washed out there was a rebound rise in $[Ca^{2+}]_i$: $[Ca^{2+}]_i$ increased gradually and reached a plateau, despite that AII was washed out 10 min before the KN93 washout. The inactive analog of KN93, KN92 (10 μM), had little or no effect. The peak $\Delta[Ca^{2+}]_i$ values in the control and AII in the presence of KN93 or KN92 were 227 ± 40 nM (n = 14), 174 ± 25 nM (n = 8) and 192 ± 35 nM (n = 8), respectively. There was no significant difference between these values. The ratios of $\Delta[Ca^{2+}]_i$ recorded during the last 1 min before the washout of the inhibitors ('a' in Fig. 6A1) and the peak $\Delta[Ca^{2+}]_i$ are shown in Fig. 6A2. Only the ratio obtained in the presence of KN93 was significantly smaller than that in the control.

By contrast, the inhibitor of protein kinase C, bisindolylmaleimide I (BIM) (100 nM and 1 μM), had concentration-dependent inhibitory effects on AII-induced $[Ca^{2+}]_i$ increase (Fig. 6B1). BIM alone did not cause significant changes on the basline $[Ca^{2+}]_i$ level (n = 6 for 100 nM, and n = 11 for 1 μM).The peak in the presence of BIM at 100 nM and 1 μM were 237 ± 44 nM (n = 6) and 231 ± 29 nM (n = 11), respectively (Fig.

6B2). Although these peak $\Delta[Ca^{2+}]_i$ values are not significantly different from the values of the control, the ratios of $\Delta[Ca^{2+}]_i$ recorded during the last 1 min before the washout of 1 μM BIM ('b' in Fig. 6B1) and the peak $\Delta[Ca^{2+}]_i$ was significantly smaller those in the control.

Moreover, involvement of phospholipace C (PLC) was also examined, as the AT1 receptor is known to couple with Gq proteins, which is coupled with PLC. AII responses in the presence of the inhibitor of PLC, U-73122 (10 μM), tended to be smaller than those in the control (Fig. 6C1) but there was no significant difference in the peak $\Delta[Ca^{2+}]_i$ value, nor in the ratio of $\Delta[Ca^{2+}]_i$ recorded during the last 1 min before the washout of 10 μM U-73122 ('c' in Fig. 6C1) and the peak $\Delta[Ca^{2+}]_i$ between the control values (Fig. 6C2).

2.7 Effects of GABA on the persistent $[Ca^{2+}]_i$ increase induced by AII

Whether the persistent $[Ca^{2+}]_i$ increase induced by AII is affected by GABA, the primary inhibitory neurotransmitter in the SFO (Honda et al., 2001; Osaka et al., 1992), was also examined. Application of GABA at 10 μM during the persistent phase of the AII-induced $[Ca^{2+}]_i$ increase, profoundly decreased $[Ca^{2+}]_i$ in a reversible manner (Fig. 7A1). GABA decreased $[Ca^{2+}]_i$ to nearly the baseline level and this inhibitory effect lasted as long as the GABA application continued. The magnitude of the GABA-induced inhibition was 23 ± 16 % (n = 16) (Fig. 7A2).

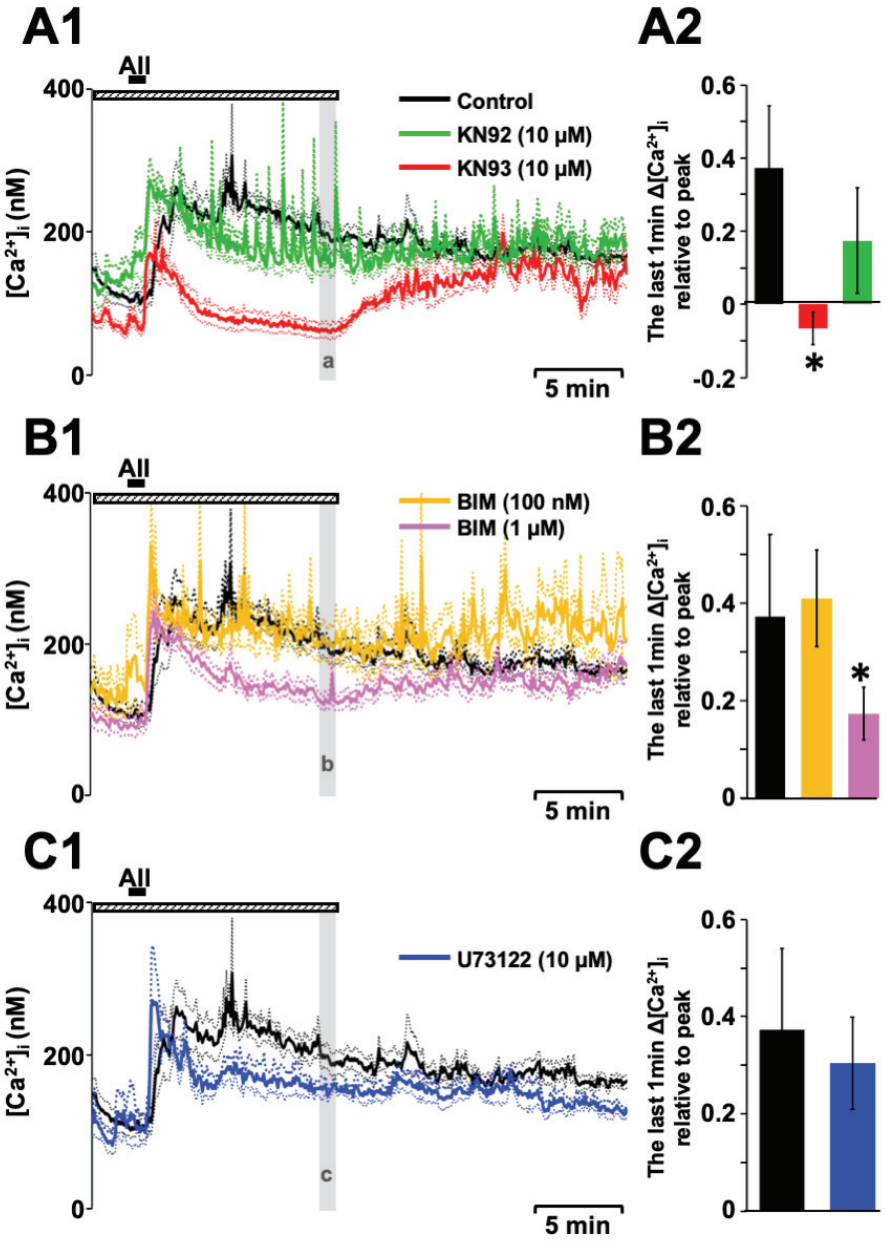

Fig. 6 Effects of inhibitors of protein kinases and phospholipase C on the AII-induced $[Ca^{2+}]_i$ increase. AII (100 nM) was administered for 1 min in this series of experiments. The time courses of $[Ca^{2+}]_i$ changes were shown by the mean ± SEM. A1, responses to AII (100 nM) recorded in the presence of inhibitor of CaMK, KN93 (10 μM), or its inactive analog, KN92 (10 μM), were superimposed on the control response to AII (100 nM). Note that the response to AII became transient in the presence of KN93, and that after KN93 was washed out $[Ca^{2+}]_i$ increased gradually and reached a persistent plateau. The numbers of the experiments are 16 (control), 8 (KN93) and 8 (KN92). A2, summary data for the effects of KN93 and KN92 on the AII-induced $[Ca^{2+}]_i$ increase. The magnitude of the inhibitory effects was expressed as the ratios of $\Delta[Ca^{2+}]_i$ recorded during the last 1 min before the washout of KN93 or KN92 ('a' in Fig. 6A1) and the peak $\Delta[Ca^{2+}]_i$. The asterisk represents statistical significance between the control value ($p < 0.05$).

B1, responses to AII (100 nM) recorded in the presence of the inhibitor of protein kinase C, bisindolylmaleimide I (BIM) (100 nM and 1 μM) (n = 6 and 11). The control response shown in A is superimposed. B2, summary data for the effects of BIM at 100 nM and 1 μM on the AII-induced $[Ca^{2+}]_i$ increase. The magnitude of the effects was expressed as the ratios of $\Delta[Ca^{2+}]_i$ recorded during the last 1 min before the washout of BIM (100 nM and 1 μM) ('b' in Fig. 6B1) and the peak $\Delta[Ca^{2+}]_i$. The asterisk represents statistical significance between the control value ($p < 0.05$). C1, responses to AII (100 nM) recorded in the presence of the inhibitor of phospholipase C, U-73122 (10 μM) (n = 6). The control response shown in A is superimposed. C2, summary data for the effects of U73122 on the AII-induced $[Ca^{2+}]_i$ increase. The magnitude of the effects was expressed as the ratio of $\Delta[Ca^{2+}]_i$ recorded during the last 1 min before the washout of U-73122 (10 μM) ('c' in Fig. 6C1) and the peak $\Delta[Ca^{2+}]_i$. 1 μM on the AII-induced $[Ca^{2+}]_i$ increase. The magnitude of the effects was expressed as the ratios of $\Delta[Ca^{2+}]_i$ recorded during the last 1 min before the washout of BIM (100 nM and 1 μM) ('b' in Fig. 6B1) and the peak $\Delta[Ca^{2+}]_i$. The asterisk represents statistical significance between the control value ($p < 0.05$). C1, responses to AII (100 nM) recorded in the presence of the inhibitor of phospholipase C, U-73122 (10 μM) (n = 6). The control response shown in A is superimposed. C2, summary data for the effects of U73122 on the AII-induced $[Ca^{2+}]_i$ increase. The magnitude of the effects was expressed as the ratio of $\Delta[Ca^{2+}]_i$ recorded during the last 1 min before the washout of U-73122 (10 μM) ('c' in Fig. 6C1) and the peak $\Delta[Ca^{2+}]_i$.

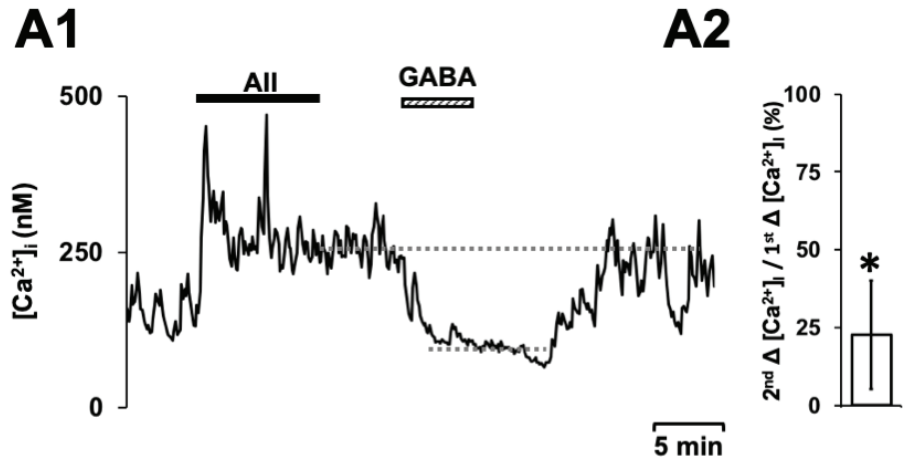

Fig. 7 Effects of the primary inhibitory neurotransmitter in the SFO, GABA, on the persistent phase of the AII-induced $[Ca^{2+}]_i$ increase. AII was administered twice just as in Fig. 5, and the magnitude of the inhibition was calculated by dividing the $\Delta[Ca^{2+}]_i$ during the last 3 min of the 5 min treatment with GABA (recorded in the second AII response) by the corresponding control $\Delta[Ca^{2+}]_i$ (recorded in the first AII response). A1, the persistent phase was strongly suppressed by application of GABA at 10 μM with a reversibly manner. A2, summary data for the inhibition by GABA on the persistent phase of AII-induced $[Ca^{2+}]_i$ increase (n = 16). The asterisk represents statistical significance ($p < 0.05$).

3. Discussion

3.1 The persistent $[Ca^{2+}]_i$ increase induced by Angiotensin II

In the present study, I have found that AII at the concentration of 1 nM or higher induces a sharp $[Ca^{2+}]_i$ rise followed by a persistent $[Ca^{2+}]_i$ increase in acutely dissociated SFO neurons. AII given at picomolar concentrations induced Ca^{2+} oscillations, which lasted for several min. However, the averaged $[Ca^{2+}]_i$ returned to the basal level after washout of picomolar concentrations of AII, which is consistent with the results presented in Chapter 1 (Izumisawa et al., 2018). The persistent phase lasted as long as observations in most SFO neurons. Moreover, none of the other stimuli I used in the present study, high K^+, glutamate, CCh and AVP, caused a similar persistent $[Ca^{2+}]_i$ increase. As the latter three are known to activate metabotropic mechanisms in neurons in the CNS, it is likely that the persistent $[Ca^{2+}]_i$ increase is specific for AII and its receptor downstream.

3.2 The mechanisms of the persistent $[Ca^{2+}]_i$ increase induced by AII

3.2.1 Receptor

It has been reported that the receptor subtype mediating the $[Ca^{2+}]_i$-raising effects of AII was blocked by the AT1 antagonist, losartan (Gebke et al., 1998). The present results that the initial $[Ca^{2+}]_i$ peak evoked by AII was blocked by losartan, and that it could be observed in the presence of the AT2 antagonist, PD123319, are consistent with the previous result. Moreover, PD123319 was without a significant inhibitory effect on the persistent $[Ca^{2+}]_i$ increase of the AII response. Taken together, these results indicate that both the initial peak and the persistent phase are due to AT1 receptor activation. However, losartan administered during the persistent phase did not reduce $[Ca^{2+}]_i$ significantly, indicating that once the persistent $[Ca^{2+}]_i$ response is initiated, activation of the AT1

receptor is no longer necessary to maintain the persistent $[Ca^{2+}]_i$ increase. This could be due to lingering metabotropic effects induced by AT1-receptor activation. It has been reported that phosphorylation of various intracellular proteins by several protein kinases is triggered in the downstream of the AT1 receptor (Higuchi et al., 2007; Kawai et al., 2017; Sumners et al., 2002).

3.2.2 Membrane channels

The persistent phase of the AII-induced $[Ca^{2+}]_i$ response was potently and rapidly suppressed by extracellular Ca^{2+} omission, but unaffected by CPA, indicating the persistent $[Ca^{2+}]_i$ increase is entirely dependent on Ca^{2+} entry through membrane channels and independent of Ca^{2+} release from intracellular Ca^{2+} stores. This is interesting, because the consistent $[Ca^{2+}]_i$-raising response to CPA observed in SFO neurons indicates that these neurons possess intracellular Ca^{2+} stores, and the AT1 receptor is known to be commonly coupled with the Gq/PLC/IP_3 pathway in CNS neurons (Seltzer et al., 1995; Verkhratsky, 2002). The reason why IP_3-dependent Ca^{2+} release was not evident in the AII-induced $[Ca^{2+}]_i$ response could be that Ca^{2+} stores in SFO neurons have small capacity, or Ca^{2+} stores are in separate intracellular compartment. This remains to be studied.

The results that the persistent phase was little affected by TTX and profoundly suppressed by Na^+ replacement suggest that some Na^+-permeating channels, but not TTX-sensitive voltage-gated Na^+ channels are involved in the persistent phase. Although TTX-insensitive voltage-gated Na^+ channels have not been found in SFO neurons, atypical Na^+ channels, Na_x channels, which have poor structural homology to voltage-gated Na^+ channels, are reported to function in the detection of Na^+ in SFO tissues

(Hiyama and Noda, 2016). However, several lines of evidence suggest that Na_x channels are expressed in SFO glial cells (Shimizu et al., 2007). It has been also reported that AII induced long-lasting depolarization and activated non-selective cation channels in SFO neurons (Ono et al., 2001). As non-selective cation channels belonging to the Transient Receptor Potential (TRP) channel superfamily are known to be activated by Gq-coupled receptors (Sharif-Naeini et al., 2010) and AII receptors are reported to activate TRP channels in peripheral tissues (Storch et al., 2012), the effects of AII reported in SFO neurons could be mediated by TRP channels. Taken together, it is suggested that persistent depolarization due to activation of non-selective cation channels by AII activated voltage-gated Ca^{2+} channels (VGCC), resulting in the persistent increase in $[Ca^{2+}]_i$. The result that TTX had insignificant effects on the persistent phase is not surprising because voltage-gated Na^+ channels (VGSC) may be inactivated during the long-lasting depolarization due to such Na^+-permeating channels.

There is another mechanism by which AII can modulate membrane potentials of SFO neurons: it is reported that AII inhibited outwardly rectifying K^+ currents (Ferguson and Li, 1996). Moreover, it is also reported that AII selectively potentiated voltage-gated Ca^{2+} currents of L- and N-types in voltage-clamp experiments (Wang et al., 2013; Washburn and Ferguson, 2001), suggesting that AII may enhance Ca^{2+} entry through these multiple ion channel mechanisms. The present results indicate that not only L-types, but also P/Q-type Ca^{2+} channels are involved in the persistent phase of AII-induced $[Ca^{2+}]_i$ response, and that L-type Ca^{2+} channels contribute most to the response. It could be that long-lasting depolarization induced by AII favored L-type channels because this type is known to have much slower inactivation than the other types (Dolphin, 2009). The present results showed that the persistent $[Ca^{2+}]_i$ increase appeared after restoring extracellular Ca^{2+},

even though AII was washed out three min before the Ca^{2+} restoration. As Ca^{2+} restoration without adding AII did not cause such persistent $[Ca^{2+}]_i$ increase, this $[Ca^{2+}]_i$ increase again suggest a lingering effect of AT1 receptor activation. It could be that when the AT1 receptor activates some intracellular metabotropic mechanisms that lead to the persistent $[Ca^{2+}]_i$ increase, some kind of auto-regenerative process may be set.

3.2.3 Intracellular signaling mechanisms

The present results that the AII-induced $[Ca^{2+}]_i$ increase became transient in the presence of KN93, but unaffected by its inactive analog, KN92, suggest that the AII-induced $[Ca^{2+}]_i$ increase can be separated into two independent processes: the 1st initial phase (causing a sharp $[Ca^{2+}]_i$ peak) and the following 2nd persistent phase. While the former is independent of CaMK, and the latter is dependent of phosphorylation by CaMK. The initial phase may be explained by the reported actions of AT1 receptor activation, such as non-selective cation channel activation, K^+ channel inhibition and Ca^{2+} channel potentiation (Ferguson and Li, 1996; Wang et al., 2013; Washburn and Ferguson, 2001).

CaMK is a multifunctional protein kinase and highly expressed in neuronal cells in the CNS. It is known to play various important roles such as synaptogenesis, memory formation, and neuronal development (Wayman et al., 2008). It is reported that CaMKII is autophosphorylated via Ca^{2+}/calmodulin binding in response to a rise in $[Ca^{2+}]_i$, and can be continuously activated even after $[Ca^{2+}]_i$ is lowered (Coultrap and Bayer, 2012). This property of CaMKII may explain the lingering feature of the persistent phase of the AII-induced $[Ca^{2+}]_i$ response observed in the present study. Another interesting finding in the present study was that after washout of KN93, a rebound rise in $[Ca^{2+}]_i$ was observed even though AII was washout 10 min before. This is the third evidence that AII

has a long-lasting lingering effect. As the persistent phase of the AII-induced $[Ca^{2+}]_i$ response was quickly and reversibly suppressed by extracellular Ca^{2+} removal (Fig. 4A), the target of CaMK-mediated phosphorylation may be the Ca^{2+} entry mechanism itself. In fact, it is reported that CaMKII phosphorylates membrane ion channels such as voltage-gated Ca^{2+} channels, cation channels, and other ion channels to modify neuronal functions (Wang et al., 2017; Wayman et al., 2008). It appears that the AT1 receptor activates voltage-dependent Ca^{2+} entry mechanisms (this forms the initial phase of the AII-response), and the resultant $[Ca^{2+}]_i$ response activates Ca^{2+}-dependent kinases such as CaMK, which in turn, augments the Ca^{2+} entry mechanisms through phosphorylation to make the $[Ca^{2+}]_i$ response persistent.

The present result also showed that BIM, a PKC inhibitor, inhibited the persistent phase of the AII-induced $[Ca^{2+}]_i$ response in a concentration-dependent manner. Our result is consistent with a previous *in vivo* study reporting that PKC within SFO is necessary for fluid intake in response to AII (Coble et al., 2014), and suggests that PKC may also be involved in the persistent response. It has been reported that AII-induced excitation as well as AII-induced inhibition of K^+ channels are medicated by both CaMK and PKC in hypothalamic neurons (Wang et al., 1996). It is possible that similar phosphorylation-mediated mechanisms exist in the downstream of the AT1 receptor in the two different groups of CNS neurons.

Although U73122, an inhibitor of PLC, tended to decrease the persistent phase of the AII-induced $[Ca^{2+}]_i$ response, there was no significant difference between the $[Ca^{2+}]_i$ averaged for the last 1 min of U73122 treatment relative to the peak $[Ca^{2+}]_i$ in the presence and absence of U73122. This could be interpreted to mean that in SFO neurons, the AT1 receptor coupled with Gq mainly activate intracellular signaling mechanisms

other than PLC. The lack of $[Ca^{2+}]_i$ response to AII in the absence of extracellular Ca^{2+} suggests that IP_3-induced Ca^{2+} release from internal Ca^{2+} stores is below the detection level in SFO neurons, and support this view. Another possibility is that PLC in SFO neurons could be relatively insensitive to the inhibition by U73122, as the concentration of U73122 I used in the present study was 10 μM, which potently suppressed PLC-mediated responses in other neuronal preparations (Sabatier et al., 1998; Zhao et al., 2011). This point remains to be elucidated.

Although I have currently no firm evidence for the question why only AII activates such persistent $[Ca^{2+}]_i$ response, there are several possibilities. It could be a difference in the signal transduction mechanisms, for example, the AT1 receptor could activate more efficiently processes that are essential to the persistent $[Ca^{2+}]_i$ response. It could also be a difference in the subcellular localization of the receptor and the intracellular machinery linked to the receptor including protein kinases. The AT1 receptor could be localized to a subcellular compartment where the intracellular machinery more efficiently linked to the receptor. The question should be answered in future studies comparing the precise intracellular signal transduction mechanisms of the receptor ligands tested in this study.

3.3 Physiological and Pathophysiological significance of the persistent $[Ca^{2+}]_i$ increase

The result that the primary inhibitory neurotransmitter in the SFO, GABA reversibly inhibited the persistent $[Ca^{2+}]_i$ increase indicates that although the persistent increase lasted for as long as more than one hour, it is stoppable by the physiological ligand. GABA may be acting on $GABA_A$ receptors and hyperpolarizing the membrane potential to the chloride equilibrium potential, thereby inhibiting the voltage-dependent Ca^{2+} entry. The result further suggests that the $[Ca^{2+}]_i$ increase is not due to an irreversible increase

in the permeability of the plasma membrane or mitochondria membrane for Ca^{2+}, which is known to occur in some pathological conditions (Giorgio et al., 2018; Martin and Bernard, 2018; Morris et al., 2018).

The plasma concentration of AII in normal rats is reported to be approximately 5 pM (Bunkenburg et al., 1991) and 40 pM (Wilcox and Dzau, 1992). It increased in dehydrated rats to approximately 150 pM (Navar et al., 1994). Another study in spontaneously hypertensive rats (SHR) reported that the AII concentration reached about 400-600 pM (Castro-Moreno et al., 2012). In humans, it is reported that the AII concentration of normal subjects was around 50 pM but that of patients with hypertension could be higher than 300 pM (Arnold et al., 2013; Catt et al., 1971; Jalil et al., 2003; Zong et al., 2015). These results indicate that the plasma AII concentration rises to a high concentration approaching 1 nM in pathophysiological conditions. The present results suggest that the threshold AII concentration that induces the persistent $[Ca^{2+}]_i$ response may be between 100 pM and 1 nM. If the plasma AII concentration reaches a level as high as the threshold concentration, even for a short period, it could initiate the persistent $[Ca^{2+}]_i$ increase. A high $[Ca^{2+}]_i$ could potently modulate various Ca^{2+}-dependent processes, such as neuronal plasticity, gene expression and cell death (Augustine et al., 2003). Particularly, the L-type Ca^{2+} channel, the importance of which in the persistent $[Ca^{2+}]_i$ increase was revealed in the present study, is known to play a major role in sending the signal from the plasma membrane to the nucleus (Deisseroth et al., 2003).

Long-term changes in synaptic transmission, synaptic plasticity, has been observed in many brain regions (Huganir and Nicoll, 2013). In addition to such synaptic changes, strong stimulation could lead to the persistent changes in intrinsic excitability, which is called the intrinsic plasticity, via changes in the activities of some types of channels (Frick

et al., 2004; Ohtsuki et al., 2012; Shim et al., 2018; Yang and Santamaria, 2016). Because I observed in the present study that a short period of AII stimulation leads to a persistent Ca^{2+} entry through VGCC, this phenomenon itself may be considered as a type of plasticity. Given that plasticity could rely on mechanisms showing threshold behavior (Kim et al., 2017; Tanaka et al., 2007), all-or-none-like concentration dependency of AII seems to also support this idea.

It may be worth of note that using manganese-enhanced magnetic resonance imaging (MEMRI), neuronal activation of the paraventricular nucleus (PVN) of the hypothalamus in response to AII injection to rats lasted for 24 hours (Zubcevic et al., 2017). In that study, the site of the initial AII action was not clear, and could be through synaptic activation through the neural circuits via SFO converging at the PVN. As the present results of the persistent $[Ca^{2+}]_i$ response to AII was obtained in isolated SFO neurons, where synaptic inputs or other cell-to-cell communication from surrounding cells can be excluded, the mechanism should be intrinsic to SFO neurons. Therefore, it is possible that SFO neurons, after sensing an increase in the AII concentration in the systemic circulation, send the excitatory signal to the PVN and other areas of the brain to modulate cardiovascular or other functions.

3.4 Conclusions

The present study revealed that AII at 1 nM or higher induces a persistent $[Ca^{2+}]_i$ increase lasting for more than 1 hour in acutely dissociated SFO neurons, and the persistent $[Ca^{2+}]_i$ increase was not induced after large $[Ca^{2+}]_i$ increases induced by high K^+ or the ligands of Gq-coupled receptors, glutamate, AVP and carbachol. The results suggest that AII-induced $[Ca^{2+}]_i$ increase is AT1 receptor-mediated, and the persistent

phase was maintained by Ca^{2+} entry. The Ca^{2+} entry may be maintained by long-lasting depolarization due to cation channel activation, and mediated, at least in part, byVGCCs of L and P/Q types. It was also demonstrated that CaMK and PKC are involved in the persistent $[Ca^{2+}]_i$ increase. The primary inhibitory neurotransmitter, GABA, reversibly inhibited the AII-induced persistent $[Ca^{2+}]_i$ increase, suggesting that the persistent increase is inhibitable by physiological ligands. The persistent $[Ca^{2+}]_i$ increase induced by AII at nanomolar concentrations may have a role in physiology and/or pathophysiology of SFO neurons.

4. Graphical abstract

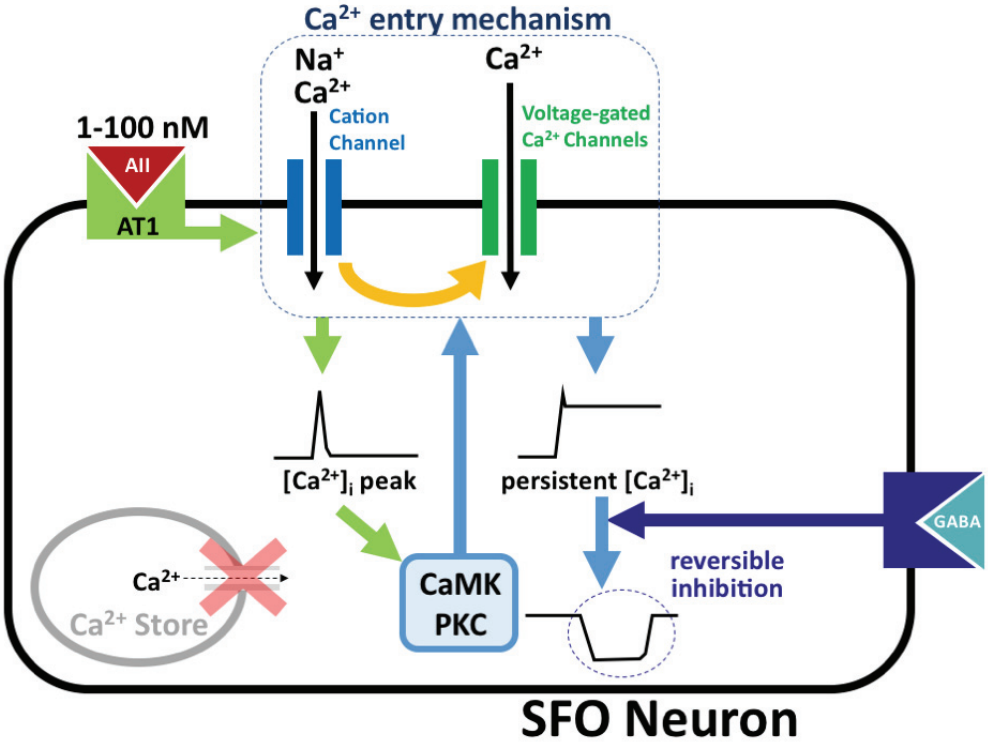

5. Experiment procedure

5.1 Solution

The standard solution used for dissociation and perfusion of SFO neurons was HEPES-buffered solution (HBS) containing (mM) NaCl, 140; KCl, 5; $CaCl_2$, 2; $MgCl_2$,1; glucose, 10 and HEPES, 10 (pH adjusted to 7.4 with Tris). For extracellular Ca^{2+}-free experiments, HBS without adding $CaCl_2$ was used, and for extracellular Na^+-free experiments, Na^+ was replaced with equimolar N-methyl-D-glucamine.

5.2 Dissociation of SFO neurons

Dissociated SFO neurons were prepared as previously described (Shibuya et al., 1998). All experiments were carried out under the control of the Ethics Committee of Animal Care and Experimentation, Tottori University, Japan. In brief, young male Wistar rats (three to four weeks of age) were deeply anesthetized with isoflurane, and SFO tissues were cut from the brain in ice-cold HBS. The SFO tissues were incubated in HBS containing pronase (Sigma, 2.3 mg/1.5 ml) for 25 min and then in a solution containing thermolysin (Sigma, 2 mg/1 ml) and DNAse (Sigma, 56 μg/50 μl) for 20 min, at 30~32 °C. The tissues were then transferred to an enzyme-free HBS and mechanically dissociated by trituration with fire-polished glass pipettes. Cells were plated onto coverslips (11mm in diameter, 0.12mm thick). The dissociated cells were incubated in oxygenated HBS solution for 40 min at room temperature (~23 °C) before loading with fura-2.

5.3 $[Ca^{2+}]_i$ measurement

The $[Ca^{2+}]_i$ in SFO neurons was measured with fura-2 according to the procedure that

I reported previously (Izumisawa et al, 2018). For fura-2 loading, dissociated SFO cells were incubated in HBS with the addition of acetoxymethyl esters of fura-2 (fura-2/AM, 1 μM) for 60 min at room temperature. The cells were then washed by perfusing with dye-free HBS before measurements of $[Ca^{2+}]_i$.

The arrangements for measuring fluorescence have been described previously (Moriya et al., 2015; Shibuya et al., 1998). In brief, cells were continuously perfused with HBS in a small volume chamber (approximately 200 μl) that had a glass coverslip bottom and that was positioned on the stage of an inverted microscope (IX71, Olympus, Tokyo, Japan). A complete change of the solution in the chamber in a few seconds at a perfusion rate of 1.5 ml/min by using peristaltic pump (Minipuls 3, Gilson, Middle- ton, WI, USA). Fluorescence images with excitation at 340 and 380 nm were recorded at 5 s intervals unless otherwise noted with CCD camera systems (AquaCosmos, Hamamatsu Photonics, Hamamatsu, Japan). The ratio of fluorescence for each pixel obtained with excitation at 340 and 380 nm (F340/F380) was used to calculate $[Ca^{2+}]_i$. A calibration curve of $[Ca^{2+}]_i$ for F340/F380 was determined using a regression curve obtained from measurements with free-acid fura-2 dissolved in series of Ca^{2+}-buffered solutions containing 0, 17, 38, 65, 100, 150, 225, 351, 602, 1350, and 39000 nM free Ca^{2+} (Life technologies, Carlsbad, CA, USA). To estimate $[Ca^{2+}]_i$ in individual cells, regions of interest (ROIs) were chosen to include the soma of each SFO cell, and average values of $[Ca^{2+}]_i$ in pixels contained in each ROI were calculated. All experiments were performed at room temperature (~23 °C).

The baseline $[Ca^{2+}]_i$ in each cell was determined by calculating the average $[Ca^{2+}]_i$ at the beginning of measurement in cells showing little or no spontaneous activity and by calculating the lowest $[Ca^{2+}]_i$ value during inter-oscillation periods in cells showing

spontaneous Ca^{2+} oscillations. Cells showing $[Ca^{2+}]_i$ responses to 50 mM K^+ that are larger than 100 nM from the baseline were regarded as healthy neurons and were used for further analysis. An increase in $[Ca^{2+}]_i$ larger than 30 nM was regarded as a meaningful response, to exclude interference from the noise of the fluorescence signal. Repeated $[Ca^{2+}]_i$ elevations larger than 30 nM were regarded as Ca^{2+} oscillations, and consequently the frequency was calculated by considering the $[Ca^{2+}]_i$ elevations larger than 30 nM as one peak during Ca^{2+} oscillations. The amplitude of $[Ca^{2+}]_i$ responses was expressed as $\Delta[Ca^{2+}]_i$, which was calculated by subtracting the average $[Ca^{2+}]_i$ before drug application from the peak $[Ca^{2+}]_i$ amplitude detected after the onset of drug application.

5.4 Drugs

Angiotensin II, arginine vasopressin (AVP), ω-conotoxin GVIA, ω-agatoxin IVA, and ω-conotoxin MVIIC were purchased from Peptide Institute (Osaka, Japan); TTX was from Nacalai Tesque (Kyoto, Japan); nicardipine, BIM, and U73122 were from Sigma-Aldrich (St. Louis, MO); PD123319 was from Cayman Chemical Company (Michigan, USA); KN-92 was from Merck (Darmstadt, Germany); fura-2/AM was from Dojindo (Kumamoto, Japan); isoflurane was from Pfizer (Tokyo, Japan); other drugs were of analytical grade from Fujifilm Wako Pure Chemical Co. (Osaka, Japan).

5.5 Statistics

All values are expressed as the mean ± SEM, and 'n' represents the number of neurons examined. A P value of < 0.05 using Student's t-test was considered statistically significant.

6. References

Arnold, A.C., Okamoto, L.E., Gamboa, A., Shibao, C., Raj, S.R., Robertson, D., Biaggioni, I., 2013. Angiotensin II, independent of plasma renin activity, contributes to the hypertension of autonomic failure. Hypertension. 61**,** 701-6.

Augustine, G.J., Santamaria, F., Tanaka, K., 2003. Local calcium signaling in neurons. Neuron. 40**,** 331-346.

Bunkenburg, B., Schnell, C., Baum, H.P., Cumin, F., Wood, J.M., 1991. Prolonged angiotensin-ii antagonism in spontaneously hypertensive rats - hemodynamic and biochemical consequences. Hypertension. 18**,** 278-288.

Castro-Moreno, P., Pardo, J.P., Hernandez-Munoz, R., Lopez-Guerrero, J.J., Del Valle-Mondragon, L., Pastelin-Hernandez, G., Ibarra-Barajas, M., Villalobos-Molina, R., 2012. Captopril avoids hypertension, the increase in plasma angiotensin II but increases angiotensin 1-7 and angiotensin II-induced perfusion pressure in isolated kidney in SHR. Auton Autacoid Pharmacol. 32**,** 61-9.

Catt, K.J., Cran, E., Zimmet, P.Z., Best, J.B., Cain, M.D., Coghlan, J.P., 1971. Angiotensin II blood-levels in human hypertension. Lancet. 1**,** 459-64.

Coble, J.P., Johnson, R.F., Cassell, M.D., Johnson, A.K., Grobe, J.L., Sigmund, C.D., 2014. Activity of protein kinase C-alpha within the subfornical organ is necessary for fluid intake in response to brain angiotensin. Hypertension. 64**,** 141-8.

Cottrell, G.T., Ferguson, A.V., 2004. Sensory circumventricular organs: central roles in integrated autonomic regulation. Regul. Pept.117**,** 11-23.

Coultrap, S.J., Bayer, K.U., 2012. CaMKII regulation in information processing and storage. Trends Neurosci. 35**,** 607-18.

Deisseroth, K., Mermelstein, P.G., Xia, H., Tsien, R.W., 2003. Signaling from synapse to nucleus: the logic behind the mechanisms. Curr Opin Neurobiol. 13**,** 354-65.

Dellmann, H.D., 1998. Structure of the subfornical organ: A review. Microsc Res Tech. 41**,** 85-97.

Dolphin, A.C., 2009. Calcium channel diversity: multiple roles of calcium channel subunits. Curr. Opin. Neurobiol. 19**,** 237-244.

Felix, D., Akert, K., 1974. The effect of angiotensin II on neurones of the cat subfornical organ. Brain Res. 76**,** 350-3.

Ferguson, A.V., Li, Z.H., 1996. Whole cell patch recordings from forebrain slices demonstrate angiotensin II inhibits potassium currents in subfornical organ neurons. Regul. Pept. 66**,** 55-58.

Fitzsimons, J.T., 1998. Angiotensin, thirst, and sodium appetite. Physiol. Rev. 78**,** 583-686.

Frick, A., Magee, J., Johnston, D., 2004. LTP is accompanied by an enhanced local excitability of pyramidal neuron dendrites. Nat Neurosci. 7**,** 126-35.

Gebke, E., Muller, A.R., Jurzak, M., Gerstberger, R., 1998. Angiotensin II-induced calcium signalling in neurons and astrocytes of rat circumventricular organs. Neuroscience. 85**,** 509-520.

Giorgio, V., Guo, L., Bassot, C., Petronilli, V., Bernardi, P., 2018. Calcium and regulation of the mitochondrial permeability transition. Cell Calcium. 70**,** 56-63.

Gross, P.M., 1992. Circumventricular organ capillaries. Progress in Brain Research. 91**,** 219-233.

Gutman, M.B., Ciriello, J., Mogenson, G.J., 1988. Effects of plasma angiotensin II and hypernatremia on subfornical organ neurons. Am. J. Physiol., Cell Physiol. 254**,** R746-R754.

Higuchi, S., Ohtsu, H., Suzuki, H., Shirai, H., Frank, G.D., Eguchi, S., 2007. Angiotensin II signal transduction through the AT_1 receptor: novel insights into mechanisms and pathophysiology. Clin Sci (Lond). 112**,** 417-28.

Hiyama, T.Y., Noda, M., 2016. Sodium sensing in the subfornical organ and body-fluid homeostasis. Neurosci Res. 113**,** 1-11.

Honda, E., Xu, S., Ono, K., Ito, K., Inenaga, K., 2001. Spontaneously active GABAergic interneurons in the subfornical organ of rat slice preparations. Neurosci Lett. 306**,** 45-8.

Huganir, R.L., Nicoll, R.A., 2013. AMPARs and synaptic plasticity: the last 25 years. Neuron. 80**,** 704-17.

Izumisawa, Y., Tanaka-Yamamoto, K., Ciriello, J., Kitamura, N., Shibuya, I., 2018. The cytosolic Ca^{2+} concentration in acutely dissociated subfornical organ (SFO) neurons of rats: spontaneous Ca^{2+} oscillations and Ca^{2+} oscillations induced by picomolar concentrations of angiotensin II. Brain Res.

Jalil, J.E., Palomera, C., Ocaranza, M.P., Godoy, I., Roman, M., Chiong, M., Lavandero, S., 2003. Levels of plasma angiotensin-(1-7) in patients with hypertension who have the angiotensin-I-converting enzyme deletion/deletion genotype. Am J Cardiol. 92**,** 749-51.

Johnson, R.F., Beltz, T.G., Sharma, R.V., Xu, Z., Bhatty, R.A., Johnson, A.K., 2001. Agonist activation of cytosolic Ca^{2+} in subfornical organ cells projecting to the

supraoptic nucleus. Am. J. Physiol. Regul. Integr. Comp. Physiol. 280**,** R1592-R1599.

Jurzak, M., Muller, A.R., Gerstberger, R., 1995a. Characterization of vasopressin receptors in cultured-cells derived from the region of rat-brain circumventricular organs. Neuroscience. 65**,** 1145-1159.

Jurzak, M., Muller, A.R., Gerstberger, R., 1995b. AVP-Fragment peptides induce Ca^{2+} transients in cells cultured from rat circumventricular organs. Brain Res. 673**,** 349-355.

Kawai, T., Forrester, S.J., O'Brien, S., Baggett, A., Rizzo, V., Eguchi, S., 2017. AT1 receptor signaling pathways in the cardiovascular system. Pharmacol Res. 125**,** 4-13.

Kim, T., Yamamoto, Y., Tanaka-Yamamoto, K., 2017. Timely regulated sorting from early to late endosomes is required to maintain cerebellar long-term depression. Nat Commun. 8**,** 401.

Li, Z., Ferguson, A.V., 1993. Angiotensin-II Responsiveness of Rat Paraventricular and Subfornical organ neurons in-vitro. Neuroscience. 55**,** 197-207.

Martin, N., Bernard, D., 2018. Calcium signaling and cellular senescence. Cell Calcium. 70**,** 16-23.

McKinley, M.J., Allen, A.M., Burns, P., Colvill, L.M., Oldfield, B.J., 1998. Interaction of circulating hormones with the brain: The roles of the subfornical organ and the organum vasculosum of the lamina terminalis. Clin. Exp. Pharmacol. Physiol. 25**,** S61-S67.

Moriya, T., Shibasaki, R., Kayano, T., Takebuchi, N., Ichimura, M., Kitamura, N., Asano, A., Hosaka, Y.Z., Forostyak, O., Verkhratsky, A., Dayanithi, G., Shibuya, I., 2015.

Full-length transient receptor potential vanilloid 1 channels mediate calcium signals and possibly contribute to osmoreception in vasopressin neurones in the rat supraoptic nucleus. Cell Calcium. 57**,** 25-37.

Morris, G., Walker, A.J., Berk, M., Maes, M., Puri, B.K., 2018. Cell Death Pathways: a Novel Therapeutic Approach for Neuroscientists. Mol Neurobiol. 55**,** 5767-5786.

Navar, L.G., Lewis, L., Hymel, A., Braam, B., Mitchell, K.D., 1994. Tubular fluid concentrations and kidney contents of angiotensins I and II in anesthetized rats. J Am Soc Nephrol. 5**,** 1153-8.

Ohtsuki, G., Piochon, C., Adelman, J.P., Hansel, C., 2012. SK2 channel modulation contributes to compartment-specific dendritic plasticity in cerebellar Purkinje cells. Neuron. 75**,** 108-20.

Okuya, S., Inenaga, K., Kaneko, T., Yamashita, H., 1987. Angiotensin II sensitive neurons in the supraoptic nucleus, subfornical organ and anteroventral third ventricle of rats in vitro. Brain Res. 402**,** 58-67.

Ono, K., Honda, E., Inenaga, K., 2001. Angiotensin II induces inward currents in subfornical organ neurones of rats. J. Neuroendocrinol. 13**,** 517-523.

Osaka, T., Yamashita, H., Koizumi, K., 1992. Inhibitory inputs to the subfornical organ from the AV3V: involvement of GABA. Brain Res Bull. 29**,** 581-7.

Pulman, K.J., Fry, W.M., Cottrell, G.T., Ferguson, A.V., 2006. The subfornical organ: A central target for circulating feeding signals. J. Neurosci. 26**,** 2022-2030.

Sabatier, N., Richard, P., Dayanithi, G., 1998. Activation of multiple intracellular transduction signals by vasopressin in vasopressin-sensitive neurones of the rat supraoptic nucleus. J Physiol. 513 (Pt 3)**,** 699-710.

Schmid, H.A., Simon, E., 1992. Effect of angiotensin II and atrial natriuretic factor on neurons in the subfornical organ of ducks and rats in vitro. Brain Res. 588**,** 324-8.

Seltzer, A.M., Zorad, S., Saavedra, J.M., 1995. Stimulation of angiotensin II AT_1 receptors in rat median eminence increases phosphoinositide hydrolysis. Brain Res. 705**,** 24-30.

Sharif-Naeini, R., Folgering, J.H., Bichet, D., Duprat, F., Delmas, P., Patel, A., Honore, E., 2010. Sensing pressure in the cardiovascular system: Gq-coupled mechanoreceptors and TRP channels. J Mol Cell Cardiol. 48**,** 83-9.

Shibuya, I., Noguchi, J., Tanaka, K., Harayama, N., Inoue, Y., Kabashima, N., Ueta, Y., Hattori, Y., Yamashita, H., 1998. PACAP increases the cytosolic Ca^{2+} concentration and stimulates somatodendritic vasopressin release in rat supraoptic neurons. J. Neuroendocrinol. 10**,** 31-42.

Shim, H.G., Lee, Y.S., Kim, S.J., 2018. The Emerging Concept of Intrinsic Plasticity: Activity-dependent Modulation of Intrinsic Excitability in Cerebellar Purkinje Cells and Motor Learning. Exp Neurobiol. 27**,** 139-154.

Shimizu, H., Watanabe, E., Hiyama, T.Y., Nagakura, A., Fujikawa, A., Okado, H., Yanagawa, Y., Obata, K., Noda, M., 2007. Glial Nax channels control lactate signaling to neurons for brain $[Na^+]$ sensing. Neuron. 54**,** 59-72.

Simpson, N.J., Ferguson, A.V., 2017. The proinflammatory cytokine tumor necrosis factor-alpha excites subfornical organ neurons. J Neurophysiol. 118**,** 1532-1541.

Simpson, N.J., Ferguson, A.V., 2018. Tumor necrosis factor alpha potentiates the effects of angiotensin II on subfornical organ neurons. Am J Physiol Regul Integr Comp Physiol.

Smith, P.M., Ferguson, A.V., 2010. Circulating signals as critical regulators of autonomic state-central roles for the subfornical organ. Am. J. Physiol. Regul. Integr. Comp. Physiol. 299**,** R405-R415.

Storch, U., Mederos y Schnitzler, M., Gudermann, T., 2012. G protein-mediated stretch reception. Am J Physiol Heart Circ Physiol. 302**,** H1241-9.

Sumners, C., Fleegal, M.A., Zhu, M., 2002. Angiotensin AT_1 receptor signalling pathways in neurons. Clin Exp Pharmacol Physiol. 29**,** 483-90.

Tanaka, J., Saito, H., Kaba, H., 1987. Subfornical organ and hypothalamic paraventricular nucleus connections with median preoptic nucleus neurons - an electrophysiological study in the rat. Exp Brain Res. 68**,** 579-585.

Tanaka, K., Khiroug, L., Santamaria, F., Doi, T., Ogasawara, H., Ellis-Davies, G.C., Kawato, M., Augustine, G.J., 2007. Ca^{2+} requirements for cerebellar long-term synaptic depression: role for a postsynaptic leaky integrator. Neuron. 54**,** 787-800.

Verkhratsky, A., 2002. The endoplasmic reticulum and neuronal calcium signalling. Cell Calcium. 32**,** 393-404.

Wang, D., Martens, J.R., Posner, P., Sumners, C., Gelband, C.H., 1996. Angiotensin II regulation of intracellular calcium in astroglia cultured from rat hypothalamus and brainstem. J Neurochem. 67**,** 996-1004.

Wang, G., Sarkar, P., Peterson, J.R., Anrather, J., Pierce, J.P., Moore, J.M., Feng, J., Zhou, P., Milner, T.A., Pickel, V.M., Iadecola, C., Davisson, R.L., 2013. COX-1-derived PGE_2 and PGE_2 type 1 receptors are vital for angiotensin II-induced formation of reactive oxygen species and Ca^{2+} influx in the subfornical organ. Am J Physiol Heart Circ Physiol. 305**,** H1451-61.

Wang, X., Marks, C.R., Perfitt, T.L., Nakagawa, T., Lee, A., Jacobson, D.A., Colbran, R.J., 2017. A novel mechanism for Ca^{2+}/calmodulin-dependent protein kinase II targeting to L-type Ca^{2+} channels that initiates long-range signaling to the nucleus. J Biol Chem. 292**,** 17324-17336.

Washburn, D.L.S., Ferguson, A.V., 2001. Selective potentiation of N-type calcium channels by angiotensin II in rat subfornical organ neurones. J. Physiol. (Lond.). 536**,** 667-675.

Wayman, G.A., Lee, Y.S., Tokumitsu, H., Silva, A.J., Soderling, T.R., 2008. Calmodulin-kinases: modulators of neuronal development and plasticity. Neuron. 59**,** 914-31.

Wilcox, C.S., Dzau, V.J., 1992. Effect of captopril on the release of the components of the renin-angiotensin system into plasma and lymph. J Am Soc Nephrol. 2**,** 1241-50.

Yang, Z., Santamaria, F., 2016. Purkinje cell intrinsic excitability increases after synaptic long term depression. J Neurophysiol. 116**,** 1208-17.

Yu, Y., Wei, S.G., Weiss, R.M., Felder, R.B., 2018. Angiotensin II Type la Receptors in the Subfornical Organ Modulate Neuroinflammation in the Hypothalamic Paraventricular Nucleus in Heart Failure Rats. Neuroscience. 381**,** 46-58.

Zhao, H., Kinch, D.C., Simasko, S.M., 2011. Pharmacological investigations of the cellular transduction pathways used by cholecystokinin to activate nodose neurons. Auton Neurosci. 164**,** 20-6.

Zong, W.N., Chen, X.M., Yang, Y.Q., Cao, J.L., Zou, H.Y.Y., Sun, H.W., Hou, M.H., Huang, H.J., Zheng, H.J., Qin, X.Y., Zhang, H., Kong, X.Q., Huang, J., Lu, X.Z., 2015. Plasma auto-antibodies to angiotensin II receptors are correlated with blood pressure and inflammatory factors in hypertension patients. Eur Heart J Suppl. 17**,** B65-B70.

Zubcevic, J., Santisteban, M.M., Perez, P.D., Arocha, R., Hiller, H., Malphurs, W.L., Colon-Perez, L.M., Sharma, R.K., de Kloet, A., Krause, E.G., Febo, M., Raizada, M.K., 2017. A Single Angiotensin II Hypertensive Stimulus Is Associated with Prolonged Neuronal and Immune System Activation in Wistar-Kyoto Rats. Front Physiol. 8**,** 592.

Chapter 3

Mechanisms of GABA-mediated inhibition of the angiotensin II-induced cytosolic Ca^{2+} increase in rat subfornical organ neurons

Highlights

1. GABA reversibly inhibited AII-induced persistent $[Ca^{2+}]_i$ increase in SFO neurons.
2. Galanin and ANP inhibited the $[Ca^{2+}]_i$ increase to a lesser extent than GABA.
3. Both $GABA_A$ and $GABA_B$ receptors play a role in the GABA-induced inhibition.
4. The $GABA_B$ agonist baclofen inhibited L-, N- and P/Q-type Ca^{2+} channels.

Abstract

Neurons in the subfornical organ (SFO) sense both neurotransmitters and circulating humoral factors such as angiotensin II (AII) and atrial natriuretic peptide (ANP), and regulate multiple physiological functions including drinking behavior. I recently reported that AII at nanomolar concentrations induced a persistent $[Ca^{2+}]_i$ increase in acutely dissociated SFO neurons and that this effect of AII was reversibly inhibited by GABA. In the present study, I studied the inhibitory mechanism of GABA using Ca^{2+} imaging and patch-clamp electrophysiology. The AII-induced persistent $[Ca^{2+}]_i$ increase was inhibited by GABA in more than 90% of AII-responsive neurons and by other two SFO inhibitory ligands, ANP and galanin, in about 60 and 30% of neurons respectively. The inhibition by GABA was mimicked by the $GABA_A$ and $GABA_B$ receptor agonists muscimol and baclofen. The involvement of both GABA receptor subtypes was confirmed by reversal of the GABA-mediated inhibition only when the $GABA_A$ and $GABA_B$ receptors antagonists bicuculline methiodide and CGP55845 were both present. The $GABA_B$ agonist baclofen rapidly and reversibly inhibited voltage-gated Ca^{2+} channel (VGCC) currents recorded in response to depolarizing pulses in voltage-clamp electrophysiology using Ba^{2+} as a charge carrier (I_{Ba}). Baclofen inhibition of I_{Ba} was antagonized by CGP55845, confirming $GABA_B$ receptor involvement; was reduced by N-ethylmaleimide, suggesting downstream Gi-mediated actions; and was partially removed by a large prepulse, indicating voltage-dependency. The magnitude of I_{Ba} inhibition by baclofen was reduced by the application of selective blockers for N-, P/Q-, and L-type VGCCs (ω-conotoxin GVIA, ω-agatoxin IVA, and nifedipine respectively). Overall, our study indicates that GABA inhibition of the AII-induced $[Ca^{2+}]_i$ increase is mediated by both $GABA_A$ and $GABA_B$ receptors, and that $GABA_B$ receptors associated

with Gi proteins suppress Ca^{2+} entry through VGCCs in SFO neurons.

1. Introduction

The subfornical organ (SFO), one of the circumventricular organs, lacks a blood-brain barrier and senses the concentrations of many different circulating signals including angiotensin II (AII) (Cottrell and Ferguson, 2004; Gross, 1992; McKinley et al., 1998; Smith and Ferguson, 2010). Upon sensing AII, the SFO induces water intake to increase the volume of body fluids (Fitzsimons, 1998). Intraventricular administration of the inhibitory amino acid neurotransmitter γ-aminobutyric acid (GABA) suppresses the effects of AII on water intake and blood pressure in rats *in vivo* (Abe et al., 1988). GABA is thought to regulate SFO neuron activity; however, the detailed mechanisms of GABA-mediated inhibition within the SFO have not yet been elucidated.

GABA is one of the most important non-proteinogenic amnio acids due to its action as an inhibitory neurotransmitter in the central nervous system (CNS). It has been estimated that at least one-third of CNS neurons utilize GABA as their primary neurotransmitter (Bloom and Iversen, 1971). The inhibitory effect of GABA is mediated by two distinct types of GABA receptors: the $GABA_A$ receptor, a ligand-gated Cl^- channel responsible for rapid inhibition; and the $GABA_B$ receptor, a metabotropic receptor that produces slow inhibition (Weindl et al., 1992; Wojcik and Holopainen, 1992; Sieghart, 2006; Bowery, 2010). $GABA_A$ receptors are present on the cell membrane of SFO neurons (Weindl et al., 1992) and GABA is thought to act through these receptors to suppress spontaneous activity in SFO neurons (Inenaga et al., 1995). Additionally, it was reported that the action of GABA via $GABA_A$ receptors was responsible for the generation of inhibitory postsynaptic currents in SFO neurons (Honda et al., 2001). From these studies, GABA is considered to play an important role in the regulation of the activity of SFO neurons, presumably through $GABA_A$ receptors.

Further, the GABAergic system in the nucleus tractus solitarius may modulate the release of noradrenaline in the SFO via both $GABA_A$ and $GABA_B$ receptors (Tanaka et al., 2002). Both receptors are also involved in modulating serotonin release in the SFO area, with the $GABA_A$ receptor mechanism implicated in the serotonergic regulatory system of body fluid balance (Takahashi et al., 2016).

While it is clear that GABAergic inhibition is of great importance in regulating SFO neuronal activity and consequent fluid balance adjustments, the underlying mechanisms of GABA-mediated inhibition in SFO neurons have not yet been elucidated. As described in Chapter 1 and 2, I found that AII at picomolar concentrations induces or enhances Ca^{2+} oscillations, and AII at nanomolar concentrations induces a persistent cytosolic Ca^{2+} concentration ($[Ca^{2+}]_i$) increase, in acutely dissociated SFO neurons (Izumisawa et al. 2019a, 2019b). I found that this AII-induced persistent $[Ca^{2+}]_i$ increase could be reversibly inhibited by GABA, yet the mechanisms by which this inhibition is mediated remain unknown. In the present study,I firstly studied whether GABA is the only ligand that can attenuate the persistent $[Ca^{2+}]_i$ increase by using fura-2-based Ca^{2+} imaging; in this regard, I examined whether two inhibitory ligands that were also reported to suppress AII-induced drinking behavior, atrial natriuretic peptide (ANP) and galanin (Nakamaru et al., 1986; Lin and Hubbard, 1992; Hirase et al., 2008), were also able to exert inhibitory actions on the AII-induced persistent $[Ca^{2+}]_i$ increase in SFO neurons. I secondly investigated the mechanism by which GABA inhibits the AII-induced persistent $[Ca^{2+}]_i$ increase in SFO neurons with selective agonists and antagonists for both $GABA_A$ and $GABA_B$ receptors. Since the analysis of the GABA receptor pharmacology revealed potential roles of $GABA_B$ receptors in the inhibitory actions of GABA, I thirdly

investigated whether or not voltage-gated Ca^{2+} channels (VGCCs) are inhibited by $GABA_B$ receptors by using whole-cell voltage-clamp electrophysiology.

I found that GABA, galanin, and ANP inhibited the AII-induced persistent $[Ca^{2+}]_i$ increase and that the inhibition by GABA is mediated through not only $GABA_A$ but also $GABA_B$ receptors. I also found that $GABA_B$ receptor activation inhibits VGCCs in a voltage-sensitive manner and the major targets of baclofen-induced inhibition were N-, P/Q-, and L-type VGCCs in SFO neurons.

2. Results

All cells in this study were stimulated with 50 mM K^+ at either the beginning or the end of experiments, and those showing K^+-induced $[Ca^{2+}]_i$ responses of >50 nM were considered to be neurons and were used for further analysis. The basic characteristics of cells acutely dissociated from SFO tissues in this study were similar to those reported in Chapter 1 and 2 (Izumisawa et al., 2019a, 2019b); that is, approximately 50% of SFO neurons responded to AII, and AII at nanomolar concentrations induced a prolonged increase in $[Ca^{2+}]_i$. A representative time course of the persistent $[Ca^{2+}]_i$ increase induced by 100 nM AII administered for 30 min is shown in Fig. 1A. AII at 100 nM induced a large, rapid spike in $[Ca^{2+}]_i$ followed by a relatively stable prolonged $[Ca^{2+}]_i$ increase throughout the 30 min AII administration period, with the elevated $[Ca^{2+}]_i$ persisting even after wash-out of AII. The total number of neurons examined with $[Ca^{2+}]_i$ measurement was 239 and the average of the basal $[Ca^{2+}]_i$ level was 146 ± 5 nM. The basal $[Ca^{2+}]_i$ level showed variations from below 100 nM to over 200 nM and the amplitude and time course of the responses to AII and high K^+ also varied from cell to cell. The reason for the variability could be due to heterogeneity or different spontaneous activity of SFO

neurons. The reason of these variations could be because the SFO consist of several heterogenous populations of neurons as reported by other groups (Ferguson and Bains, 1997; Sunn et al., 2003).

2.1 The effects of the inhibitory transmitters GABA, galanin, and ANP on the AII-induced persistent $[Ca^{2+}]_i$ increase

First, I used the prolonged AII-evoked $[Ca^{2+}]_i$ response to investigate the actions of physiologically relevant inhibitory ligands for SFO neurons; namely GABA, galanin, and ANP. When the $[Ca^{2+}]_i$ had reached a stable AII-induced level, the three ligands GABA (10 μM), galanin (100 nM), and ANP (100 nM) were administered sequentially in randomized order to each SFO neuron (n = 64), with each ligand separated by a wash-out period. The concentration of each ligand was close to its respective maximally effective concentration for SFO neurons in previous studies (Björkstrand et al., 1993; Kai et al., 2006; Schmid and Simon, 1992; Inenaga et al., 1995). The AII-induced $[Ca^{2+}]_i$ increase was sensitive to inhibition by at least one of the three ligands in 97% of neurons tested. Of the three ligands, GABA most consistently suppressed the AII-induced persistent $[Ca^{2+}]_i$ increase (58/64 neurons, 90%), with fewer cells showing inhibition by galanin (39/64 neurons, 60%) or ANP (20/64 neurons, 31%). In 14% of neurons, all three ligands inhibited the AII-induced $[Ca^{2+}]_i$ increase, while only GABA and galanin suppressed this increase in 41% of neurons. Representative examples of the two types of response are shown in Fig. 1B and C, respectively. I found that there was an overlap in the neuron groups responsive to GABA, galanin, and ANP: 74% of the GABA-responsive neurons were also inhibited by either galanin, ANP, or both, while only 3% of the AII-responsive neurons showed responses to both galanin and ANP (Fig. 1D).

Further, I examined the strength of inhibition for each ligand by calculating the inhibition rate (the magnitude of the ligand-induced $[Ca^{2+}]_i$ decrease as a proportion of the AII-induced persistent $[Ca^{2+}]_i$ increase; Fig. 1E). When considering all 64 neurons tested, GABA caused the largest suppression of the AII-induced persistent $[Ca^{2+}]_i$ increase, often reducing the $[Ca^{2+}]_i$ below the pre-AII baseline (as seen in Fig. 1B), while the magnitude of inhibition by galanin and ANP inhibition was smaller than that of GABA (Fig. 1E, open bars). Only ANP did not show significant inhibition of the AII-induced $[Ca^{2+}]_i$ increase. This pattern of results persisted when considering only the neurons that were responsive to the relevant ligand (GABA, n = 58; galanin, n = 39; ANP, n = 20), with GABA showing the strongest inhibition and galanin and ANP showing lesser inhibition of the AII-induced $[Ca^{2+}]_i$ increase (Fig. 1E, closed bars). Our results indicate that GABA has a powerful suppressive effect on the AII-induced $[Ca^{2+}]_i$ response in the vast majority of AII-responsive SFO neurons.

Next, I investigated the GABA-induced suppression of the AII-induced persistent $[Ca^{2+}]_i$ increase in more detail. To examine the concentration-response relationship of the suppression of the AII-induced persistent $[Ca^{2+}]_i$ increase (Fig. 1A) by GABA, I administered GABA at concentrations between 0.1–100 μM (Fig. 2A) during the continuous phase of the AII-induced persistent $[Ca^{2+}]_i$ increase. GABA at 10 and 100 μM caused significant inhibition and the maximal inhibition was obtained by GABA at 10 μM. The concentration of GABA required for 50% inhibition (IC_{50}) was estimated to be 1.1 μM from the regression curve (Fig. 2B).

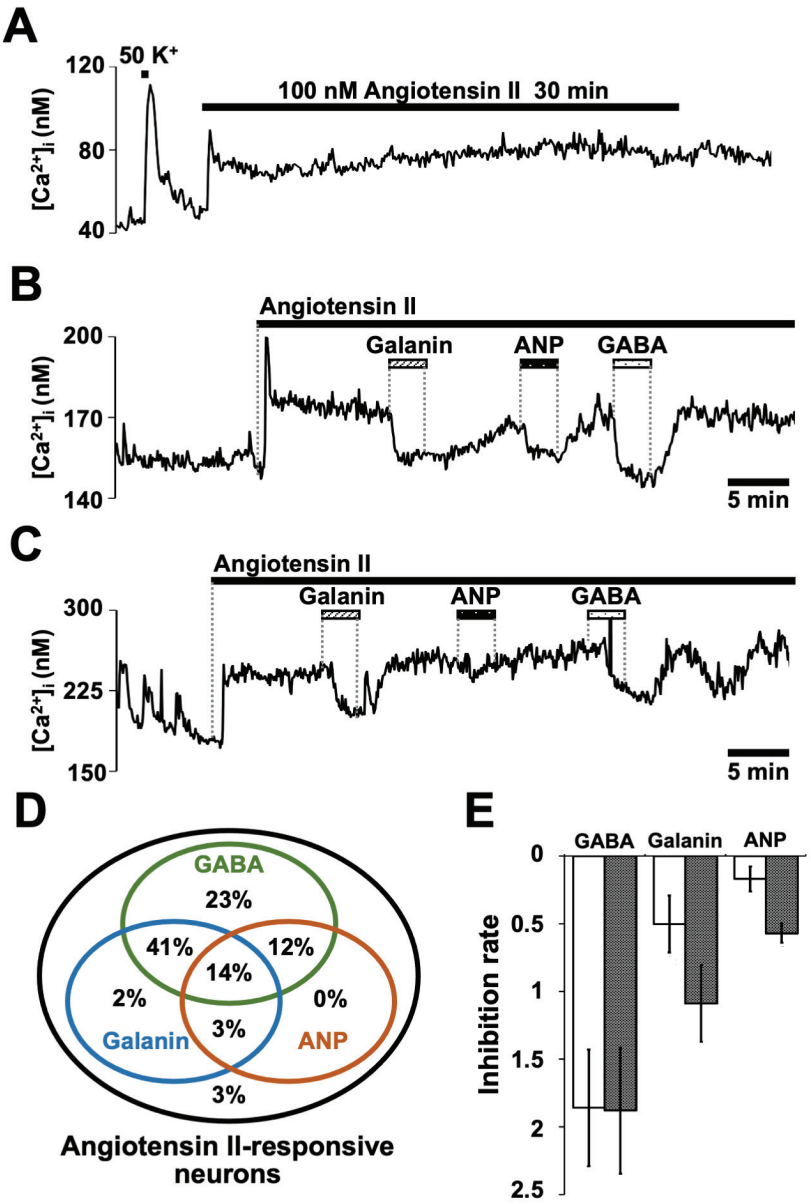

Fig. 1 The effects of the inhibitory ligands γ-aminobutyric acid (GABA), galanin, and atrial natriuretic peptide (ANP) on the angiotensin II (AII)-induced persistent cytosolic calcium concentration ($[Ca^{2+}]_i$) increase in rat subfornical organ (SFO) neurons. **A** Representative time course of persistent $[Ca^{2+}]_i$ increases induced by the application of AII (100 nM) for 30 min. **B** Representative $[Ca^{2+}]_i$ trace showing an SFO neuron in which the persistent $[Ca^{2+}]_i$ increase induced by 100 nM AII could be inhibited by all three ligands GABA (10 μM), galanin (100 nM), and ANP (100 nM). **C** Representative $[Ca^{2+}]_i$ trace showing an SFO neuron in which the AII-induced persistent $[Ca^{2+}]_i$ increase was inhibited by galanin and GABA, but not by ANP. **D** Venn diagram showing the overlap of inhibitory responses in SFO neurons (n = 64) to GABA, galanin, and ANP. The values have been rounded to whole numbers. **E** Summary data for the inhibition rate of GABA, galanin, and ANP on the AII-induced persistent $[Ca^{2+}]_i$ increase. The inhibition rates were calculated by dividing the magnitude of the ligand-induced $[Ca^{2+}]_i$ decrease (measured during the last 30 s of 3 min treatment) by the AII-induced increase ($\Delta[Ca^{2+}]_i$, measured during the last 30 s of AII treatment before addition of the ligand). Open bars show summary inhibition rate data calculated using all 64 AII-responsive neurons; closed bars show summary inhibition rate data calculated using only the AII-responsive neurons that exhibited significant responses to GABA (n = 58), galanin (n = 39), and ANP (n = 20). Graph shows mean ± standard error of the mean (SEM).

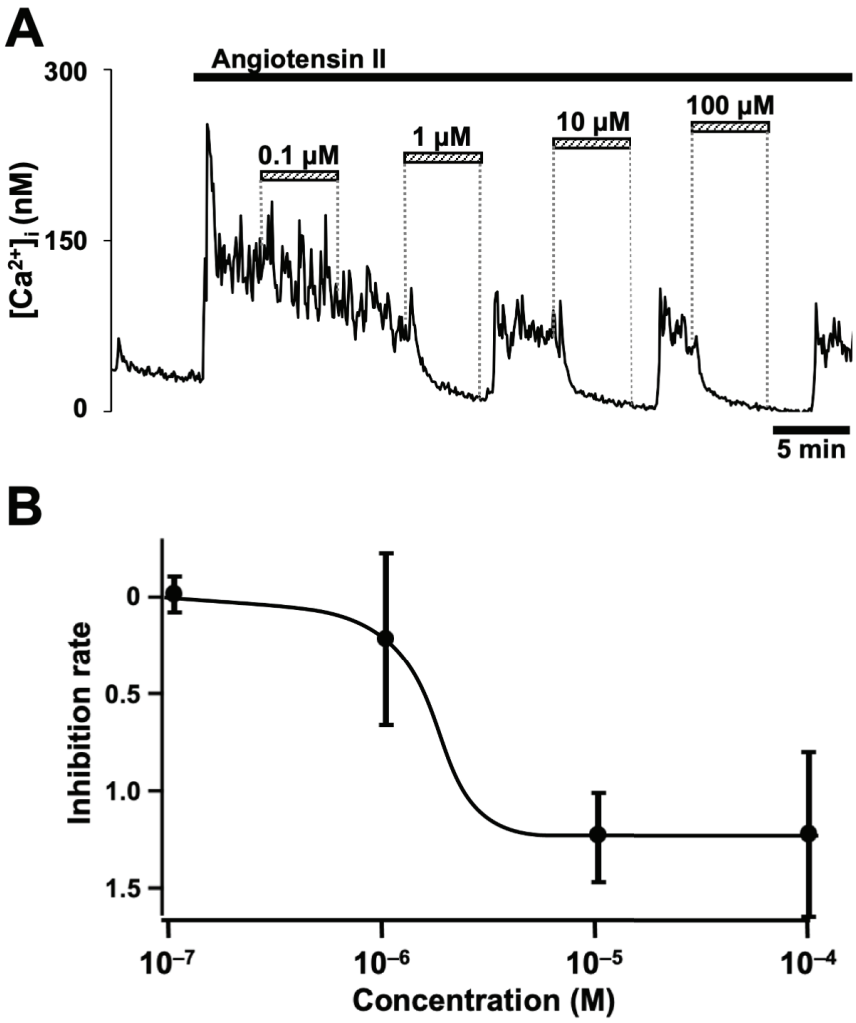

Fig. 2 The concentration-response relationship of GABA-mediated suppression of the AII-induced persistent $[Ca^{2+}]_i$ increase. **A** Representative $[Ca^{2+}]_i$ trace showing concentration-dependent suppression of the AII-induced persistent $[Ca^{2+}]_i$ increase from GABA applied at 0.1–100 μM. GABA-mediated inhibition was reversible and the magnitude of inhibition increased with increasing GABA concentration. **B** The concentration-response relationship between GABA concentration and inhibition of AII-induced persistent $[Ca^{2+}]_i$ increase. The regression curve was obtained by the least squares method using the equation $y = a/(1+\exp(-x-b))$. The concentration of GABA required for 50% inhibition (IC_{50}) calculated from the curve was 1.1 μM.

2.2 The GABA receptor subtype responsible for inhibition of the AII-induced persistent $[Ca^{2+}]_i$ increase

The two major subclasses of GABA receptors, $GABA_A$ and $GABA_B$ receptors, are reported to be expressed in the SFO (Weindl et al., 1992; Inenaga et al., 1995; Honda et al., 2001). Here, I used selective agonists and antagonists of $GABA_A$ and $GABA_B$ receptors to identify the subtype responsible for mediating GABA inhibition of the AII-induced persistent $[Ca^{2+}]_i$ increase (Fig. 3 and 4). First I applied muscimol and baclofen, selective agonists of the $GABA_A$ and $GABA_B$ receptors respectively, during the AII-induced persistent $[Ca^{2+}]_i$ increase (Fig. 3A) at levels close to their maximally effective concentrations (Shibuya et al., 1997). Similar to GABA, both muscimol and baclofen induced an obvious inhibition of the AII-induced persistent $[Ca^{2+}]_i$ increase (Fig. 3A). Calculations of the inhibition rate for GABA (10 μM, n = 68), baclofen (100 μM, n = 12), and muscimol (10 μM, n = 13) showed that all three compounds significantly inhibited the AII-induced persistent $[Ca^{2+}]_i$ increase (Fig. 3B). These results showed that inhibition of the AII-induced persistent $[Ca^{2+}]_i$ increase by GABA could be mimicked by both muscimol and baclofen, suggesting that both $GABA_A$ and $GABA_B$ receptors play a role in GABA-induced inhibition.

Next, to more clearly determine the dual involvement of both GABA receptor subtypes, selective antagonists of $GABA_A$ and $GABA_B$ receptors (bicuculline methiodide [BMI, 30 μM] and CGP55845 [CGP, 10 μM], respectively) were applied in an step-wise additive manner during the AII-induced persistent $[Ca^{2+}]_i$ increase, starting with either CGP (n = 22, Fig. 4A and B) or BMI (n = 12, Fig. 4C and D). CGP alone (Fig. 4A and B) or BMI alone (Fig. 4C and D) had no inhibitory effect on the AII-induced $[Ca^{2+}]_i$ increase, and the inhibitory effect of GABA was unaffected by the presence of either

antagonist (CGP + GABA, Fig. 4A; BMI + GABA, Fig. 4C; summary data in Fig. 4B and D). However, GABA-mediated inhibition of the AII-induced $[Ca^{2+}]_i$ increase was attenuated when both receptor antagonists were present (CGP + GABA + BMI, Fig. 4A; BMI + GABA + CGP, Fig. 4C; summary data in Fig. 4B and D). These results indicate that inhibition of the AII-induced persistent $[Ca^{2+}]_i$ increase by GABA can be mediated not only through $GABA_A$ receptors, but also through $GABA_B$ receptors.

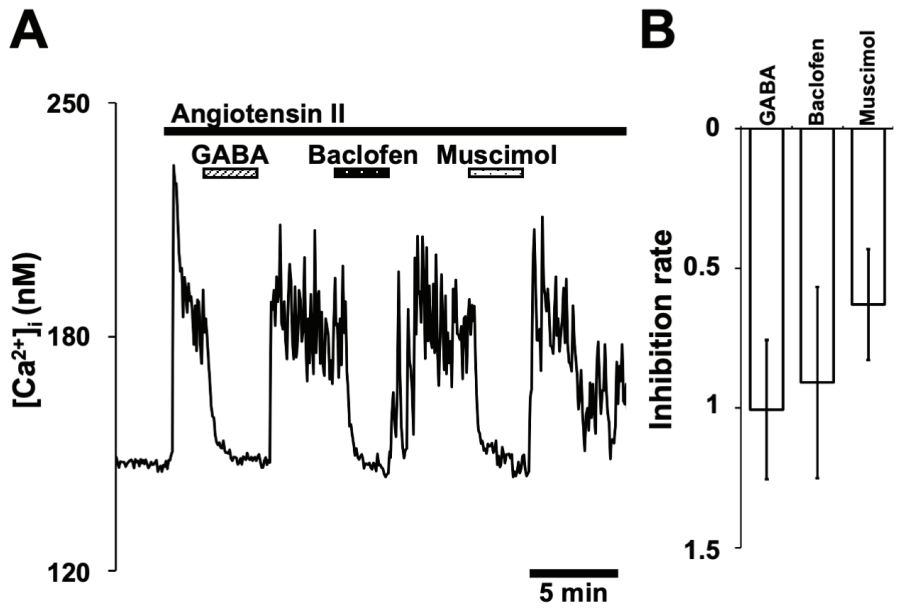

Fig. 3 Inhibition of the AII-induced persistent $[Ca^{2+}]_i$ by GABA was mimicked by either of the selective agonists of $GABA_A$ and $GABA_B$ receptors muscimol and baclofen, respectively. **A** Representative $[Ca^{2+}]_i$ trace showing suppression of the AII (100 nM)-induced persistent $[Ca^{2+}]_i$ increase by GABA (10 μM), baclofen (100 μM), and muscimol (10 μM). **B** Summary data for the inhibition of the AII-induced persistent $[Ca^{2+}]_i$ increase by GABA (n = 68), baclofen (n = 12), and muscimol (n = 13). Graph shows mean ± SEM.

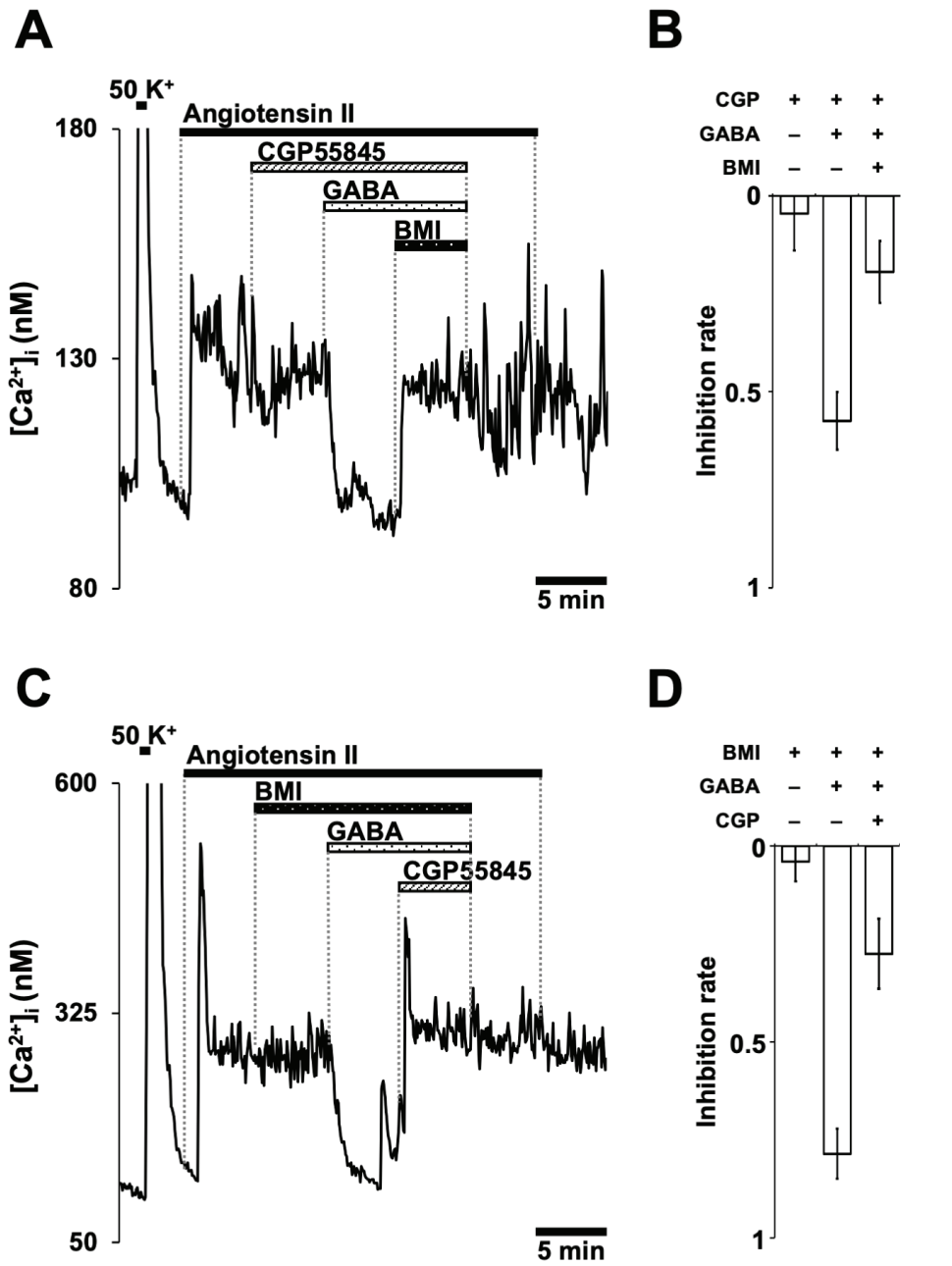

Fig. 4 Inhibition of the AII-induced persistent increase in $[Ca^{2+}]_i$ by GABA was attenuated by dual application of the selective $GABA_A$ and $GABA_B$ receptor antagonists bicuculline methiodide (BMI) and CGP55845 (CGP), respectively. **A** Representative $[Ca^{2+}]_i$ trace showing that application of CGP alone (10 μM) had no effect on AII-induced persistent $[Ca^{2+}]_i$ increase, and that inhibition of the AII-induced persistent $[Ca^{2+}]_i$ increase by GABA (10 μM) persisted in the presence of CGP but was attenuated upon co-application of BMI (30 μM) with CGP. **B** Summary data for the inhibition rate of the AII-induced $[Ca^{2+}]_i$ increase by CGP, GABA, and BMI (n = 22). **C** Representative $[Ca^{2+}]_i$ trace showing that application of BMI alone had no effect on the AII-induced persistent $[Ca^{2+}]_i$ increase, and that inhibition by GABA persisted in the presence of BMI but was attenuated upon co-application of CGP with BMI. **D** Summary data for the inhibition rate of the AII-induced persistent $[Ca^{2+}]_i$ increase by BMI, GABA, and CGP (n = 12). Inhibition rates for solo antagonists or GABA were calculated using the average of the last 30 s of the 5 min application; and during the 5 min where both antagonists were present the rate was calculated using the average of the 30 s where the effect of adding the second antagonist was most evident. Graphs show mean ± SEM.

2.3 The effects of GABA and baclofen on the $[Ca^{2+}]_i$ increase evoked by membrane depolarization

Although an inhibitory role for $GABA_A$ receptors in SFO neurons has been identified previously (Takahashi et al., 2016; Inenaga et al., 1995; Honda et al., 2001), inhibitory mechanisms of $GABA_B$ receptors in SFO neurons have not yet been described. As $GABA_B$ receptor activation is known to inhibit voltage-gated Ca^{2+} channels (VGCCs) (Wojcik and Holopainen, 1992), I next examined whether GABA and the $GABA_B$ agonist baclofen inhibit $[Ca^{2+}]_i$ increases induced by membrane depolarization. As I described in Chapter 1 and 2 (Izumisawa et al., 2019a, 2019b), SFO neurons respond to 50 mM K^+ with a large, rapid increase in $[Ca^{2+}]_i$ (Fig. 5A and B). Application of GABA (10 μM) inhibited the $[Ca^{2+}]_i$ increase induced by 50 mM K^+ (Fig. 5A and C), but application of baclofen (100 μM) had no significant effect (Fig. 5B and C). The inhibition rates for GABA and baclofen on the 50 mM K^+-evoked $[Ca^{2+}]_i$ increase were calculated separately in AII-responsive (Fig. 5C, open bars) and AII-unresponsive (Fig. 5C, closed bars) SFO neurons. Both types of neurons showed significant inhibition of the 50mM K^+-evoked $[Ca^{2+}]_i$ response by GABA but not by baclofen. These results indicate that the GABAergic inhibition of the 50 mM K^+-evoked $[Ca^{2+}]_i$ increase occurs via $GABA_A$ receptors.

However, I did find that baclofen (100 μM) significantly suppressed the $[Ca^{2+}]_i$ increase induced by a lower concentration (10 mM) of extracellular K^+, in both AII-responsive (Fig. 5E, open bar) and AII-unresponsive (Fig. 5E, closed bar) SFO neurons. These results suggest that $GABA_B$ receptors are indeed capable of inhibiting VGCC currents in SFO neurons; however, this inhibition is reduced in a depolarization-dependent manner.

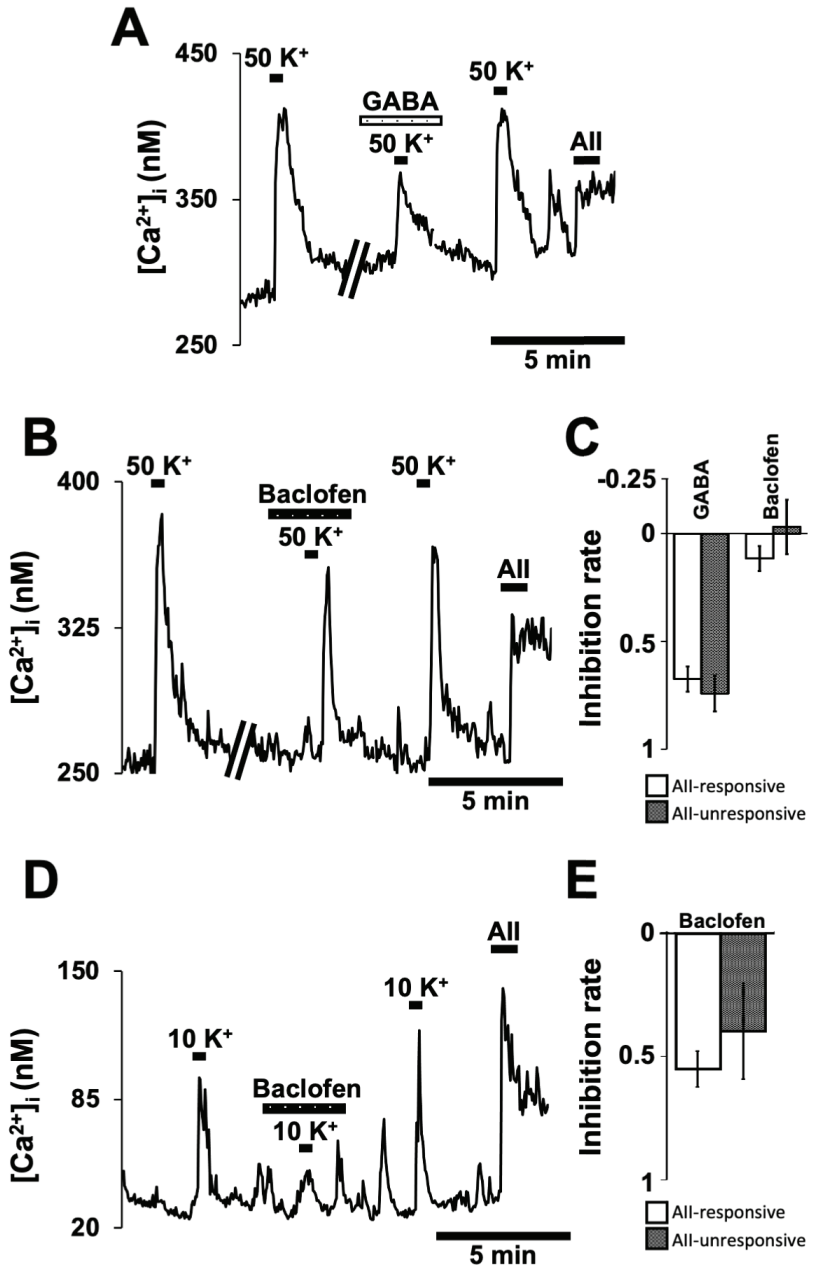

Fig. 5 The effects of baclofen and GABA on the $[Ca^{2+}]_i$ increase evoked in SFO neurons by high concentrations (10 and 50 mM) of K^+. **A** Representative $[Ca^{2+}]_i$ trace showing that the application of GABA (10 μM) diminished the 50 mM K^+-evoked $[Ca^{2+}]_i$ increase in an AII-responsive neuron. **B** Representative $[Ca^{2+}]_i$ trace showing that the application of baclofen (100 μM) had little effect on the 50 mM K^+-evoked $[Ca^{2+}]_i$ increase in an AII-responsive neuron. **C** Summary data for the inhibition of the 50 mM K^+-evoked $[Ca^{2+}]_i$ increase on AII-responsive (open bars) and AII-unresponsive (closed bars) neurons by GABA (open bar, n = 21; closed bar, n = 8) and baclofen (open bar, n = 6; closed bar, n = 8). The inhibition rate was calculated by dividing the response to 50 mM K^+ during baclofen or GABA application by the average of the pre- and post-drug control responses to 50 mM K^+. **D** Representative $[Ca^{2+}]_i$ trace showing that the application of baclofen suppressed the $[Ca^{2+}]_i$ increase evoked by 10 mM K^+. **E** Summary data for the inhibition rate of the 10 mM K^+-evoked $[Ca^{2+}]_i$ increase in AII-responsive (open bar, n = 30) and AII-unresponsive (closed bar, n = 10) neurons by baclofen. Graphs show mean ± SEM.

2.4 The effects of baclofen on the VGCC currents in rat SFO neurons

Having identified a potential role for $GABA_B$ receptors in inhibiting Ca^{2+} increases and VGCCs in SFO neurons, I studied the inhibition of VGCC currents by $GABA_B$ receptors using patch-clamp electrophysiology. I used 10 mM Ba^{2+} as a charge carrier to record VGCC current responses in SFO neurons (Fig. 6). The neurons were voltage-clamped at −80 mV in a whole-cell configuration. Currents through voltage-gated Na^+ and K^+ channels were blocked using tetrodotoxin (TTX), tetraethylammonium (TEA), and 4-aminopyridine (4AP). To record current responses through high-voltage-activated (HVA) VGCCs, a series of voltage pulses to between −60 and +30 mV was applied with an interval of 15 s (Fig. 6A). After recording current responses to the series of voltage pulses, 100 μM Cd^{2+} was applied to inhibit VGCC-mediated currents in all cells tested. In the absence of Cd^{2+}, clear inward currents were evoked by potentials more positive than −30 mV. In the presence of Cd^{2+}, most inward currents were abolished, indicating that the vast majority of the inward current was Ba^{2+} currents (I_{Ba}) through HVA Ca^{2+} channels. I considered the net current, which was calculated by subtracting the remaining current in the presence of Cd^{2+} from the current in the absence of Cd^{2+}, to be the current through VGCCs.

Baclofen (100 μM) reduced the amplitude of the I_{Ba} response to depolarizing voltage pulses in virtually all SFO neurons examined (Fig. 6A and B show example traces without and with baclofen, respectively). Two types of inhibition of I_{Ba} were observed when baclofen was applied to SFO neurons, namely kinetic slowing and steady-state inhibition; these two types of inhibition have previously been observed for VGCC inhibition in various other types of CNS neurons (Scholz and Miller, 1991; Pearson et al., 1993; Harayama et al., 2014). Here, the extent of kinetic slowing was assessed by calculating

the ratio between I_{Ba} recorded 5–10 and 40–45 ms after the onset of depolarizing pulses. Out of the 88 SFO neurons examined, 48 (55%) showed kinetic slowing as demonstrated by I_{Ba} inhibition together with a reduction of more than 0.05 in the ratio (5–10/40–45ms) in response to baclofen.

To assess the voltage-dependency of baclofen-induced I_{Ba} inhibition, I examined the current-voltage (IV) relationship for I_{Ba} in the presence and absence of baclofen (100 μM) in 9 neurons (Fig. 6C). As the IV curve showed that the I_{Ba} peak amplitude and inhibition by baclofen were maximal at −10 mV, I used a depolarizing pulse to −10mV for 50 ms (10 s intervals) for further analysis. When examining the concentration-dependency of baclofen-induced I_{Ba} inhibition, I found that baclofen caused significant inhibition at 1–100 μM and the maximal inhibition was observed at 100 μM. Using the depolarization paradigm of pulses to −10 mV with 10 s intervals for optimal baclofen inhibition of I_{Ba}, I confirmed that inhibition by baclofen was reversible and that the two types of inhibition, kinetic slowing (Fig. 7A) and steady-state inhibition (Fig. 7B), could be observed in SFO neurons. I also noted that I_{Ba} tended to undergo rundown during experiments lasting 10–20 min or longer when using depolarizing pulses to −10 mV at 10 s intervals. While the extent of rundown differed from cell to cell, the average rundown rate was 0.073% ± 0.01%/s (n = 58). To minimize the influence of rundown on the estimation of the inhibitory effects of baclofen and other drugs on I_{Ba}, drug effects were calculated by dividing the I_{Ba} amplitude obtained during drug application by the average of pre- and post-drug I_{Ba} amplitudes. I confirmed the involvement of $GABA_B$ receptors in baclofen-induced inhibition of I_{Ba} by showing that the $GABA_B$ antagonist CGP was indeed able to reverse the I_{Ba} inhibition by baclofen (Fig. 8A and B) in a concentration-dependent manner. The maximal recovery of I_{Ba} was obtained at 10 μM CGP (Fig. 8C),

which was consistent with the recovery by CGP of $GABA_B$-induced inhibition of the AII-induced $[Ca^{2+}]_i$ increase.

In our calcium-imaging experiments I observed potential voltage-dependency in the ability of baclofen to inhibit K^+-induced Ca^{2+} increases; thus, I examined the voltage-dependency of the baclofen-induced inhibition of I_{Ba}, using a prepulse to +120 mV lasting for 100 ms (Fig. 9A). The strongly depolarizing prepulse significantly reduced baclofen-induced inhibition of I_{Ba} (Fig. 9B, $P < 0.05$). In particular, the baclofen-induced kinetic slowing was almost eliminated by the prepulse, as clearly demonstrated in Fig. 9C where the ratio of I_{Ba} amplitudes at 5–10 ms and 40–45 ms during baclofen inhibition is almost equal to that without baclofen (Fig. 9C). After the prepulse, the remaining inhibition of I_{Ba} by baclofen became a pattern of steady-state inhibition.

The βγ subunits released from Gi-type trimeric GTP binding proteins are known to mediate inhibition of neuronal VGCC currents (Ruiz-Velasco and Ikeda, 2000). To determine whether the $GABA_B$-mediated pathway of VGCC inhibition in the present study involves Gi protein βγ subunits, I examined the effect of N-ethylmaleimide (NEM), a sulfhydryl alkylating agent that quickly and potently occludes Gi protein-mediated actions (Shapiro et al., 1994; Harayama et al., 1998; Harvey and Stephens, 2004), on the inhibition of I_{Ba} by baclofen (Fig. 9D). NEM significantly attenuated the baclofen-induced inhibition of I_{Ba}, and on average reduced the inhibitory effect of baclofen to 35% ± 10% of non-NEM control (n = 4). These results indicate that the inhibition of VGCC currents via $GABA_B$ receptors is mediated at least in part by βγ subunits released from Gi proteins, which are known to induce voltage-dependent inhibition.

Three previous studies of SFO neuronal VGCC currents have revealed that SFO neurons possess multiple types of HVA VGCCs, namely N- and L-types (Kolaj et al.,

2004; Fry et al., 2008; Wang et al., 2013). Thus, I investigated which type of VGCC is involved in baclofen-induced inhibition in SFO neurons, using type-selective VGCC blockers at their maximally effective concentrations as reported in SFO and other CNS neurons (Mintz and Bean, 1993; Tottene et al., 2000; Kolaj et al., 2004). The selective blockers of N- and P/Q-type VGCCs, ω-conotoxin GVIA and ω-agatoxin IVA respectively, irreversibly inhibited I_{Ba} (Fig. 10A and B); as such, baclofen was added immediately after I_{Ba} reached a steady level following treatment with either of these toxins. In contrast, the selective blockers of L- and R-type VGCCs, nifedipine and SNX-482 respectively, caused at least partially reversible inhibition (Fig. 10C and D); in these experiments, baclofen was administered in the presence of the blocker. The proportion of inhibition by the blockers of N-, P/Q-, L- and R-type VGCCs, calculated using I_{Ba} amplitudes during 5–10 ms after the onset of the depolarizing pulse, are shown in Fig. 10E. The proportion of each VGCC-blocker-sensitive component in the baclofen-sensitive component was calculated by determining the difference between the baclofen-induced I_{Ba} reduction in the presence and absence of a selective blocker, and dividing this difference by the total baclofen-sensitive current. The proportions of N-, P/Q-, L- and R-types VGCC currents in the baclofen-sensitive currents were 41 ± 18% (n = 6), 50 ± 11% (n = 5), 41 ± 7.8% (n = 7), and 12 ± 11% (n = 5), respectively (Fig. 10F). Both the total inhibition calculated by adding the values from all VGCC types and the total proportion of baclofen-sensitive currents well exceeds 100%. This may be caused by overestimation of the magnitude of inhibition due to the rundown of I_{Ba}. These results indicate that the major targets of baclofen-induced inhibition were N-, P/Q-, and L-type VGCCs in SFO neurons.

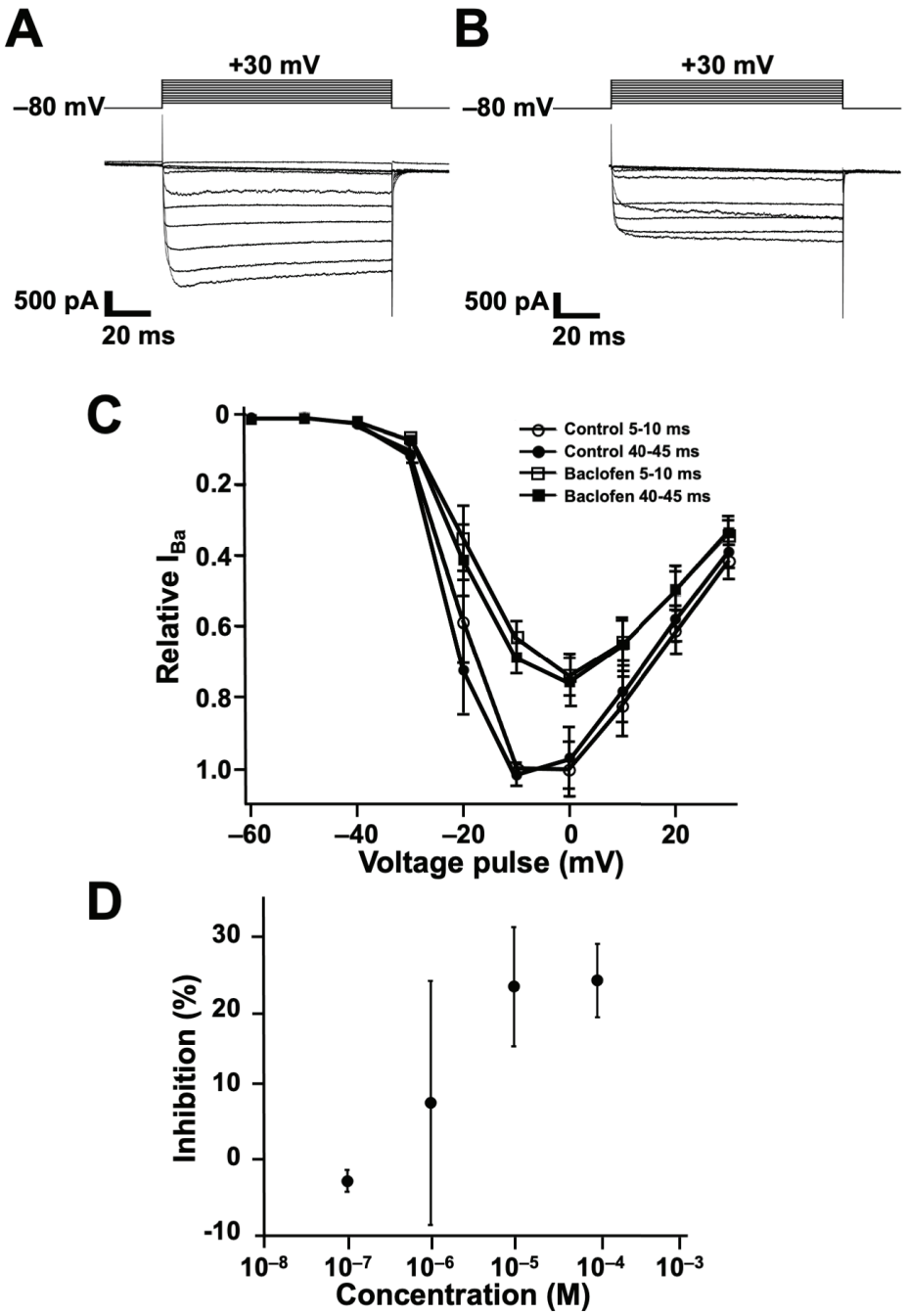

Fig. 6 The current-voltage relationship of voltage-gated Ca^{2+} channel (VGCC) currents recorded in the absence and presence of baclofen in rat SFO neurons. **A, B** Representative I_{Ba} evoked by 50 ms depolarizing voltage pulses from –80 mV to potentials ranging between –60 and +30 mV (10 mV steps) in SFO neurons in the absence (**A**) and presence (**B**) of baclofen (100 μM). **C** Summarized current-voltage relationship of I_{Ba} in the absence (circles) and presence (squares) of baclofen (n = 9 neurons, averages during 5–10 ms [open points] and 40–45 ms [closed points] after the onset of depolarizing pulses). I_{Ba} amplitudes were normalized to the peak amplitude of I_{Ba} evoked by a voltage pulse to –10 mV during 5–10 ms after the onset of the voltage step. **D** Concentration-dependency of baclofen-induced I_{Ba} inhibition (10^{-7} M, n = 4; 10^{-6} M, n = 5; 10^{-5} M, n = 6; 10^{-4} M, n = 11), with average I_{Ba} recorded during 10–15 ms after the onset of depolarizing pulses. Graphs show mean ± SEM.

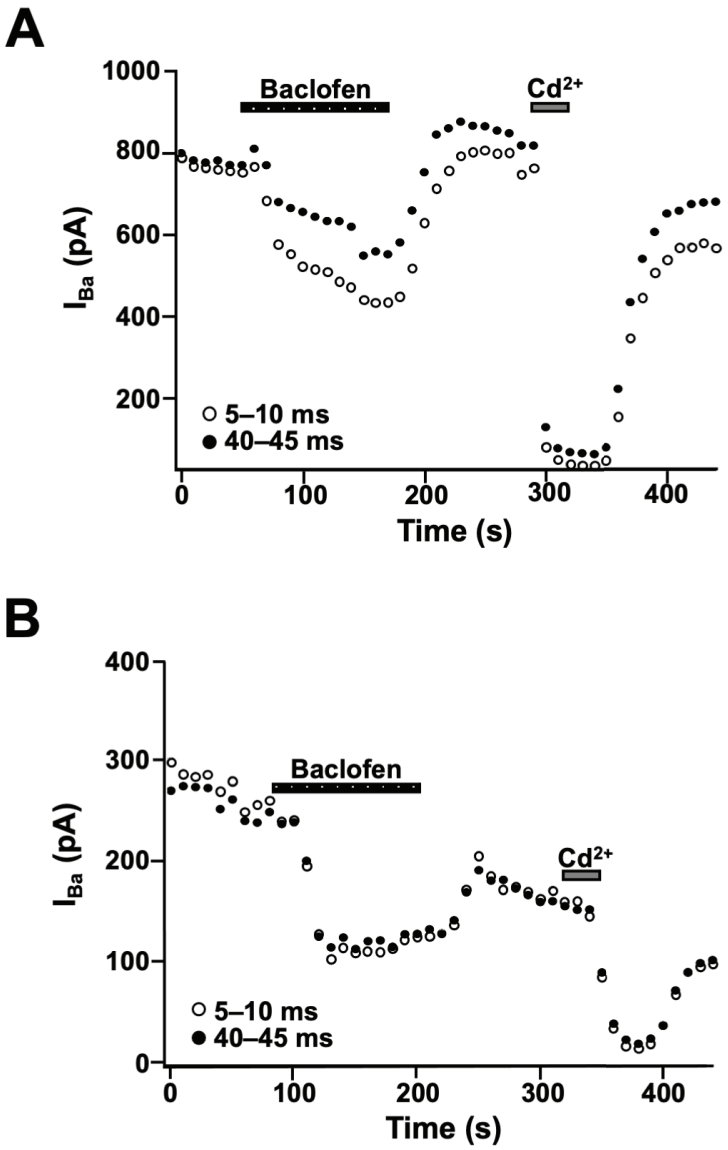

Fig. 7 The time course of baclofen-induced inhibition of VGCC currents. **A**, **B** Representative I_{Ba} traces in response to pulses from the holding potential of –80 mV to –10 mV (10 s interval) recorded before, during, and after baclofen (100 μM) application. The open and closed circles represent I_{Ba} amplitudes calculated during 5–10 ms and 40–45 ms, respectively, after the onset of depolarizing pulses. The trace in **A** clearly shows a larger inhibition for I_{Ba} at 5–10 ms than 40–45 ms, indicative of kinetic slowing, whereas the trace in **B** shows similar inhibition in I_{Ba} at 5–10 and 40–45 ms, indicative of steady-state inhibition.

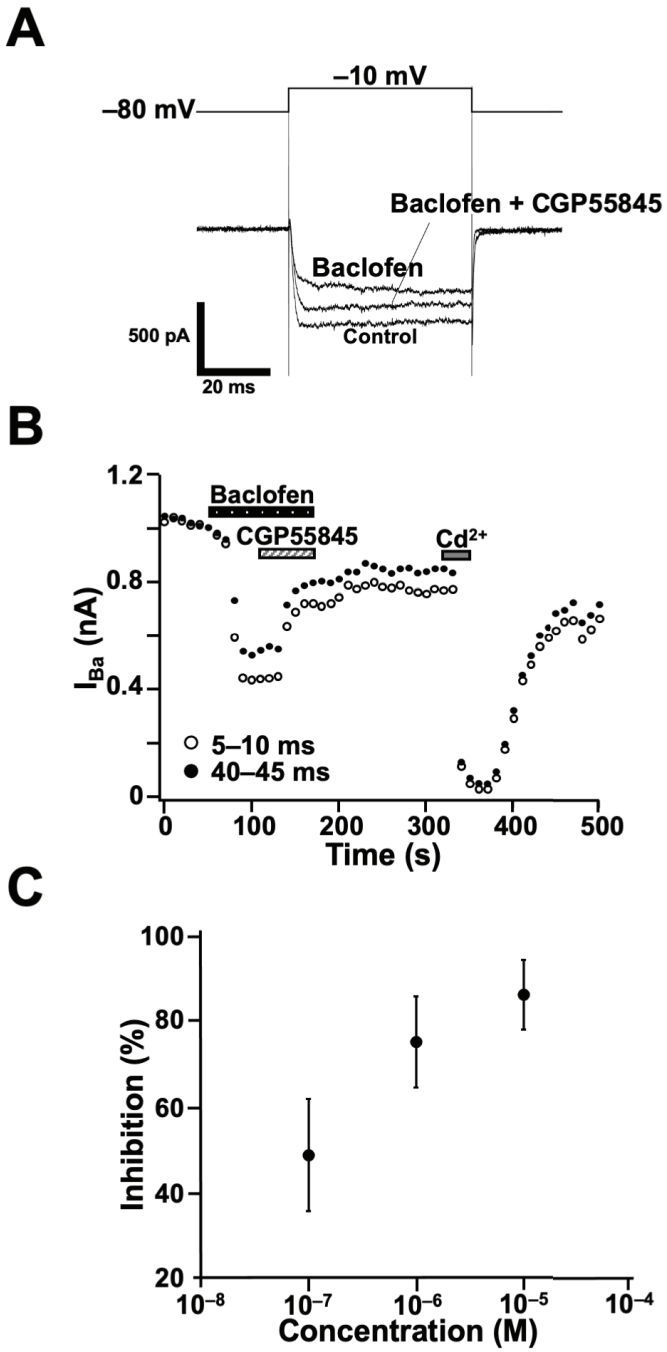

Fig. 8 The effect of CGP55845 on baclofen-induced inhibition of VGCC currents. **A** Representative I_{Ba} traces in response to depolarizing pulses from the holding potential of –80 mV to –10 mV (10 s interval) recorded before and during baclofen (100 µM) application, and during co-application of CGP (10 µM) and baclofen. **B** Representative time course of I_{Ba} showing the effects of baclofen (100 µM) and CGP (10 µM). The open and closed circles represent I_{Ba} amplitudes during 5–10 ms and 40–45 ms, respectively, after the onset of depolarizing pulses. **C** Concentration-dependency of the blockade of baclofen-induced inhibition of I_{Ba} by CGP (10^{-7} M, n = 7; 10^{-6} M, n = 9; 10^{-5} M, n = 4). The magnitude of the blockade was calculated from the average of I_{Ba} recorded 10–15 ms after the onset of depolarizing pulses. Graphs show mean ± SEM.

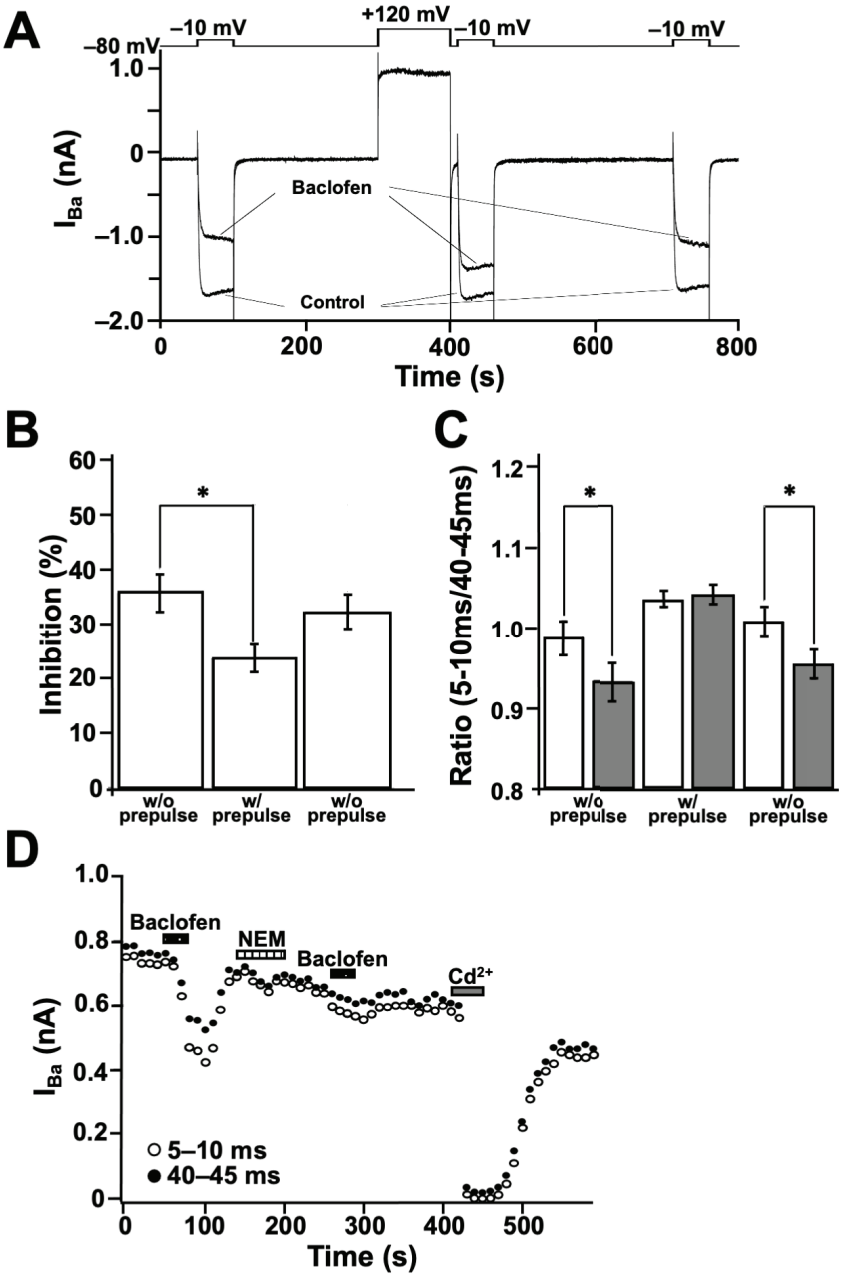

Fig. 9 The effects of a large prepulse and N-ethylmaleimide (NEM) on baclofen-induced inhibition of I_{Ba}. **A** Representative I_{Ba} traces in response to three step pulses from the holding potential of –80 mV to –10 mV (20 s interval) recorded with and without baclofen (100 μM). The second step pulse was preceded by a large prepulse (to +120 mV, 100 ms) to observe voltage-dependent removal of inhibition by baclofen (100 μM). Note that the kinetic slowing of I_{Ba} was not observed after the prepulse. **B** Summary data for the magnitude of the baclofen-induced inhibition of I_{Ba} (recorded 10–15 ms after the onset of depolarizing pulses) with (w/) and without (w/o) prepulse (n = 11); *$P < 0.05$ by one-way ANOVA with post-hoc Tukey test. **C** Summary data for the ratio of I_{Ba} amplitudes measured 5–10 ms and 40–45 ms after the onset of depolarizing pulses (n = 11) to examine kinetic slowing; *$P < 0.05$ by paired Student's *t*-test. Open and closed bars represent the ratios of the I_{Ba} amplitudes recorded in the absence and presence of baclofen, respectively. **D** Representative time course showing the effect of baclofen on I_{Ba} before and after the application of NEM (100 μM). I_{Ba} was recorded during depolarizing pulses from –80 mV to –10 mV for 50 ms applied with 10 s intervals. The open and closed circles represent I_{Ba} amplitudes measured at 5–10 ms and 40–45 ms, respectively, after the onset of depolarizing pulses. Graphs show mean ± SEM.

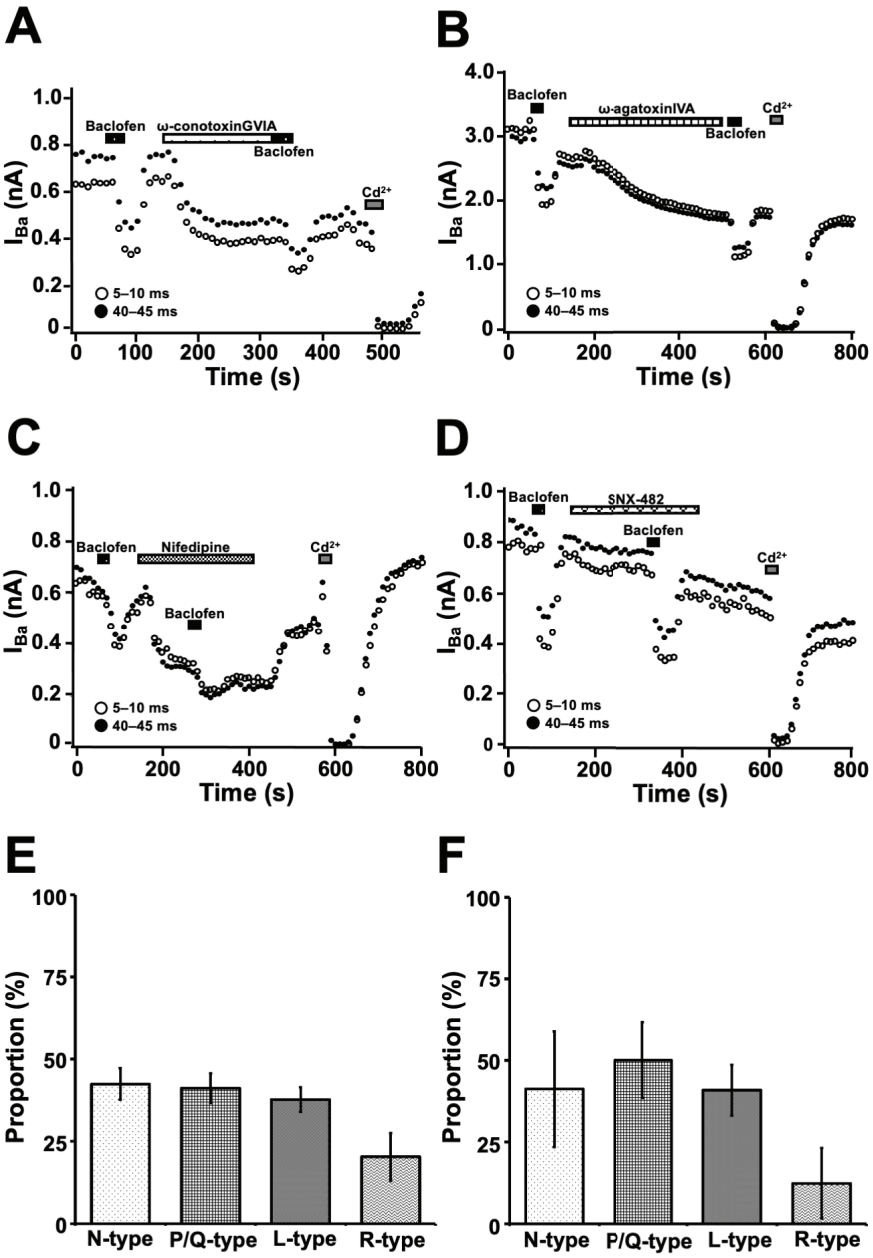

Fig. 10 The effects of selective blockers for high-voltage-activated Ca^{2+} channels (N-, P/Q-, L- and R-types) on I_{Ba} and baclofen (100 μM)-induced I_{Ba} inhibition. I_{Ba} was recorded with depolarizing pulses from –80 mV to –10 mV for 50 ms applied at 10 s intervals. The open and closed circles represent I_{Ba} amplitudes during 5–10 ms and 40–45 ms, respectively, after the onset of depolarizing pulses. **A–D** Representative time courses of changes in I_{Ba} amplitude, showing baclofen responses before and during the application of selective blockers for N-type (**A**, ω-conotoxin GVIA, 1 μM), P/Q-type (**B**, ω-agatoxin IVA, 0.1 μM), L-type (**C**, nifedipine, 10 μM), or R-type (**D**, SNX-482, 0.2 μM) VGCCs. **E** Summary data for the magnitude of the inhibition of I_{Ba} by the four VGCC blockers. The magnitude of the I_{Ba} inhibition was calculated by dividing the difference between I_{Ba} recorded just before and just after blocker application by the control I_{Ba}. **F** Summary data for the proportion of baclofen-sensitive currents through each subtype of the VGCC. The proportions of I_{Ba} sensitive to each blocker in the baclofen-sensitive I_{Ba} was calculated by dividing the difference between the total baclofen-induced current reduction and that during the blocker treatment by the total baclofen-sensitive current in the absence of any blockers. Graphs in **E** and **F** show mean ± SEM from experiments using N-type (n = 6), P/Q-type (n = 6), L-type (n = 7), and R-type (n = 5) VGCCs.

3. Discussion

Although the previous literature suggested that only $GABA_A$ receptors were involved in the inhibitory effects of GABA on SFO neuron functions, I identified here a dual role for $GABA_A$ and $GABA_B$ receptors.

3.1 The effects of the inhibitory transmitters GABA, galanin, and ANP on AII-induced persistent $[Ca^{2+}]_i$ increase in SFO neurons

In the present study I examined the inhibitory actions of the three physiologically relevant inhibitory ligands for SFO neurons, GABA, galanin, and ANP, on persistent $[Ca^{2+}]_i$ increase induced by application of angiotensin II (AII). GABA is the primary inhibitory neurotransmitter in the SFO (Jones and Mogenson, 1982; Unger et al., 1983; Abe et al., 1988). Injection of ANP into the ventricles or SFO attenuates water intake induced by AII (Nakamaru et al., 1986; Lin and Hubbard, 1992), while co-injection of galanin with intracerebroventricular AII also significantly inhibits AII-induced water intake (Hirase et al., 2008). Here, I demonstrated that all three ligands significantly inhibited the persistent AII-induced $[Ca^{2+}]_i$ increase in SFO neurons, consistent with their actions countering the behavioral effects of AII. GABA exhibited the most potent inhibition of the three ligands, often inhibiting not only the AII-induced $[Ca^{2+}]_i$ increase but also the maintenance of basal $[Ca^{2+}]_i$. Moreover, inhibition by GABA was observed in more than 90% of AII-responsive neurons, compared to galanin in 60% or ANP in around 30% of AII-responsive neurons. Our results indicate that GABA has the largest suppressive effect on AII-responsive SFO neurons among these three ligands.

3.2 The importance of $GABA_B$ receptors in suppression of the AII-induced persistent $[Ca^{2+}]_i$ increase in SFO neurons

In Chapter 2, I reported that the AII-induced $[Ca^{2+}]_i$ increase is mediated by the angiotensin II type 1 receptor and the persistent phase is maintained entirely by Ca^{2+} entry, with the prolonged Ca^{2+} entry likely enabled by long-lasting depolarization due to cation channel activation and mediated at least in part by L- and P/Q-type VGCCs (Izumisawa et al., 2019b). I also reported that the AII-induced $[Ca^{2+}]_i$ increase is inhibited by GABA (Izumisawa et al., 2019b), but the subtype of GABA receptor responsible for this inhibition had not yet been identified. In the present study, I used selective agonists and antagonists of $GABA_A$ and $GABA_B$ receptors to demonstrate that both $GABA_A$ and $GABA_B$ receptors are involved in the actions of the physiological ligand GABA in suppressing the AII-induced persistent $[Ca^{2+}]_I$ increase in SFO neurons. Our results are in accordance with previous studies showing an inhibitory effect of GABA through $GABA_A$ receptors in the SFO (Weindl et al., 1992, Inenaga et al., 1995). Both the $GABA_A$ agonist muscimol and $GABA_B$ agonist baclofen were reported to inhibit release of noradrenaline (Tanaka et al., 2002) and serotonin (Takahashi et al., 2016) in the SFO area, and it was also reported that baclofen induced membrane potential hyperpolarization and decreased firing rate in a subset of SFO neurons (Inenaga et al., 1995) . However, all three previous reports pertaining to the effects of $GABA_B$ receptor activation on neuronal function in the SFO either used the agonist baclofen only and omitted GABA from their experiments or failed to observe a blockade of the GABA effect by the $GABA_B$ antagonist phaclofen. Importantly, the presence of baclofen-induced effects does not necessarily mean that the $GABA_B$ receptor is involved in inhibition by the physiological ligand GABA. In our current study, I discovered that

$GABA_B$ receptors are definitively involved in the inhibitory effect of GABA on the AII-induced $[Ca^{2+}]_i$ increase in SFO neurons, using the $GABA_B$ agonist baclofen to mimic and the $GABA_B$ antagonist CGP to attenuate the effect of GABA. To the best of our knowledge our study is the first report showing that $GABA_B$ receptors play a physiological role in the inhibition of SFO neurons by GABA.

Thus, I suggest that inhibition of the AII-induced persistent $[Ca^{2+}]_i$ increase by GABA is mediated by the dual GABA receptor mechanisms. Similar inhibitory effects mediated by both GABA receptor subtypes are reported in a study of spontaneous $[Ca^{2+}]_i$ oscillations in toad melanotrophs (Shibuya et al., 1997). Although mediation through both subtypes may appear redundant, $GABA_A$ and $GABA_B$ receptors act via different intracellular mechanisms and their dual involvement could assure that inhibition of SFO neurons could be maintained in conditions where Gi-protein-coupled inhibitory mechanisms were impaired, chloride equilibrium potential was shifted to a less negative potential, or ligand-gated channels were desensitized.

3.3 The intracellular mechanisms of GABA-induced suppression of $[Ca^{2+}]_i$ increases in SFO neurons

The cellular mechanisms by which $GABA_A$ and $GABA_B$ receptors modulate neuronal cell functions have been well documented. The $GABA_A$ receptor is a ligand-gated Cl^- channel whose opening mediates hyperpolarization (Sieghart, 2006). The $GABA_B$ receptor is a seven-transmembrane G-protein-coupled receptor (GPCR) (Weindl et al., 1992; Wojcik and Holopainen, 1992; Bowery, 2010); the binding of GABA to the $GABA_B$ receptor inhibits adenylate cyclase to reduce intracellular cyclic AMP concentration, activates G-protein-coupled inwardly-rectifying potassium (GIRK)

channels to hyperpolarize the membrane potential, and inhibits VGCC activity to reduce Ca^{2+} entry (Misgeld et al., 1995; Bettler et al., 2004). βγ subunits released from the Gi protein can act directly on GIRK channels and VGCCs (Gage, 1992; Ruiz-Velasco and Ikeda, 2000; Dolphin, 2003; Zamponi and Currie, 2013; Jurčić et al., 2019). I consider it likely that hyperpolarization via dual types of GABA receptors closes the VGCCs opened by AII (Izumisawa et al., 2019b) and suppresses the AII-induced $[Ca^{2+}]_i$ increase.

$GABA_A$ receptors were implicated in the inhibition of depolarization-induced calcium influx by our results showing that GABA, but not baclofen, significantly inhibited the 50 mM K^+-evoked $[Ca^{2+}]_i$ increase. As the equilibrium potential of Cl^- in neurons is hyperpolarized compared with the resting potential, activation of $GABA_A$ receptor Cl^- channel by GABA would hyperpolarize the membrane via influx of extracellular Cl^- and interfere with the depolarization evoked by the high extracellular concentration of K^+. Thus, I assume that the $GABA_A$ receptor-mediated action of GABA on the 50 mM K^+-evoked $[Ca^{2+}]_i$ increase is via prevention, rather than inhibition, of depolarization.

The role of $GABA_B$ receptors may be more complex than that of $GABA_A$ receptors in GABA-induced inhibition of SFO neurons. Our results show that the $GABA_B$ agonist baclofen inhibited VGCCs currents (I_{Ba}) in response to depolarization in voltage-clamp electrophysiology experiments, but did not inhibit the $[Ca^{2+}]_i$ increase evoked by 50 mM K^+. The lack of inhibition by baclofen following 50 mM K^+ application may be due to $GABA_B$ receptor activation opening GIRK potassium channels and making neurons more sensitive to the raised extracellular K^+ concentration. This could be interpreted to mean that the $GABA_B$ receptor-mediated pathway in SFO neurons is coupled with K^+ channels but not with VGCCs. There are several reports showing that a certain combination of β and γ subunits has preferential effects on VGCC inhibition over GIRK activation (Ito et

al., 1992; Clapham and Neer, 1993; Wickman et al., 1994; Yamada et al., 1994; Isomoto et al., 1997). Whether or not other combinations of βγ subunits have reversed preferential effects on these two channels remains to be elucidated.

However, $GABA_B$ receptors are also known to have another mechanism to inhibit depolarization-induced $[Ca^{2+}]_i$ increase, namely the direct closure of VGCCs. When I applied a more mild depolarizing stimulus of 10 mM K^+ and induced a smaller $[Ca^{2+}]_i$ increase, I found that baclofen was capable of inhibiting the evoked $[Ca^{2+}]_i$ increase; thus, the coupling of the $GABA_B$ receptor pathway with VGCCs may be voltage-dependent in SFO neurons. Inhibition of VGCCs by Gi-coupled receptors via βγ subunits is reduced by strong depolarization (Zamponi and Currie, 2013), and indeed I found that baclofen-induced inhibition of VGCC currents was at least partially abolished by a strong depolarizing prepulse, suggesting that $GABA_B$ activation directly inhibits VGCCs by Gi protein βγ subunits. Supporting the invovlement of Gi proteins, I found that the inhibition by baclofen was attenuated with pretreatment with the Gi-inhibitor NEM. Our results indicate that $GABA_B$ receptors couple with VGCCs via Gi proteins to exert voltage-dependent inhibition of calcium influx in SFO neurons.

3.4 The $GABA_B$ receptor-mediated inhibition of voltage-gated Ca^{2+} channel subtypes in SFO neurons

Our patch-clamp results showed that $GABA_B$ receptor activation resulted in potent inhibition of VGCC currents in SFO neurons. $GABA_B$ receptors have been shown to inhibit VGCCs in various types of CNS and peripheral nervous system (PNS) neurons (Dolphin, 1995; Bowery and Enna, 2000). Multiple types of HVA VGCCs, but no low-voltage-activated VGCCs, have been identified in SFO neurons (Kolaj et al., 2004; Fry

et al., 2008; Wang et al., 2013). Two studies reported that L- and N- type VGCCs were preferentially potentiated by prostaglandin E_2 (Wang et al., 2013) and AII (Washburn and Ferguson, 2001), respectively; however, there are no reports regarding inhibition of specific VGCCs in SFO neurons to date.

Here, I used selective VGCC blockers to demonstrate that not only N- and L-type channels, but also P/Q- and R-type HVA Ca^{2+} channels, are present in SFO neurons. I found that N-, P/Q-, and L-type channels are the major baclofen-sensitive VGCCs in SFO neurons. $GABA_B$ receptors have been reported to preferentially inhibit N- and P/Q-type VGCCs at the somato-dendritic region in various types of CNS and PNS neurons (Doze et al., 1995; Connor and Christie, 1998; Harayama et al., 1998; Chieng and Bekkers, 1999; Carbone et al., 2001) and in presynaptic VGCCs at nerve terminals (Huston et al., 1995; Satake et al., 2004). Preferential coupling of $GABA_B$ receptors with N- and P/Q-type VGCCs, rather than GIRK channels, has been previously reported in supraoptic neurons (Harayama et al., 2014). Moreover, $GABA_B$ receptors in retinal neurons facilitate L-type VGCCs while inhibiting N-type VGCCs (Shen and Slaughter, 1999). Inhibition of L-type channels by Gi-coupled GPCRs is rare in neuronal cells (Wojcik et al., 1990) but is more common in endocrine cells, where inhibition of L-type channels via Gi-coupled receptors including $GABA_B$ receptors has been reported in pituitary endocrine cells, adrenal chromaffin cells, pancreatic islet cells, and enterochromaffin cells (Tallent et al., 1996; Tanaka et al., 1998; Zeng et al., 1999; Carbone et al., 2001; Braun et al., 2008). As there are several known isoforms of the L-type channel pore-forming $\alpha 1$ subunit, it is possible that inhibition of L-type channels by GPCRs requires particular combinations of L-type channel subclass and intracellular downstream signaling molecules. The precise mechanisms of inhibition of L-type VGCCs by $GABA_B$

receptors should be studied by examining the molecular subclass of L-type channels in SFO neurons, for which no data exists at present.

Our present finding of inhibition of L- and P/Q-type VGCCs through $GABA_B$ receptors matches our previous result where the AII-induced $[Ca^{2+}]_I$ increase was significantly reduced by blockers of L- and P/Q-type VGCCs (Izumisawa et al., 2019b), consistent with the notion that L- and P/Q-type VGCCs are involved in the persistent phase of the $[Ca^{2+}]_I$ response to AII (Izumisawa et al., 2019b). The N-type channel blocker also tended to inhibit the AII-induced $[Ca^{2+}]_i$ increase, but its statistical significance was not confirmed because of the relatively large variation. It may be possible that N-type channels are also involved in the baclofen-induced inhibition of the AII-induced $[Ca^{2+}]_i$ increase in a subset of SFO neurons. Furthermore, the lack of effect of the $GABA_A$ receptor antagonist BMI on GABA-induced inhibition of the $[Ca^{2+}]_i$ increase at a physiological concentration as low as 10 μM suggests that a considerable $GABA_B$-receptor-mediated component exists in the action of GABA, and that the VGCCs in SFO neurons may be under tonic inhibitory control by Gi-coupled $GABA_B$ receptors *in vivo*.

3.5 The possible mechanisms of action for the inhibitory ligands ANP and galanin

In the present study, I found that both ANP and galanin directly act on SFO neurons to attenuate the AII-induced persistent $[Ca^{2+}]_i$ increase. In the SFO, a radioimmunoassay study reported a large number of ANP binding sites (Quirion, 1989) but detection with ANP antisera showed few immunopositive reactions of ANP (Kawata et al., 1985). Therefore, ANP may regulate SFO neurons as a circulating humoral factor rather than as a neurotransmitter released from nerve endings projecting to the SFO. In contrast, nerve

terminals in the rat SFO show a galanin-like immune response (Kai et al., 2006), suggesting that galanin may regulate SFO as a neurotransmitter.

Our finding that ANP inhibited the AII-induced persistent $[Ca^{2+}]_i$ increase is consistent with previous results showing that ANP counteracts the actions of AII in studies of electrophysiology and drinking behavior (Nakamaru et al, 1986; Hattori et al., 1988; Lin and Hubbard, 1992). However, in the present study only 30% of AII-responsive neurons were inhibited by ANP and the magnitude of the inhibition by ANP was considerably smaller than that of GABA or galanin. It seems unlikely that the weak influence of ANP observed in the present study explains the potent counteractions of ANP on the action potential discharge or drinking behavior induced by AII in SFO neurons. It is possible that our dissociation method selectively collected ANP-insensitive SFO neurons, which would result in underestimation of the ANP influence. It is also possible that ANP has direct and more potent actions on AII-unresponsive SFO neurons innervating AII-responsive neurons, thereby suppressing the effects of AII.

The inhibitory effect of galanin was also observed a previous electrophysiological study (Kai et al., 2006) and it has been suggested that galanin acts on SFO neurons mainly via GalR1 to inhibit the AII-induced persistent $[Ca^{2+}]_I$ increase. In the present study, I found that more than half of the AII-responsive neurons were inhibited by galanin and that the inhibition rate by galanin was nearly 100%, suggesting that galanin is potent enough to eliminate the $[Ca^{2+}]_i$-increasing effect of AII. The inhibitory action of galanin in other areas of the brain, such as the locus coeruleus and supraoptic nucleus neurons, is thought to be due to increased K^+ conductance across the cell membrane (Papas and Bourque 1997; Ren et al., 2001). AII suppresses outward-rectifying K^+ current in SFO neurons (Ferguson and Li, 1996); therefore, it is possible that galanin hyperpolarizes the

cell membrane and suppresses SFO neuronal activation by opening K^+ channels which were closed by AII or other K^+ channels on which AII did not act. As I found that the AII-induced persistent $[Ca^{2+}]_i$ increase has voltage-dependent component (Izumisawa et al., 2019b); the inhibition by galanin may be explained, at least in part, by the above-mentioned effects on K^+ channels. Moreover, as galanin receptors are known to couple with Gi proteins in a similar manner to $GABA_B$ receptors (Bartfai et al., 1992), it would be reasonable to assume galanin inhibits VGCCs to suppress Ca^{2+} entry. Preliminary results in our laboratory indicate that galanin also inhibits VGCCs and suggest that a similar mechanism to the one I revealed for $GABA_B$ receptors may underlie the inhibitory action of galanin. The detailed mechanisms by which ANP and galanin inhibit the persistent $[Ca^{2+}]_i$ increase induced by AII should be clarified in future experiments.

3.6. The physiological significance of inhibition of the persistent $[Ca^{2+}]_i$ increase in SFO neurons

In the present study, I used the persistent $[Ca^{2+}]_i$ increase induced by continuous administration of AII at nanomolar concentrations as the paradigm to examine the effects of inhibitory ligands and their underlying mechanisms. However, it is unclear whether the plasma AII concentration could reach sufficiently high levels to expose SFO neurons to nanomolar AII under physiological or pathological circumstances. Elevation of the plasma AII concentration to nanomolar levels *in vivo* may be caused by a sudden decrease in blood pressure, acute dehydration-induced disruption of the circulation, or pathological conditions such as chronic hypertension. In fact, it was reported that the plasma concentration of AII increases to 150 pM in dehydrated rats (Navar et al., 1994) and to above 600 pM in spontaneously hypertensive rats (Castro-Moreno et al., 2012), and that

such high levels of AII induce persistent hypertension in rodents (Girouard et al., 2008; Iulita et al., 2019). In our previous report, I conclude that the persistent $[Ca^{2+}]_i$ increase induced by AII at nanomolar concentrations may play important roles in the physiology and/or pathophysiology of SFO neurons (Izumisawa et al., 2019b). In the present study I found that the persistent $[Ca^{2+}]_I$ increases mediated by AII in SFO neurons can be rapidly and reversibly suppressed by physiologically relevant inhibitory ligands. This reversibility of the $[Ca^{2+}]_i$ increase induced by nanomolar AII supports the notion that the calcium response is a physiologically relevant response, rather than an irreversible increase in plasma membrane or mitochondria membrane Ca^{2+} permeability, which is known to occur in some pathological conditions (Giorgio et al., 2018; Martin and Bernard, 2018; Morris et al., 2018). Our patch-clamp recordings suggest that $GABA_B$ receptors are involved in the inhibitory regulation in virtually all SFO neurons, although our $[Ca^{2+}]_i$ measurements indicate that they are involved in the majority of AII-responsive neurons. As the SFO consists of several heterogenous populations of neurons (Sunn et al., 2003; Ferguson and Bains, 1997), our results indicate that $GABA_B$-mediated inhibition is particularly important within the SFO. Future studies will need to address the intriguing question of how the function of the SFO is altered as a consequence of a persistent $[Ca^{2+}]_i$ increase, and how this putative functional alteration is regulated by the interplay between AII and the inhibitory ligands GABA, galanin, and ANP *in vivo*.

4. Graphical abstract

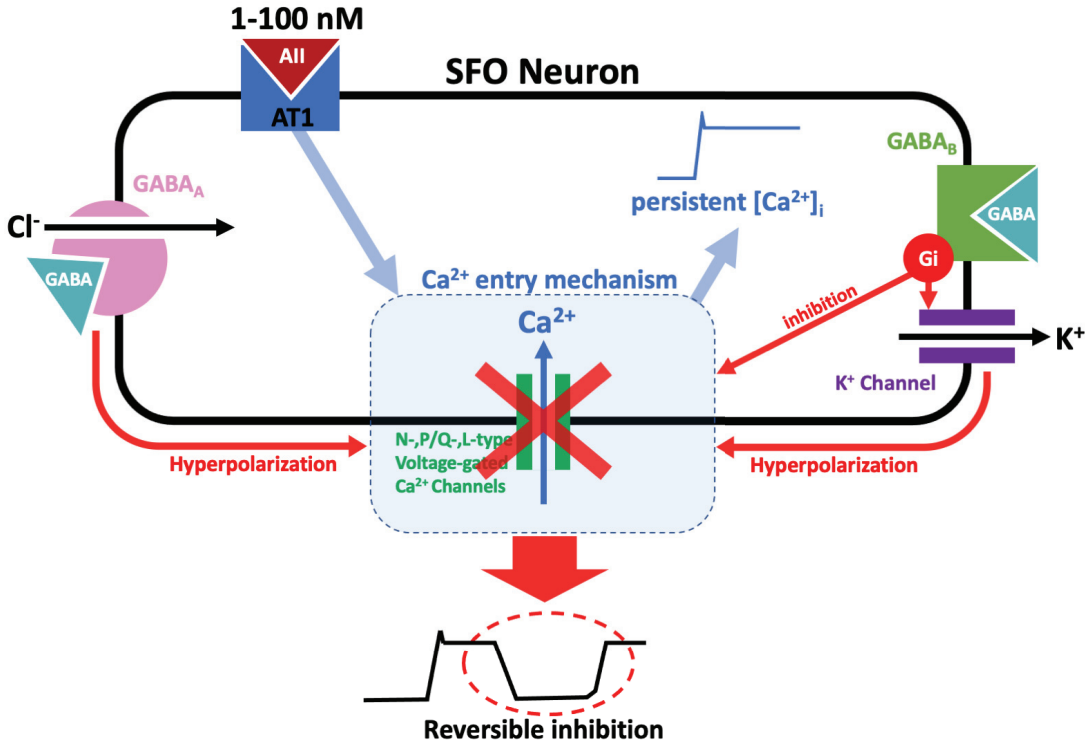

5. Experimental procedures

5.1 Solutions

As described in Chapters 1 and 2 (Izumisawa et al. 2019a, 2019b), SFO neurons were dissociated and perfused in HEPES-buffered solution (HBS) containing (in mM) 140 NaCl, 5 KCl, 2 $CaCl_2$, 1 $MgCl_2$, 10 glucose, and 10 HEPES (pH adjusted to 7.4 with Tris). The osmolality of the HBS was 298 ± 6 mOsmol/kg (n=5). For 50 mM K^+ (high K^+) solution, 45 mM Na^+ was replaced with equimolar K^+.

5.2 Dissociation of SFO neurons

Dissociated SFO neurons were prepared as previously described (Shibuya et al. 1998, Izumisawa et al. 2019b). All experiments were carried out under the control of the Ethics Committee of Animal Care and Experimentation, Tottori University, Japan. In brief, young male Wistar rats (three to four weeks of age) were deeply anesthetized with isoflurane, and brains were removed to ice-cold HBS. The SFO tissues were isolated from brains and then enzymatically and physically dissociated as previously described (Shibuya et al. 1998, Izumisawa et al. 2019b). The dissociated SFO cells were plated on coverslips (11 mm diameter, 0.12 mm thickness) and incubated in oxygenated HBS for 40 min at room temperature (22–24°C) before loading with fura-2.

5.3 $[Ca^{2+}]_i$ measurement

The $[Ca^{2+}]_i$ in SFO neurons was measured with fura-2 according to the protocol I reported previously (Izumisawa et al. 2019a, 2019b). For fura-2 loading, dissociated SFO cells were incubated in HBS with the addition of membrane-permeable acetoxymethyl esters of fura-2 (fura-2/AM, 1 μM) for 60 min at room temperature. The cells were then

washed by perfusing with dye-free HBS before measurements of $[Ca^{2+}]_i$.

The arrangements for measuring fluorescence have been described previously (Shibuya et al., 1998, Moriya et al., 2015, Izumisawa et al., 2019a, 2019b). In brief, cells were continuously perfused with HBS in a small-volume chamber (approximately 200 μL) that had a glass coverslip bottom and was positioned on the stage of an inverted microscope (IX71, Olympus, Tokyo, Japan). The solution in the chamber was completely changed in a few seconds at a perfusion rate of 1.5 mL/min using peristaltic pump (Minipuls 3, Gilson, Middleton, WI, USA). Fluorescence images with excitation at 340 and 380 nm were recorded at 5 s intervals unless otherwise noted with CCD camera systems (AquaCosmos, Hamamatsu Photonics, Hamamatsu, Japan). The ratio of fluorescence for each pixel obtained with excitation at 340 and 380 nm (F340/F380) was used to calculate $[Ca^{2+}]_i$. A calibration curve for F340/F380 was obtained from measurements with free-acid membrane-impermeable fura-2 dissolved in series of Ca^{2+}-buffered solutions containing 0, 17, 38, 65, 100, 150, 225, 351, 602, 1350, and 39000 nM free Ca^{2+} (Life Technologies, Carlsbad, CA, USA). To estimate $[Ca^{2+}]_i$ in individual cells, regions of interest (ROIs) were chosen to include the soma of each SFO cell, and average values of $[Ca^{2+}]_i$ in pixels included in each ROI were calculated. All experiments were performed at room temperature (22–24°C).

The baseline $[Ca^{2+}]_i$ in each cell was determined by calculating the average $[Ca^{2+}]_i$ at the beginning of measurement in cells showing little or no spontaneous activity, or by calculating the lowest $[Ca^{2+}]_i$ value during inter-oscillation periods in cells showing spontaneous Ca^{2+} oscillations. All cells were stimulated with 50 mM K^+ either at the beginning or at the end of experiments, and those showing 50 mM K^+-induced $[Ca^{2+}]_i$ responses >50 nM from baseline were regarded as healthy neurons and were used for

further analysis. The amplitude of $[Ca^{2+}]_i$ responses was expressed as $\Delta[Ca^{2+}]_i$, which was calculated by subtracting the averaged basal $[Ca^{2+}]_i$ before drug application from the peak $[Ca^{2+}]_i$ detected after the onset of drug application. The $[Ca^{2+}]_i$ responses to AII was assessed by calculating the ratio of $\Delta[Ca^{2+}]_i$ recorded 30 s before application of any other drug. The $[Ca^{2+}]_i$ responses to other stimuli was assessed by calculating the ratio of $\Delta[Ca^{2+}]_i$ recorded 30 s before wash-out of drugs.

5.4 Patch-clamp recording

Currents through VGCCs were measured with standard whole-cell voltage-clamp techniques as previously described (Fukumoto et al. 2012). Patch pipettes were pulled from micro glass capillaries (GD-1.5, Narishige, Japan) by a framed puller (P-97, Sutter, USA). Pipettes with 2.5–5 MΩ tip resistance were used. When VGCC currents were recorded, cells were perfused with the I_{Ba} solution that consisted of (in mM): 115 NaCl, 6 KCl, 10 $BaCl_2$, 1 $MgCl_2$, 10 D-glucose, and 10 HEPES (pH adjusted to 7.4 with NaOH). To reduce contamination of VGCC currents by voltage-gated Na^+ and K^+ currents, the bath solution was supplemented with TTX (1 μM, Tocris Bioscience, UK), TEA (10 mM, Sigma-Aldrich, USA), and 4-AP (1 mM, Sigma-Aldrich, USA). Ca^{2+} in the bath solution was replaced with 5 mM Ba^{2+} as a charge carrier and VGCC currents were recorded as Ba^{2+} current (I_{Ba}). Neurons were dialyzed with a pipette solution that consisted of (in mM): 110 CsCl, 20 CsOH, 1.3 $CaCl_2$, 2 $MgCl_2$, 10 EGTA, 10 D-glucose, 2 ATP, 0.3 GTP (pH adjusted to 7.3 with HCl). Cells were continuously perfused with the bath solution at a flow rate of 1 mL/min by gravity and overflow solution was removed with an electronic pump. At the end of each measurement, $CdCl_2$ (100 μM) was added to the I_{Ba} solution and the residual currents were recorded. The amplitude of VGCC currents

were calculated by subtracting these residual currents from recorded I_{Ba}. An agar bridge containing 2% agar and 154 mM NaCl in conjunction with an Ag-AgCl wire was used as the reference electrode. As liquid-junction potentials between the bath and pipette solutions were measured to be smaller than ±3 mV, they were not corrected. The patch-clamp amplifier used was Axopatch 200B (Axon Instruments, USA). Membrane potentials were controlled and whole-cell currents were sampled and stored using Axograph software (Axon Instruments) running on Macintosh (Apple, USA). Capacitance in each cell was determined by reading the dial for the C-slow compensation of the amplifier. Stored data were analyzed by IGOR Pro (WaveMetrics, USA). All electrophysiological experiments were performed at room temperature (22–24 ºC).

5.5 Drugs

Angiotensin II, ANP (Rat), galanin (Rat), ω-agatoxin IVA, ω-conotoxin GVIA and SNX-482 were purchased from Peptide Institute (Osaka, Japan); γ-aminobutyric acid (GABA), muscimol hydrobromide, baclofen, bicuculline methiodide, 4-aminopyridine (4-AP), and N-ethylmaleimide (NEM) were from Sigma-Aldrich (St. Louis, MO); CGP55845 hydrochloride was from TOCRIS bioscience (Bristol, UK); $CdCl_2$ was from FUJIFILM Wako Pure Chemical Corporation (Osaka, Japan); nifedipine was from Tokyo Chemical Industry Co., Ltd. (Tokyo, Japan); Fura-2/AM was from Dojindo (Kumamoto, Japan); and isoflurane was from Pfizer (Tokyo, Japan).

5.6 Statistics

All values are expressed as the mean ± SEM, and ‘n’ represents the number of neurons examined. The value of change relative to the internal control of each neuron was

assessed by paired Student's *t*-test or one-way ANOVA with Tukey's post-hoc test. Actual values of $[Ca^{2+}]_i$ measured in nM were assessed by using paired Student's *t*-test. The inhibition rates were assessed by using in one-way ANOVA with post-hoc Tukey test. A *P* value of < 0.05 was considered statistically significant.

6. References

Abe, M., T. Tokunaga, K. Yamada, and T. Furukawa. 1988. Gamma-aminobutyric acid and taurine antagonize the central effects of angiotensin II and renin on the intake of water and salt, and on blood pressure in rats. Neuropharmacology. 27 (3): 309-18.

Bartfai, T., G. Fisone, and U. Langel. 1992. Galanin and galanin antagonists: molecular and biochemical perspectives. Trends Pharmacol. Sci. 13 (8): 312-7.

Bettler, B., K. Kaupmann, J. Mosbacher, and M. Gassmann. 2004. Molecular structure and physiological functions of GABA(B) receptors. Physiol. Rev. 84 (3): 835-67.

Björkstrand, E., A. L. Hulting, B. Meister, and K. Uvnäs-Moberg. 1993. Effect of galanin on plasma levels of oxytocin and cholecystokinin. Neuroreport. 4 (1): 10-2.

Bloom, F. E., and L. L. Iversen. 1971. Localizing 3H-GABA in nerve terminals of rat cerebral cortex by electron microscopic autoradiography. Nature. 229 (5287): 628-30.

Bowery, N. G., and S. J. Enna. 2000. γ -Aminobutyric Acid$_B$ Receptors: first of the functional metabotropic heterodimers. Journal of Pharmacol Exp. Ther 292 (1): 2-7.

Bowery, N. G. 2010. Historical perspective and emergence of the GABA$_B$ receptor. Adv Pharmacol. 58: 1-18.

Braun, M., R. Ramracheya, M. Bengtsson, Q. Zhang, J. Karanauskaite, C. Partridge, P. R. Johnson, and P. Rorsman. 2008. Voltage-gated ion channels in human pancreatic beta-cells: electrophysiological characterization and role in insulin secretion. Diabetes. 57 (6): 1618-28.

Carbone, E., V. Carabelli, T. Cesetti, P. Baldelli, J. M. Hernández-Guijo, and L. Giusta. 2001. G-protein- and cAMP-dependent L-channel gating modulation: a manyfold system to control calcium entry in neurosecretory cells. Pflugers Arch. 442 (6): 801-13.

Castro-Moreno, P., J. P. Pardo, R. Hernandez-Munoz, J. J. Lopez-Guerrero, L. Del Valle-Mondragon, G. Pastelin-Hernandez, M. Ibarra-Barajas, and R. Villalobos-Molina. 2012. Captopril avoids hypertension, the increase in plasma angiotensin II but increases angiotensin 1-7 and angiotensin II-induced perfusion pressure in isolated kidney in SHR. Auton. Autacoid Pharmacol.32 (3 Pt 4): 61-9.

Chieng, B., and J. M. Bekkers. 1999. $GABA_B$, opioid and $\alpha 2$ receptor inhibition of calcium channels in acutely-dissociated locus coeruleus neurones. Br J Pharmacol. 127 (7): 1533-8.

Clapham, D. E., and E. J. Neer. 1993. New roles for G-protein β γ -dimers in transmembrane signalling." Nature. 365 (6445): 403-6.

Connor, M., and M. J. Christie. 1998. Modulation of Ca^{2+} channel currents of acutely dissociated rat periaqueductal grey neurons. J. Physiol.509 (Pt 1): 47-58.

Cottrell, G. T., and A. V. Ferguson. 2004. Sensory circumventricular organs: central roles in integrated autonomic regulation. Regul. Pept. 117 (1): 11-23.

Dolphin, A. C. 2003. G protein modulation of voltage-gated calcium channels. Pharmacol Rev.

Dolphin, A. C. 1995. The G.L. Brown Prize Lecture. Voltage-dependent calcium channels and their modulation by neurotransmitters and G proteins. Exp Physiol. 80 (1): 1-36.

Doze, V. A., G. A. Cohen, and D. V. Madison. 1995. Calcium channel involvement in GABAB receptor-mediated inhibition of GABA release in area CA1 of the rat hippocampus. J Neurophysiol. 74 (1): 43-53.

Ferguson, A. V., and J. S. Bains. 1997. Actions of angiotensin in the subfornical organ and area postrema: Implications for long term control of autonomic output. Clin. Exp. Pharmacol. Physiol. 24 (1): 96-101.

Ferguson, A. V., and Z. H. Li. 1996. Whole cell patch recordings from forebrain slices demonstrate angiotensin II inhibits potassium currents in subfornical organ neurons. Regul. Pept. 66 (1-2): 55-58.

Fry, M., G. T. Cottrell, and A. V. Ferguson. 2008. Prokineticin 2 influences subfornical organ neurons through regulation of MAP kinase and the modulation of sodium channels. Am J Physiol Regul Integr Comp Physiol. 295 (3): R848-56.

Fukumoto, N., N. Kitamura, K. Niimi, E. Takahashi, C. Itakura, and I. Shibuya. 2012. Ca^{2+} channel currents in dorsal root ganglion neurons of P/Q-type voltage-gated Ca^{2+} channel mutant mouse, rolling mouse Nagoya. Neurosci Res. 73 (3): 199-206.

Gage, P. W. 1992. Activation and modulation of neuronal K^+ channels by GABA. Trends Neurosci. 15 (2): 46-51.

Giorgio, V., L. Guo, C. Bassot, V. Petronilli, and P. Bernardi. 2018. Calcium and regulation of the mitochondrial permeability transition. Cell Calcium. 70: 56-63.

Girouard, H., A. Lessard, C. Capone, T. A. Milner, and C. Iadecola. 2008. The neurovascular dysfunction induced by angiotensin II in the mouse neocortex is sexually dimorphic. Am J Physiol Heart Circ Physiol. 294 (1): H156-63.

Gross, P. M. 1992. Circumventricular Organ Capillaries. Prog. Brain Res. 91: 219-233.

Harayama, N., T. Kayano, T. Moriya, N. Kitamura, I. Shibuya, K. Tanaka-Yamamoto, Y. Uezono, Y. Ueta, and T. Sata. 2014. Analysis of G-protein-activated inward rectifying K^+ (GIRK) channel currents upon $GABA_B$ receptor activation in rat supraoptic neurons. Brain Res. 1591: 1-13.

Harayama, N., I. Shibuya, K. Tanaka, N. Kabashima, Y. Ueta, and H. Yamashita. 1998. Inhibition of N- and P/Q-type calcium channels by postsynaptic $GABA_B$ receptor activation in rat supraoptic neurones. J Physiol. 509 (Pt 2): 371-83.

Harvey, V. L., and G. J. Stephens. 2004. Mechanism of GABA receptor-mediated inhibition of spontaneous GABA release onto cerebellar Purkinje cells. Eur J Neurosci. 20 (3): 684-

Hattori, Y., M. Kasai, S. Uesugi, M. Kawata, and H. Yamashita. 1988. Atrial natriuretic polypeptide depresses angiotensin II induced excitation of neurons in the rat subfornical organ in vitro. Brain Res. 443 (1-2): 355-9.

Honda, E., S. Xu, K. Ono, K. Ito, and K. Inenaga. 2001. Spontaneously active GABAergic interneurons in the subfornical organ of rat slice preparations. Neurosci Lett. 306 (1-2): 45-8.

Hirase, M., K. Ono, H. Yamashita, and K. Inenaga. 2008. Central injection of galanin inhibits angiotensin II-induced responses in rats. Neuroreport. 19 (3): 323-6.

Huston, E., G. P. Cullen, J. R. Burley, and A. C. Dolphin. 1995. The involvement of multiple calcium channel sub-types in glutamate release from cerebellar granule cells and its modulation by $GABA_B$ receptor activation. Neuroscience. 68 (2): 465-78.

Inenaga, K., T. Nagatomo, E. Honda, Y. Ueta, and H. Yamashita. 1995. GABAergic inhibitory inputs to subfornical organ neurons in rat slice preparations. Brain Res. 705 (1-2): 85-90.

Isomoto, S., C. Kondo, and Y. Kurachi. 1997. Inwardly rectifying potassium channels: their molecular heterogeneity and function. Jpn J Physiol. 47 (1): 11-39.

Ito, H., R. T. Tung, T. Sugimoto, I. Kobayashi, K. Takahashi, T. Katada, M. Ui, and Y. Kurachi. 1992. On the mechanism of G protein beta gamma subunit activation of the muscarinic K^+ channel in guinea pig atrial cell membrane. Comparison with the ATP-sensitive K^+ channel. J Gen Physiol. 99 (6): 961-83.

Iulita, M. F., S. Duchemin, D. Vallerand, T. Barhoumi, F. Alvarez, R. Istomine, C. Laurent, J. Youwakim, P. Paradis, N. Arbour, C. A. Piccirillo, E. L. Schiffrin, and H. Girouard. 2019. CD4. J Am Heart Assoc. 8 (1): e009372.

Izumisawa, Y., K. Tanaka-Yamamoto, J. Ciriello, N. Kitamura, and I. Shibuya. 2019. The cytosolic Ca^{2+} concentration in acutely dissociated subfornical organ (SFO) neurons of rats: spontaneous Ca^{2+} oscillations and Ca^{2+} oscillations induced by picomolar concentrations of angiotensin II. Brain Res. 1704:137-149.

Izumisawa, Y., K. Tanaka-Yamamoto, J. Ciriello, N. Kitamura, and I. Shibuya. 2019. Persistent cytosolic Ca^{2+} increase induced by angiotensin II at nanomolar concentrations in acutely dissociated subfornical organ (SFO) neurons of rats. Brain Res 1718:137-147.

Jones, D. L., and G. J. Mogenson. 1982. Central injections of spiperone and GABA: attenuation of angiotensin II stimulated thirst. Can J Physiol Pharmacol. 60 (5): 720-6.

Jurčić, N., G. Er-Raoui, C. Airault, J. Trouslard, N. Wanaverbecq, and R. Seddik. 2019. GABA. J Physiol. 597 (2): 631-651.

Kawata, M., K. Nakao, N. Morii, Y. Kiso, H. Yamashita, H. Imura, and Y. Sano. 1985. Atrial natriuretic polypeptide: topographical distribution in the rat brain by radioimmunoassay and immunohistochemistry. Neuroscience. 16 (3): 521-46.

Kai, A., K. Ono, H. Kawano, E. Honda, O. Nakanishi, and K. Inenaga. 2006. Galanin inhibits neural activity in the subfornical organ in rat slice preparation. Neuroscience. 143 (3):769-77.

Kolaj, M., D. Bai, and L. P. Renaud. 2004. $GABA_B$ receptor modulation of rapid inhibitory and excitatory neurotransmission from subfornical organ and other afferents to median preoptic nucleus neurons." J Neurophysiol. 92 (1): 111-22.

Lin, N., and J. I. Hubbard. 1992. ANP and naloxone reduce postdeprivation drinking after subfornical organ lesions. Brain Res Bull. 28 (5): 769-74.

Martin, N., and D. Bernard. 2018. Calcium signaling and cellular senescence. Cell Calcium 70: 16-23.

McKinley, M. J., A. M. Allen, P. Burns, L. M. Colvill, and B. J. Oldfield. 1998. Interaction of circulating hormones with the brain: The roles of the subfornical organ and the organum vasculosum of the lamina terminalis. Clin. Exp. Pharmacol. Physiol. 25: S61-S67.

Mintz, I. M., and B. P. Bean. 1993. Block of calcium channels in rat neurons by synthetic omega-Aga-IVA. Neuropharmacology. 32 (11): 1161-9.

Misgeld, U., M. Bijak, and W. Jarolimek. 1995. A physiological role for $GABA_B$ receptors and the effects of baclofen in the mammalian central nervous system. Prog Neurobiol. 46 (4): 423-62.

Moriya, T., R. Shibasaki, T. Kayano, N. Takebuchi, M. Ichimura, N. Kitamura, A. Asano, Y. Z. Hosaka, O. Forostyak, A. Verkhratsky, G. Dayanithi, and I. Shibuya. 2015. Full-length transient receptor potential vanilloid 1 channels mediate calcium signals and possibly contribute to osmoreception in vasopressin neurones in the rat supraoptic nucleus. Cell Calcium. 57 (1):25-37.

Morris, G., A. J. Walker, M. Berk, M. Maes, and B. K. Puri. 2018. Cell Death Pathways: a Novel Therapeutic Approach for Neuroscientists. Mol Neurobiol. 55 (7): 5767-5786.

Nakamaru, M., R. Takayanagi, and T. Inagami. 1986. Effect of atrial natriuretic factor on central angiotensin II-induced responses in rats. Peptides. 7 (2): 373-5.

Navar, L. G., L. Lewis, A. Hymel, B. Braam, and K. D. Mitchell. 1994. Tubular fluid concentrations and kidney contents of angiotensins I and II in anesthetized rats. J Am Soc Nephrol. 5 (4): 1153-8.

Papas, S., and C. W. Bourque. 1997. Galanin inhibits continuous and phasic firing in rat hypothalamic magnocellular neurosecretory cells. J Neurosci. 17 (16): 6048-56.

Pearson, H. A., K. G. Sutton, R. H. Scott, and A. C. Dolphin. 1993. Ca^{2+} currents in cerebellar granule neurones: role of internal Mg^{2+} in altering characteristics and antagonist effects. Neuropharmacology. 32 (11): 1171-83.

Quirion, R. 1989. Receptor sites for atrial natriuretic factors in brain and associated structures: an overview. Cell Mol Neurobiol. 9 (1): 45-55.

Ren, J., H. Z. Hu, A. M. Starodub, and J. D. Wood. 2001. Galanin suppresses calcium conductance and activates inwardly rectifying potassium channels in myenteric neurones from guinea-pig small intestine. Neurogastroenterol Motil. 13 (3): 247-54.

Ruiz-Velasco, V., and S. R. Ikeda. 2000. Multiple G-protein betagamma combinations produce voltage-dependent inhibition of N-type calcium channels in rat superior cervical ganglion neurons. J Neurosci. 20 (6): 2183-91.

Satake, S., F. Saitow, D. Rusakov, and S. Konishi. 2004. AMPA receptor-mediated presynaptic inhibition at cerebellar GABAergic synapses: a characterization of molecular mechanisms. Eur J Neurosci. 19 (9): 2464-74.

Schmid, H. A., and E. Simon. 1992. Effect of angiotensin II and atrial natriuretic factor on neurons in the subfornical organ of ducks and rats in vitro. Brain Res. 588 (2):324-8.

Scholz, K. P., and R. J. Miller. 1991. $GABA_B$ receptor-mediated inhibition of Ca^{2+} currents and synaptic transmission in cultured rat hippocampal neurones. J Physiol. 444: 669-86.

Shapiro, M. S., L. P. Wollmuth, and B. Hille. 1994. Modulation of Ca^{2+} channels by PTX-sensitive G-proteins is blocked by N-ethylmaleimide in rat sympathetic neurons. J Neurosci. 14 (11 Pt 2): 7109-16.

Shen, W., and M. M. Slaughter. 1999. Metabotropic GABA receptors facilitate L-type and inhibit N-type calcium channels in single salamander retinal neurons. J Physiol. 516 (Pt 3): 711-8.

Shibuya, I., S. Kongsamut, and W. W. Douglas. 1997. Both $GABA_A$ and $GABA_B$ receptors participate in suppression of $[Ca^{2+}]_i$ pulsing in toad melanotrophs. Eur J Pharmacol. 321 (2): 241-6.

Shibuya, I., J. Noguchi, K. Tanaka, N. Harayama, Y. Inoue, N. Kabashima, Y. Ueta, Y. Hattori, and H. Yamashita. 1998. PACAP increases the cytosolic Ca^{2+}

concentration and stimulates somatodendritic vasopressin release in rat supraoptic neurons. J Neuroendocrinol. 10 (1):31-42.

Sieghart, W. 2006. Structure, pharmacology, and function of $GABA_A$ receptor subtypes. Adv Pharmacol. 54: 231-63.

Smith, P. M., and A. V. Ferguson. 2010. Circulating signals as critical regulators of autonomic state-central roles for the subfornical organ. Am. J. Physiol. Regul. Integr. Comp. Physiol. 299 (2): R405-R415.

Sunn, N., M. J. McKinley, and B. J. Oldfield. 2003. Circulating angiotensin II activates neurones in circumventricular organs of the lamina terminalis that project to the bed nucleus of the stria terminalis. J Neuroendocrinols. 15 (8): 725-31.

Takahashi, M., M. Nomura, and J. Tanaka. 2016. GABAergic modulation of serotonin release in the rat subfornical organ area. Neurosci Lett. 630: 114-119.

Tallent, M., G. Liapakis, A. M. O'Carroll, S. J. Lolait, M. Dichter, and T. Reisine. 1996. Somatostatin receptor subtypes SSTR2 and SSTR5 couple negatively to an L-type Ca^{2+} current in the pituitary cell line AtT-20. Neuroscience. 71 (4): 1073-81.

Tanaka, K., I. Shibuya, N. Kabashima, Y. Ueta, and H. Yamashita. 1998. Inhibition of voltage-dependent calcium channels by prostaglandin E_2 in rat melanotrophs. Endocrinology. 139 (12): 4801-10.

Tanaka, J., N. Mashiko, A. Kawakami, A. Ushigome, and M. Nomura. 2002. GABAergic systems in the nucleus tractus solitarius regulate noradrenaline release in the subfornical organ area in the rat. Auton Neurosci. 100 (1-2): 58-65.

Unger, T., F. Bles, D. Ganten, R. E. Lang, R. Rettig, and N. A. Schwab. 1983. Gabaergic stimulation inhibits central actions of angiotensin II: pressor responses, drinking and release of vasopressin. Eur J Pharmacol. 90 (1): 1-9.

Tottene, A., S. Volsen, and D. Pietrobon. 2000. α_{1E} subunits form the pore of three cerebellar R-type calcium channels with different pharmacological and permeation properties. J Neurosci. 20 (1): 171-8.

Wang, G., P. Sarkar, J. R. Peterson, J. Anrather, J. P. Pierce, J. M. Moore, J. Feng, P. Zhou, T. A. Milner, V. M. Pickel, C. Iadecola, and R. L. Davisson. 2013. COX-1-derived PGE2 and PGE2 type 1 receptors are vital for angiotensin II-induced formation of reactive oxygen species and Ca^{2+} influx in the subfornical organ. Am J Physiol Heart Circ Physiol. 305 (10): H1451-61.

Washburn, D. L. S., and A. V. Ferguson. 2001. Selective potentiation of N-type calcium channels by angiotensin II in rat subfornical organ neurones. J. Physiol. (Lond.) 536 (3): 667-675.

Wickman, K. D., J. A. Iñiguez-Lluhl, P. A. Davenport, R. Taussig, G. B. Krapivinsky, M. E. Linder, A. G. Gilman, and D. E. Clapham. 1994. Recombinant G-protein beta gamma-subunits activate the muscarinic-gated atrial potassium channel. Nature. 368 (6468): 255-7.

Wojcik, W. J., R. A. Travagli, E. Costa, and M. Bertolino. 1990. Baclofen inhibits with high affinity an L-type-like voltage-dependent calcium channel in cerebellar granule cell cultures. Neuropharmacology. 29 (10): 969-72.

Weindl, A., J. Bufler, B. Winkler, T. Arzberger, and H. Hatt. 1992. Neurotransmitters and receptors in the subfornical organ. Immunohistochemical and electrophysiological evidence. Prog Brain Res. 91: 261-9.

Wojcik, W. J., and I. Holopainen. 1992. Role of central $GABA_B$ receptors in physiology and pathology. Neuropsychopharmacology. 6(4):201-14.

Yamada, M., Y. K. Ho, R. H. Lee, K. Kontanill, K. Takahashill, T. Katadall, and Y. Kurachi. 1994. Muscarinic K^+ channels are activated by beta gamma subunits and inhibited by the GDP-bound form of alpha subunit of transducin. D Biochem Biophys Res Commun. 200 (3)

Zamponi, G. W., and K. P. Currie. 2013. Regulation of Ca_V2 calcium channels by G protein coupled receptors. Biochim Biophys Acta. 1828 (7): 1629-43.

Zeng, N., C. Athmann, T. Kang, J. H. Walsh, and G. Sachs. 1999. Role of neuropeptide-sensitive L-type Ca^{2+} channels in histamine release in gastric enterochromaffin-like cells. Am J Physiol. 277 (6): G1268-80.

SUMMARY

INTRODUCTION & PURPOSE

The subfornical organ (SFO) is one of the circumventricular organs, which lack the blood-brain barrier. It induces water intake when it detects angiotensin II (AII) and as a result, increases the volume of body fluids. It is also known that the SFO evokes an increase of blood pressure through the sympathetic nervous system. The relationship between the SFO and the hypertension is currently attracting attention. The purpose of this study was to investigate the basic $[Ca^{2+}]_i$ kinetics of acutely dissociated SFO neurons, which lack synaptic and humoral influence from the surrounding tissues. The preparation allows to study intrinsic properties of these neurons, and direct effects of various neurotransmitters and humoral factors on these neurons. Furthermore, the properties and mechanisms of the $[Ca^{2+}]_i$ increase by AII, which is one of the most important physiological substances that regulate SFO neuron functions, at low concentrations (1 to 100 pM) and high concentrations (1 nM or more), and the inhibitory mechanism by GABA, which is the major inhibitory neurotransmitter in the SFO, were investigated.

MATERIALS AND METHODS

Neurons were acutely dissociated from SFO of Wistar rats (3-4 weeks old, male) by enzymatic and mechanical treatments. The $[Ca^{2+}]_i$ of SFO neurons was optically measured using the fura-2-based microfluorometry. In addition, the voltage-gated Ca^{2+} channel (VGCC) current with Ba^{2+} as the charge carrier (I_{Ba}) was measured using the whole-cell patch clamp method.

RESULTS

(1) More than a half of the acutely dissociated SFO neurons showed increases and decreases of $[Ca^{2+}]_i$ occurring repeatedly (Ca^{2+} oscillations), and the rest of the neurons maintained a nearly stable and low $[Ca^{2+}]_i$. Application of AII at low concentrations (1 to 100 pM) increased both the frequency and amplitude of Ca^{2+} oscillations in the former neurons and induced Ca^{2+} oscillations in the latter neurons.

(2) Both spontaneous and AII-induced Ca^{2+} oscillations were inhibited by extracellular Ca^{2+} and Na^{+} removal. In addition, it was also inhibited by Cd^{2+} which is a non-specific VGCC blocker, nicardipine which is a selective L-type VGCC blocker, and TTX, which is a selective voltage-gated Na^{+} channel blocker.

(3) Application of AII at high concentrations (1 nM or more) for a time period as short as 30 sec caused persistent $[Ca^{2+}]_i$ increases which lasted for 1 hour or longer.

(4) Spontaneous Ca^{2+} oscillations and persistent $[Ca^{2+}]_i$ increase induced by AII were reversibly suppressed by GABA.

(5) The persistent $[Ca^{2+}]_i$ increase induced by AII was completely inhibited by the AT1 antagonist, losartan.

(6) The persistent $[Ca^{2+}]_i$ increase was also completely inhibited by removal of extracellular Ca^{2+}. However, suppression of Ca^{2+} release from the Ca^{2+} store by the selective inhibitor of store Ca^{2+} pump, cyclopiazonic acid, had no effect on the persistent $[Ca^{2+}]_i$ increase. In addition, it was significantly inhibited by selective L-type and P / Q-type VGCC blockers and CaMK and PKC inhibitors.

(7) In more than 90% of AII-responsive neurons, the persistent $[Ca^{2+}]_i$ increase was inhibited by GABA, and the $[Ca^{2+}]_i$ increase was inhibited also by galanin and ANP in about 60% and 30%, respectively, of the SFO neurons.

(8) The inhibition by GABA was mimicked by the selective agonists of $GABA_A$ and $GABA_B$ receptors, muscimol and baclofen, respectively.

(9) The GABA-mediated inhibition was inhibited only when both the selective antagonists of $GABA_A$ and $GABA_B$ receptors, bicuculline and CGP55845, respectively, were administered.

(10) Baclofen rapidly and reversibly inhibited I_{Ba} in a concentration-dependent mannor, and the inhibition was antagonized by CGP55845.

(11) The inhibition of I_{Ba} by baclofen was reduced by the application of selective blockers of N-type, P / Q-type, and L-type VGCCs.

DISCUSSION & CONCLUSION

First, this study revealed that spontaneous Ca^{2+} oscillations occur in more than 50% of SFO neurons. It was also found that low concentrations of AII induce and enhance Ca^{2+} oscillations. It is suggested that spontaneous Ca^{2+} oscillations is due to Ca^{2+} influx from the extracellular space partly via L-type Ca^{2+} channels. Although several groups have reported basic characteristics of $[Ca^{2+}]_i$ of SFO neurons, there has been no report of spontaneous Ca^{2+} oscillations to date. It may be that the use of dissociated preparations in this study is the reason of the discovery of spontaneous Ca^{2+} oscillations and this could be one of the intrinsic properties of SFO neurons. Second, this study also revealed that high-concentrations of AII induce persistent $[Ca^{2+}]_i$ increase. The persistent $[Ca^{2+}]_i$ increase involves the AT1 receptor triggering Ca^{2+} influx through activation of voltage-gated Na^{2+} and Ca^{2+} channels as well as non-selective cation channels, rather than intracellular Ca^{2+} release. In addition, it is considered that protein phosphorylation by

both CaMK and PKC is involved in the persistent nature of the $[Ca^{2+}]_i$ response. Finally, this study further revealed that the persistent $[Ca^{2+}]_i$ increase is suppressed all of the three physiologically relevant inhibitory agents, GABA, galanin and ANP. It is suggested that the persistent $[Ca^{2+}]_i$ increase is stoppable and therefore not a result of damage of neurons. It is suggested that the inhibition by GABA is mediated by both $GABA_A$ and $GABA_B$ receptors, and that the inhibition via the $GABA_B$ receptor involve suppression of VGCCs of N-, P / Q-, and L-types. This is the first report of involvement of the $GABA_B$ receptor, and of inhibition of VGCCs in SFO neurons.

It has been reported that the plasma concentration of AII in normal rats is about 5 to 40 pM, and that in dehydrated or hypertention rats reaches about 150 to 600 pM. In this study, the induction and enhancement of Ca^{2+} oscillations were observed at 1 pM to 100 pM, which is close to the plasma concentration in normal rats. Moreover, the threshold concentration of AII causing the persistent $[Ca^{2+}]_i$ increase is between 100 and 1 nM, which is close to the AII concentrations in dehydrated rats and hypertension rats. Therefore, it is suggested that Ca^{2+} oscillations of SFO neurons may play an important role in the maintenance and regulation of the physiological function of SFO neurons *in vivo*, and the persistent $[Ca^{2+}]_i$ increase could be related to the pathophysiological functional change of SFO neurons. Moreover, since GABA, galanin and ANP all reversibly suppressed both Ca^{2+} oscillations and persistent $[Ca^{2+}]_i$ increase, it is suggested that the $[Ca^{2+}]_i$ kinetics of SFO is bidirectionally regulated by AII and the three inhibitory agents *in vivo*.

ACKNOWLEDGEMENTS

I would like to express the deepest appreciation to my supervisor, Dr. Izumi Shibuya, Professor, Department of Veterinary Medicine, Faculty of Agriculture, Tottori University, Japan, for his elaborated guidance, mentorship, considerable encouragement and invaluable discussion which made my research of great achievement and my study life unforgettable.

I would also like to express my deepest appreciation to my supervisor, Dr. Naoki Kitamura, Associate professor, Department of Veterinary Medicine, Faculty of Agriculture, Tottori University, Japan, for his invaluable supervision, kind support and tutelage.

I sincerely wish to appreciate Dr. Keiko Tanaka-Yamamoto, Principle Researcher, Center for Functional Connectomics, Korea Institute of Science and Technology, Seoul, Republic of Korea, Dr. John Ciriello, Professor, Department of Physiology and Pharmacology, Schulich School of Medicine and Dentistry, University of Western Ontario London, Ontario, Canada, Dr. Takahiko Shiina, Associate Professor, Department of Basic Veterinary Science, Laboratory of Physiology, The United Graduate School of Veterinary Sciences, Gifu University, Yanagido, Gifu, Japan, and Dr. Masashi Higuchi, Associate professor, Laboratory of Veterinary Biochemistry, Joint Department of Veterinary Medicine, Faculty of Agriculture, Japan, for their intimate advice and comments to my research projects and thesis.

I am very grateful also to Dr. Kenji Ito, Senoo Animal Hospital (Okayama, Japan), Dr. Keisuke Sugita, Assistant Chief, Koshigaya city, Saitama, Dr. Tazuyo Arai, Awaji Livestock hygiene service center, Hyogo, Japan, Hina Kokudo, student in our laboratory and the all students in this laboratory for their valuable cooperation in my experiments.

My appreciation also goes out to my family and friends for their encouragement and support all through my studies.

Finally, I would like to thank and pay my respects to animals for giving excellent data in my study.